Preparation and Characterization of Cell Membranes for Cancer Immunotherapy

by

Lukasz Jakub Ochyl

A dissertation submitted in partial fulfillment
of the requirements for the degree of
Doctor of Philosophy
(Pharmaceutical Sciences)
in the University of Michigan
2018

Doctoral Committee:

Assistant Professor James J. Moon, Chair
Associate Professor Wei Cheng
Professor Joerg Lahann
Research Associate Professor Qiao Li

Lukasz J. Ochyl

ochyl@umich.edu

ORCID iD: 0000-0001-9040-3679

Acknowledgements

The work presented in this thesis spanned a six-year period and a lifetime of preparation, all of which was aided by countless contributions of others. I greatly appreciate all and any assistance, however big or small.

I would like to thank my doctoral committee chair, Dr. James Moon, for taking me on as a student and serving a role of a tireless mentor. He has provided me with invaluable feedback at every step of the way, starting with introduction to new laboratory techniques, establishing experimental procedures, designing experiments, and communicating the results. I greatly appreciate all of the patience, thoughtfulness, and effort that have gone into shaping me into a scientist. I would like to also acknowledge my doctoral committee consisting of Dr. Wei Cheng, Dr. Joerg Lahann, Dr. Qiao Li, and Dr. Steven Schwendeman, for the great amount of feedback that they have provided. Your suggestions and advice over the years had given direction and scope for my work.

I would like to acknowledge everyone that has sparked my interest in science and contributed to my education starting with my high school chemistry teacher, Mr. Kenneth Warren. I would like to acknowledge the faculty at University of Wisconsin and in particular Dr. Michelle Harris and Dr. Ann Palmenberg (along with her entire lab, specifically Dr. Bradley Brown and Dr. Holly Basta) for introducing me to scientific research. The faculty at University of Michigan and in particular the College of Pharmacy had provided the necessary education and guidance.

I would like to thank all of the Moon Lab members who had assisted me with their feedback, time, and labor. Dr. Preety Sahdev has established the early lab space and introduced me to numerous experimental procedures. Joseph Bazzill has provided scientific input, troubleshooting ideas, and aided in a number of experiments over the years that would not have been feasible on my own. Dr. Rui Kuai, Dr. Jutaek Nam, and Charles Park have provided feedback and insight into my work. Yao Xu has worked tirelessly in ensuring that the lab operates smoothly and assisted with laborious experiments.

A lot of input and assistance came from outside of the lab due to the collaborative environment of the University of Michigan. Flow cytometry core, and specifically Dr. Dave Adams, Ann Marie Deslauriers-Cox, and Mark Savary, have been invaluable with their feedback and help. Biointerfaces Institute established possibilities and connections with scientists of various backgrounds generating unique perspectives. I would like to thank Dr. Joseph Labuz, Joe Nguyen, Dr. Molly Kozminsky, Priyan Weerappuli, Dr. Ryan Oliver, and labs of Dr. Joerg Lahann, Dr. Lonnie Shea, and Dr. Steven Schwendeman.

Thank you to all of the friends that I have made along the way and who have supported me. In particular I would like to mention Dr. Joseph Madak for all of the kind words and the good times. Joseph Bazzill has been a good friend inside and outside of the lab, along with Dr. Patrick Grogan, Karl Olsen, Dr. Chitra Subramanian, and Mark Nelson.

Finally, I would never have accomplished anything without my family. My parents have worked tirelessly, sacrificed themselves, and always stressed the importance of education. They supported me when I needed help and pushed me to excel. My brother, Michal, has always been an incredibly positive influence and someone I could always lean on. Most importantly, I would like to thank my amazing wife, Mari, for all of her support, patience, and confidence in me.

Table of Contents

List of Figures

Abstract

Cancer immunotherapy has advanced rapidly over the past decade leading to clinical approval of immune checkpoint blockade and adoptive cell transfer therapies. Further efforts into development of therapeutic vaccines had generated promising results in pre-clinical and clinical studies. Here, we demonstrate novel methodology for preparation of cell membranes into nano-sized vesicles and the development of characterization methods via nanoparticle flow cytometry. Cancer cell membranes from murine melanoma cell line expressing model antigen, ovalbumin, were used for generation of PEGylated vehicles (PEG-NPs), which efficiently delivered endogenous membrane-associated cancer antigens to the draining lymph nodes after subcutaneous administration. PEG-NPs were efficiently taken up by dendritic cells and, when dosed with a potent adjuvant, led to antigen-specific T cell activation and proliferation approximately 4-fold greater than treatment with traditional freeze-thaw lysates. In combination with immune checkpoint blockade (anti-PD-1 treatment), our vaccination approach led to therapeutic cure of 63% of mice and persistent memory responses rejecting additional tumor rechallenge. We further utilized our nanoparticle platform by using adjuvant-matured dendritic cells (DCs) generating MPLA-activated dendritic cell membrane vesicles ((MPLA)DC-MVs). This preparation led to nanoparticles carrying T cell activation ligands (CD80 and CD86) and promoted their proliferation activation in vitro compared to antigen peptide alone, as demonstrated by 2-fold increase in proliferation and 5- to 8-fold increase in live cell numbers and expression of CD25 activation marker. In addition, (MPLA)DC-MVs, but not unstimulated

DC-MVs, resulted in activation of immature dendritic cells in vitro, indicated by 2- and 1.3-fold greater expression of CD40 and CD80, respectively. Administration of this formulation in vivo together with OVA peptide epitope led to 2-fold enhanced expansion and maintenance of antigen-specific T cells compared to peptide alone in mice that received adoptive cell transfer or had established OVA-expressing tumors. These studies had demonstrated the use for cell membranes in immunotherapy as vaccine vehicles, but further characterization and optimization could allow for improved efficacy, prompting us to adopt flow cytometry methods aimed at nanoparticle analysis. The technique was established by analysis of lipid-based synthetic formulations focused on demonstrating effective fluorescence detection and separation of individual particle populations. Proof of concept studies were used to confirm presence of ovalbumin on membrane-derived vesicles with antibody staining. Finally, we had utilized this technique to examine antigen display on hepatitis virus C vaccine formulation in order to determine if broadly neutralizing antibodies can bind efficiently and thus if they can be raised in mice immunized with these formulations. Our studies demonstrate that similar levels of broadly neutralizing antibody binding to nanoparticles translate to similar level of protection against cross-strain viral challenge. Taken together, this work has generated a foundation for further research into the use of cell membranes as nanoparticles for immunotherapeutic approaches and techniques necessary for their characterization.

Chapter 1: Introduction

1.1 Melanoma: Current Therapies and Challenges

Cancer is the second leading cause of death in the United States claiming nearly 600,000 American lives each year [1]. Over 90,000 Americans with a median age of 60 years old are expected to be diagnosed with melanoma in 2018 demonstrating an increase of 15,000 new per cases per year since 2014. [1-3]. Approximately 16% of these new cases involve distant metastases, which in 2012 have been associated with very poor prognosis with an approximately 15% 5-year survival rate and resulting in almost 10,000 deaths per year [1, 2]. With the advent of newly developed immunotherapies, melanoma prognoses have been becoming more optimistic with the expected 5-year survival expected to at least double, if not triple over the next decade, while still leaving room for therapeutic improvement and decrease in side effects [4].

Melanoma has been linked to prolonged exposure to ultraviolet light and genetic predisposition, generally arising as a local lesion which can advance to metastatic disease [5]. Early diagnosis of melanoma following surgical resection is associated with good prognosis as the cancerous growth can be entirely removed. If left untreated, cancerous cells spread to the local lymph nodes and then disseminate throughout the body often establishing metastases in the brain, lungs, and liver [5]. For many decades there were only few FDA-approved therapies, which can be categorized into three groups: 1) chemotherapy (Dacarbazine), 2) BRAF/MEK inhibitors (Dabrafenib, Trametinib, and Vemurafenib), and 3) immune system stimulatory agents

(Aldesleukin). Within the past ten years, the field of immunotherapy has undergone tremendous progress, leading to the approval of immune checkpoint blockade therapies, which target PD-1 and CTLA4 (pembrolizumab/nivolumab and ipilimumab, respectively) [6].

Dacarbazine is an alkylating agent used in the clinic for over forty years characterized by very low average response rate of 15.3%, mostly comprised of partial responses leading to modest progression free survival of 6.4 months [7, 8]. This traditional chemotherapeutic approach has recently fallen out of use and has been replaced by more effective targeted and immunotherapeutic approaches as described below. Common activating mutation in the V600 residue of BRAF has been identified in approximately 50% of melanoma cases and has been generally associated with poor prognosis [9, 10]. Inhibition of BRAF or MEK in the MAPK pathway has been believed to result in an effective therapy for metastatic disease, which has led to recent development and FDA approval for three small molecule drugs: vemurafenib, dabrafenib, and trametinib [9]. In the most successful trial, combination of dabrafenib and trametinib resulted in an increase of the overall response rate to 76% and progression-free survival of 9.4 months for patients with the V600 BRAF mutation [11]. Even though these kinase inhibitors represent a modern breakthrough in treatment of metastatic melanoma they provide modest benefits due to known resistance mechanisms [12].

Aside from general chemotherapy and the specific MAPK pathway inhibition, immunotherapy has been the only other approach to show efficacy in patients with metastatic melanoma. Interleukin-2 (IL-2) has been identified for its anti-tumoral approved for clinical trials in very high doses (HD IL-2, under commercial name Aldesleukin) [13]. IL-2 is a potent activating T-cell cytokine associated with severe toxicities, which require treatment to be

stopped. Analysis of various clinical trials indicates durable complete response rate of 6% and partial response rate of 10% leading to 5.9 month progression-free survival [13].

Ipilimumab is an immunostimulatory agent recently developed for the wide, nonspecific activation of T-cell immunity, which acts by blocking inhibitory signaling through a T-cell transmembrane receptor CTLA-4 [14]. Recent clinical trials indicate 11% and 15.2% overall response when administered as monotherapy or together with dacarbazine, respectively, which is comparable to the results obtained using HD IL-2 [14, 15]. Ipilimumab benefits from a markedly decreased number of severe side effects, but also does not seem to lead to durable complete responses (1.5% and 0.8% for the previously mentioned trials) compared to the HD IL-2 therapy (6% complete response) [13-15]. Results from the HD IL-2 and ipilimumab studies provide evidence that the immune system can combat cancer, further supported by positive correlation between tumor infiltrating lymphocyte counts and survival in patients with melanoma [16].

Another approach in this area focuses on blocking inhibitory signaling through interaction between programmed death 1 (PD-1) receptor expressed by T cells and programmed death 1 ligand (PD-1L) expressed in the tumor microenvironment [5]. Two promising monoclonal antibodies, pembrolizumab (anti-PD-1) and nivolumab (anti-PD-1L) have demonstrated decreased toxicity, increased response rate (between 17% and 44%), and comparable frequencies of durable responses as HD IL-2 [17-19]. In fact, response to pembrolizumab was not influenced by previous treatment with ipilimumab suggesting that synergy may be achieved when targeting these two pathways, which was supported by promising results from an early clinical trial consisting of ipilimumab + nivolumab therapy [18, 20]. The most recent analysis demonstrates 58% three-year survival, which was unmatched with other

approaches, while one third of the patients have shown lack of disease progression during the three years hinting at durable, long-term cures [4].

However, while immune checkpoint inhibition is considered generally safe, high grade toxicities may occur during treatment, with the loosened reins on the immune system. Generally, decreasing the dose or abandoning therapy allows the side effects to subside, but the therapeutic efficacy may be lost. It is important to remember the purpose of immune checkpoints, where in healthy adults they prevent of autoimmune disease and excessive tissue damage during inflammation [21]. As these biologic drugs make their way through the clinic, monitoring and analysis of long term effects is necessary as demonstrated recently by evidence of cardiotoxicity following CTLA4 and PD-1 therapy [22]. Treatment protocols are currently being optimized, thus establishing efficacious and safe therapies – however, due to this delicate balance, other treatment modalities may be needed to provide the necessary improvements.

While many advances have been made, the currently available therapies for metastatic melanoma had demonstrated either low levels of response or short duration. In addition, the MAPK pathway inhibitors are generally well tolerated but resistance rapidly develops resulting in small benefit to overall survival. BRAF inhibitors were successful because of their high level of specificity, whereas immunotherapies exploited the specificity of the body's own immune system, but were effective in only a small fraction of patients. It appears that not only activation, but also guidance of the immune system may be necessary to achieve durable responses in majority of patients, which has led to attempts to develop therapeutic cancer vaccines explored below.

1.2 Introduction to the Immune System

The immune system has developed to protect the host from a variety of pathogens such as bacteria and viruses. It can be divided into two branches of innate and adaptive immunity. The former plays an important role in eradication and/or containment of infectious pathogens at an early stage. Innate immunity relies on common and evolutionarily preserved elements of viruses and bacteria known as pathogen-associated molecular patterns (PAMPs) for recognition using pathogen recognition receptors (PRRs) [23]. This early response provides time for the adaptive immunity to form, where antigen presenting cells (APCs) sample pathogens for immunogenic antigens and present them to the effector cells of the adaptive immunity (T and B cells), giving rise to a specific and effective response. This process has also been recognized to identify and kill abnormal cells with tumorigenic properties, supported by increased incidence rates of cancer among immunocompromised populations [24].

1.2.1 Antigen Presentation

Antigen presenting cells (APCs) bridge innate and adaptive immunity by capturing pathogens and delivering antigens to the effector T and B cells. Relatively recently recognized dendritic cells (DCs) play a major role in this process and have been termed professional APCs. DCs function by continually sampling their environment and preferentially recognizing pathogens through the action of PRRs in a similar way to macrophages [25]. However, rather than upregulating phagocytic behavior and trafficking pathogens to lysosomes for degradation, DCs process and conserve antigens and begin their migration to the local lymph node [26]. Once there, antigens are presented on the cell surface along with an array of stimulatory transmembrane proteins in order to activate antigen-specific T cells. In particular, certain DC subsets possess a unique ability of cross-presentation, a process involving presentation of

extracellular antigens on major histocompatibility complex class I (MHC-I), strictly necessary for cytotoxic T cell response [27].

MHC-I is expressed by every cell in the body and in a traditional antigen-presentation pathway functions as a surveillance mechanism for viral and intracellular infections [28]. Cells continuously turn over cytosolic proteins through the action of proteasome, which cleaves them into short amino acid chains. These peptides are then transported into the endoplasmic reticulum (ER) via TAP1/2, where they bind to MHC-I producing unique peptide-MHC-I complexes, which are then trafficked to the plasma membrane, allowing healthy cells to present self-antigens on their surface [29]. Infected cells contain bacterial or viral proteins, which are processed in the exact same way, leading to foreign antigen display on the plasma membrane. These cells are then readily recognized and killed by antigen-specific cytotoxic T lymphocytes.

Normal cells fail to express immunostimulatory molecules such as CD80/86 to activate and expand the antigen-specific CTL clone, thus for the traditional antigen-presentation pathway to work, APCs would have to be infected directly, which may be a rare and unreliable event. Because of this, a process of cross-presentation has evolved, where APCs can take up antigens from the extracellular space and present them on MHC-I [27]. This complex and still not fully understood process involves antigen capture and trafficking into endosomes, which can briefly fuse with the ER and extract the necessary machinery for cross-presentation. Proteins can then be degraded directly by endosomal proteases and loaded onto MHC-I, which is known as the vacuolar pathway, or they can be translocated into the cytoplasm with the assistance of Sec61 protein, degraded by the proteasome, and trafficked back via TAP1/2 complex to be loaded onto MHC-I [27].

Cross-presentation often occurs due to the naturally occurring cues, such as TLR signaling. It is also very difficult to induce artificially and has been the major challenge in eliciting CTL responses. A few strategies have been employed to circumvent this issue by disrupting the endosomal membrane and thus allowing the antigens to enter the cytosol. One of these approaches involves conjugation of fusogenic or cell-penetrating peptides to the surface of nanoparticles. These peptides are generally composed of positively charged amino acids and can adsorb and disrupt the negatively charged lipid bilayer. In one particular case, OVA-loaded liposomes were modified with octaarganine (R8) leading to 5- and 55-fold increase in OVA presentation on MHC-I compared to cationic liposomes and soluble OVA, respectively [30]. Another strategy employed conjugation of pH-dependent fusogenic polymer (linear 3-methylglutarylated poly(glycidol)) to liposomal surface and induced high OVA delivery to the cytosol, thus increasing CTL responses and providing protective immunity against challenges with OVA-expressing murine lymphoma model and retarding growth of established tumors [31]. Other approaches involve biomimetic incorporation of listeriolysin O, a pathogenic element which induces endosomal lysis in response to decreasing pH, leading to increased cytosolic delivery of OVA and significantly higher cross-presentation efficiency [32]. In the end, more advanced strategies for successful antigen delivery to dendritic cells and stimulation of pathways involved in surface peptide-MHC-I display are necessary to achieve strong anti-tumor CTL responses.

1.2.2 Cytotoxic T Lymphocyte Response

$CD8^+$ T cells or cytotoxic T lymphocytes (CTLs) are very important for combating intracellular infection as well as cancer. During $CD8^+$ T cell development in the thymus, the T-cell receptor (TCR) gene undergoes recombination in order to create unique antigen binding sites

[33]. TCRs are then exposed to MHC-I-self-peptide complexes presented by thymus-resident cells; if the binding is too weak, cells undergo apoptosis as their TCR cannot functionally bind to MHC-I, but if the binding is too strong, there's a potential for autoimmunity and those cells are deleted as well. Thus only T cells with intermediate affinity for self-peptides develop fully, which makes cancer immunotherapy directed at tumor associated antigens difficult, as the high affinity clones are eliminated in the process.

Following development, naïve T cells circulate throughout the body, traveling to lymph nodes and various tissues, where they can become activated. In order to fully promote T cell expansion, three different signaling events must take place [34]. Signal 1 is delivered through the interaction of TCR and MHC-I-peptide complex presented on APCs. Signal 2 comes from CD28 expressed on T cells and its binding to CD80 or CD86, which is expressed on mature and fully activated dendritic cells. Once sufficient activation occurs, T cells upregulate another surface receptor, CTLA4, which binds to CD80 and CD86 with a much higher affinity than CD28 and leads to inhibitory signaling. This mechanism serves to stop uncontrollable T cell expansion after activation and has been a target to increase immunogenicity with the use of CTLA4-specific monoclonal antibodies [14]. Finally, IL-2 produced by $CD4^+$ T cells or $CD8^+$ T cells themselves is necessary for functional development of CTLs and is considered to be Signal 3.

Once T cells are activated they can travel to sites of inflammation following cytokine gradients and seek out their targets by screening MHC-I-peptide complexes expressed on cell surfaces. Following recognition of the specific antigen, CTLs secrete granzymes and perforins which can effectively lyse the plasma membrane of target cells and induce signal transduction cascade leading to apoptosis [28]. After stimulation with IFNγ, healthy cells at the sites of inflammation upregulate Programmed Death Ligand 1 (PD-L1), which can bind to Programmed

Death 1 (PD-1) receptor on T-cells and induce their apoptosis [35]. This mechanism is necessary to prevent overly active immune response and prevent damage to the healthy tissue. Unfortunately, many tumors have hi-jacked this approach and create a severely immunosuppressive environment where CTLs cannot function properly. This interaction has been a target of recently developed monoclonal antibodies, which show efficacy as monotherapies, but may have an even greater impact when combined with cancer vaccines.

Although direct activation of $CD8^+$ T cells by APCs is considered to play the central role in anti-tumoral immune response, T helper (Th), or $CD4^+$, cells are also of particular importance. Aside from assisting with humoral responses, they are responsible for secretion of IL-2 necessary for effective $CD8^+$ T cell proliferation and IFNγ, which enhances maturation and functionality of dendritic cells [36]. In addition, Th cells also transiently express CD40L, which feeds back to DCs leading to further activation and upregulation of costimulatory factors and cytokines such as IL-12, necessary for functional CTL development and prolonged action at the site of the tumor [37, 38]. Finally, Th cells play a substantial role in eliciting memory phenotype, which allows for CTL persistence and thus increased efficacy against metastases and relapse [37]. There are a few differentiation paths that Th cells can take including Th1 and Th2 phenotype most commonly elicited by vaccines, which favor CTL and humoral responses respectively. Thus, it is important for cancer vaccine formulations to induce the Th1 response as it would aid CTLs most effectively. The advantage of subunit and whole tumor cell lysate over peptide vaccination is also evident here, considering that epitopes for MHC-I and MHC-II would be present thus allowing for direct activation of CTL and Th responses.

1.3 Vaccine Components

Vaccination has been claimed as the most effective form of preventative medicine in decreasing healthcare costs, human suffering, and death. Development of cancer vaccination has begun in early 1990s, aimed at the use of peptides and whole tumor cell lysates, and despite significant advancements still faces major challenges [39]. Many factors can influence vaccine efficacy including site of the injection and timing of the primary and booster immunizations. However, the vaccine composition has a predominant effect on the type and strength of immunity which can be achieved. Antigens are generally fragments of proteins which can be recognized by the effector component of the immune system. In addition, the immune action against that antigen must be triggered, thus there must be an activating component associated with every vaccine, which can range from emulsifying of the antigen to inclusion of various immunostimulatory molecules (adjuvants).

1.3.1 Antigens

Melanoma-specific proteins involved in melanin production have been identified as potential vaccine targets and include glycoprotein 100 (gp100), Melan-A/MART-1, and tyrosinase [40]. Other potential targets include common tumor-restricted antigens such as MART-2, MAGE-1, MAGE-3 and NY-ESO-1. Peptide vaccinations may prove more efficacious due to their effective dose at delivery and lack of necessity for cross-presentation. In addition, due to the differences between the protein cleavage properties of cellular proteasome and the DC-expressed immunoproteasome, effective immunity against a particular epitope may not always be achieved with the use of whole protein vaccination and peptides may need to be employed (e.g. melanoma-associated MART 1 immunogenic epitope failed to be presented on MHC-I in DCs transduced to express the protein in the cytosol) [41]. Problems stemming from

the localization of peptides *in vivo* prevent direct administration and require nanoparticle formulations or emulsification agents.

Administration of gp100 immunogenic peptide emulsified in Montanide ISA-51 together with Interleukin-2 led to increased response rate (20% vs 10%) and greater median overall survival (17.8 vs 11.1 months) compared to the IL-2 only treatment [42]. Immunization with gp100 together with ipilimumab did not improve efficacy over ipilimumab treatment alone, presenting the complexity of the cancer vaccination challenge, but can also be explained by the heterogeneity of most tumors and insufficient immune response [14]. Administration of dendritic cells pulsed *ex vivo* with five immunogenic peptides derived from melanoma tumor proteins (gp100, tyrosinase, MAGE-A2, MAGE-A3, and MART-1) demonstrated improved overall survival [43]. Other approaches aimed at eliciting multivalent responses focused on tumor cell lysate administration tested in multiple clinical trials, but were met with low response rates and insufficient benefits [40]. These issues may be explained by lack of immunogenicity of tumor cell lysates and low cross-presentation efficiency, which are currently being addressed with the use of various adjuvants and nanoparticle formulations.

Aside from development of the immune checkpoint blockade over the past decade, there has been a major shift in the antigens targeted by today's vaccines. The focus has gone away from poorly immunogenic self-antigens, which have had limited efficacy and continuous concerns about potential autoimmunity, but rather, due to the highly mutagenic cancer genome (resulting from diminished capabilities of DNA repair and resistance to apoptosis), fell on a new class of epitopes [44]. Often, as a result of single point mutation or shift in the reading frame, the primary amino acid structure will be affected leading to generation of a new sequence. This may lead to a new epitope, termed neo-antigen, which may be immunogenic due to enhanced cellular

processing, MHC-I binding affinity, or T cell receptor recognition. The past five years have shown translation from initial mouse studies focusing on identification of neo-antigens in cell lines and showing efficacy in pre-clinical studies [45, 46] to the first reports of human trials demonstrating complete and durable cures [47, 48]. There is no doubt that this approach has tremendous promise in the future of cancer immunotherapy, prompting extensive research in formulation and delivery of neo-antigen vaccines [49].

1.3.2 Adjuvants

Cancer therapeutic vaccines struggle with poorly immunogenic antigens and lack of proper adjuvants for induction of cross-presentation and strong CTL responses [50]. Current clinically-used adjuvants include aluminum salts (Alum) and squalene-based oil-in-water emulsions (MF59 and AS03), which induce inflammatory responses and thus recruit APCs to the site of the injection allowing antigen sampling, providing immunogenic cues, and most commonly resulting in increased humoral responses [51]. Additionally, receptors involved in recognition of pathogen associated molecular patterns (PAMPs) have been identified as key players in APC activation and include primarily studied Toll-like receptors (TLRs), as well as less understood nucleotide-binding domain (NOD) receptors, NOD-like receptors (NLRs), RIG-1-like receptors, integrins and C-type lectins. The latter receptors have been receiving increasing amounts of attention lately, but it is the better-understood TLR agonists that have made it into the clinic thus far.

Double stranded RNA (dsRNA) associated with viral infections activates TLR3 in the endosomal compartment and promotes Th1-skewed responses, which favor involvement of CTLs [50]. Additionally, dsRNA molecules such as synthetic polyinosinic:cytidylic acid (polyI:C) can also activate cytosolic receptors such as retinoic acid-inducible gene-1(RIG-I) and

melanoma differentiation associated gene 5 (MDA5), which together with TLR3 signaling may induce synergistic effects and induce increased IL-12 and type I interferon (IFN) secretion. PolyI:C can be administered in a complex with poly-L-lysine in order to increase stability and counter the highly negative charge, thus allowing for effective topical administration currently showing safety and efficacy in clinical trials against glioblastoma [52]. Additionally, polyI:C can be freely administered as a soluble adjuvant along with nanoparticle formulations via intratracheal route in order to boost mucosal CTL responses [53]. Finally, co-loading of OVA and polyI:C into fusogenic liposomes led to superior anti-tumoral effects compared to OVA-polyI:C complexes, thus suggesting that cytosolic delivery of the dsRNA may induce MDA5-mediated signaling and improved efficacy, although this causality was not tested by the authors [54].

TLR4 has been identified for its role in recognition of lipopolysaccharide (LPS) and induction of adaptive immunity [55]. Non-pyrogenic LPS analog, monophosphoryl lipid A (MPLA) is associated with Th1-skewed response and has been FDA approved for use in Cervarix and Fendrix, aluminum-salt-based vaccines against human papilloma virus (HPV) and hepatitis B virus (HBV), respectively [51]. Lipid-based particles provide an additional advantage in delivery of MPLA at dose-sparing amounts, as it can partition effectively into the hydrophobic membrane. Efficacy of TLR signaling was demonstrated by increased upregulation of splenic DC maturation markers, when cells were co-cultured with MPLA-containing particles compared to adjuvant free formulation, and induction of high levels of antigen-specific CTL response *in vivo* [56].

TLR7 and TLR8 expressed in the endosomal compartment are responsible for detection of single stranded RNA (ssRNA) rich in guanosine and uridine [50]. Considering that RNA is

inherently unstable, small molecule compounds capable of activating TLR7 (Imiquimod) and TLR7/8 (Resiquimod or R848) were developed, which do not show efficacy when administered as a soluble vaccine, possibly due to high hydrophobicity, thus strongly affecting their co-localization with the antigen. Approaches involving conjugation of these agonists to antigens and nanoparticle formulation have been used in order to achieve responses. Due to high permeability, Imiquimod has also been used as a 5% cream for topical administration at tumor sites in various benign skin neoplasms, but also as experimental immunotherapy for melanoma patients which has shown increased T cell activation alone, and together with CpG/Melan A peptide vaccination, promoted strong antigen-specific central memory phenotype CTL responses [57, 58].

Human DNA contains methylated CpG motifs which are not present in bacteria and viruses, thus providing a marker for pathogenic DNA recognized by TLR9 [50]. TLR9 is not expressed in human myeloid DCs, known for their superior cross-presentation efficiency, but activation of TLR9 in plasmacytoid DCs is believed to promote high level of IFNγ production responsible for antibody responses, promotion of T cell proliferation, survival and memory phenotype, as well as strong polarization of the T helper cell phenotype to CTL-supportive Th1 [59]. CpG has been used in various cancer therapeutic vaccine approaches and has most made it into clinical trials incorporated into water-in-oil emulsion (Montanide) together with immunogenic peptide from melanoma-specific protein, Melan-A [60]. It has also been extensively explored as an adjuvant for numerous vaccine approaches intended for various cancers and infectious diseases demonstrating relatively safety when given at lower doses [61].

TLR3 and some TLR4 signaling relies strongly on TRIF adaptor molecule and leads to activation of type I IFN production, whereas remaining TLRs signal through Myd88 associated

with activation of NF-κB transcription factor. These signaling cascades as well activation of the two different transcription factors have been shown to elicit synergistic effects and are associated with stronger and broader immune responses [51]. In particular, simple intraperitoneal administration of CpG and PolyI:C together led to increased levels of cytokine production including IL-12 and enhanced anti-tumoral response against established melanoma lung metastases compared to either adjuvant alone [62]. Overall, it is difficult to predict which combinations will work and generally must be tested on a case by case basis, thus providing opportunities for development of multiadjuvant therapies.

1.4 Immunotherapies in Development

Currently approved immunotherapeutic agents, HD IL-2 and checkpoint blockade inhibitors, act systemically by nonspecific activation of T-cell immunity leading to low response rate, but produce durable effects making immunotherapy a very promising field. Directing the immune response toward anti-tumor responses via vaccination has been suggested for decades, but quite difficult to achieve, due to central tolerance and lack of visible objective responses, often associated with the "adaptive resistance" [21]. Due to the immune infiltration and inflammation, local production of IFNγ fuels upregulation of PD-1L on tumors cells, which in turn decreases T cell function and promotes immunosuppressive environment. Introduction and development of immune checkpoint blockade allowed for vaccine-mediated tumor antigen-specific T cell expansion to kill tumor cells efficiency and without any hindrance, which led to extensive progress in tumor vaccine development.

1.4.1 Dendritic-cell-based Therapies

Provenge is the only cancer vaccine currently approved by the FDA and is associated with a 4.1 month increase in median overall survival of patients with advanced prostate cancer [63]. Cancer therapeutic vaccinations involve presentation of tumor associated antigens (TAAs) in an immunogenic setting to induce anti-tumoral responses, but so far the results have been limited and disappointing [39]. Current methods of TAA delivery vary and generally include pulsing *ex vivo* cultured DCs with tumor cell lysates or peptide antigens, which have been the only therapies associated with notable responses [39, 64, 65]. Dendritic cell vaccinations have been explored for nearly two decades following discovery and verification of these professional antigen presenting cells (APCs) and led to hundreds of DC-based vaccines in clinical trials across the United States [66]. Unfortunately, even though promising results have been observed since the late 1990s, most therapies fail to elicit sufficient response ultimately preventing further development.

A phase II clinical trial, in which *ex vivo* cultured DCs were pulsed with a cocktail containing five melanoma peptide antigens (gp100, tyrosinase, MAGE-A2, MAGE-A3, and MART-1), has shown significant improvement in overall survival of patients from 7.3 to 13.6 months [43]. In addition, outcome was strongly correlated to the level of immune response as determined by an ELISPOT assay, and the overall survival for high-responding patients was 21.9 months compared to 8.1 months in low-responding patients. Another phase II clinical trial focused on DC-based vaccination using irradiated autologous tumor cells with self-renewing and proliferative characteristics (indicative of the CSC populations) and resulted in a five-year survival rate of 54% [67]. In a comparative study DC-vaccinated patients achieved two-year survival rate of 72% compared to 31% in patients who only received irradiated tumor cells [68].

These promising results led to a promising launch of a large scale phase III clinical trial for melanoma (NCT01875653).

Dendritic cells are generated from *ex vivo* cultured monocytes or $CD34^+$ progenitor cells obtained from patients' peripheral blood, although recent reports indicate that these artificial DCs may not be as effective as naturally occurring plasmacytoid dendritic cells, thus recognizing an area for future progress [69]. Utilization of dendritic cells has shown clinical efficacy, but involves labor-intensive and expensive methods, such as FDA-approved Provenge dendritic cell vaccine, which requires a four day process at cGMP (current good manufacturing practice) facilities and costs $93,000 per therapy [70]. It is not surprising that a lot of different therapies and approaches are being studied, but due to young age and significant challenges in the field, have not yet made the transition to the bedside just yet. Overall, cancer immunotherapy has become a very attractive field in the recent years, as it employs very specific and often durable responses compared to treatments with toxic chemotherapy or small molecule inhibitors often associated with resistance mechanisms.

1.4.2 Pre-clinical Whole Tumor Cell Therapies

Importance of CTL responses in cancer immunotherapy has prompted numerous studies focused on cytosolic delivery of tumor associated antigens and promoting their immunogenicity. Several murine cancer models (i.e. B16 melanoma and EL4 lymphoma) have been developed in order to aid with research in immunocompetent animals. In addition, these cell lines have been transduced with stable expression of ovalbumin (OVA), providing important models for studying immunogenic delivery of this model antigen. Granted that generation of an immune response with the aid of an exogenous antigen is less challenging, these results need to be examined carefully and reevaluated with the use of tumor associated self-antigens.

Advantages of using whole tumor cell antigen repertoire include multivalent responses as well as idea of personalized medicine, but the approach has not been very successful thus far. Studies aiming at inducing immune responses include incorporation of whole tumor cell lysates into particle formulations, which can benefit *ex vivo* pulsed DCs by eliciting superior level of cross-presentation [71]. These benefits were extended by direct immunization with fusogenic liposomes encapsulated with B16BL6 lysates, which decreased tumor growth in mice [72]. In addition, encapsulation of E.G7 into PLGA microspheres with CpG and PolyI:C and *in vivo* administration, led to expansion of E.G7-specific and functional CTLs and regression of established subcutaneous tumors in mice [73].

Administration of inactivated tumor cells is also explored as the *in vivo* immunogenic tumor cell death is believed to promote anti-tumoral responses. A recent study focused on nanoparticle-induced loading of IL-2 and GM-CSF into irradiated Lewis lung carcinoma (LLC) tumor cells followed by subcutaneous administration [74]. Together with the immunogenic death of the cells, the controlled release of cytokines, which can attract DCs, led to improved infiltration of CTLs into the tumor site, prophylactic and therapeutic responses in tumor models, and decreased metastatic behavior of established tumors.

Other approaches involve implantation of antigen and adjuvant co-loaded scaffolds. A recent study used poly(D,L-lactide-co-glycolide) (PLG) matrices co-loaded with tumor cell lysates obtained from digested primary tumors, DC-activation granulocyte macrophage colony-stimulating factor (GM-CSF), and three different TLR agonists: PolyI:C, MPLA, and CpG [75]. The findings indicted that PolyI:C and CpG prolonged stimulation and homing of dendritic cells to the local lymph nodes which correlated with improved therapeutic responses (tumor volume and overall survival) in mice with established tumors compared to the use MPLA. In addition,

using a knock-out model, it was demonstrated that $CD8^+$ DCs, known for their role in cross-presentation, are necessary for induction of effective CTL response. IL-12 and granulocyte colony-stimulating factor (G-CSF) production correlated positively with anti-tumoral response, thus providing potential biomarkers for future studies. Finally, feasibility of immunization using whole tumor cell lysates from a primary source sample was demonstrated.

Focus of current studies includes enhancing cross-presentation of tumor associated antigens as well as promoting Th1-skewed cytokine responses. Approaches using tumor cell lysates as the source of antigens have been shown to elicit responses in the laboratory, although a lot of improvement is still needed as no therapies achieved objective responses in clinical studies [40]. Important questions currently being investigated involve the vehicle and the combination of adjuvant needed to elicit a potent CTL response.

1.5 Nanoparticle Delivery Systems

Induction of an effective response against self-antigens is difficult and requires the use of adjuvants to provide immunostimulatory cues as described above. Simple mixing of the adjuvant and the antigen prior to administration is also insufficient due to many reasons. For example, the antigen can be degraded prior to being taken up by an antigen presenting cell (APC) or it can be taken up separately from the adjuvant, thus inducing a tolerogenic response [76].

Nanoparticle formulations have been used successfully in the past for vaccination, as they effectively increase antigen delivery to APCs. This occurs due to endocytosis-inducing size and shape of the particles, which mimic characteristics of pathogens. Additionally, particle size and charge may strongly affect biodistribution and retention time of the particles in lymph nodes and spleens, thus enhancing exposure to APCs and affecting the type and level of response [77-79].

Another major benefit of nanoparticle systems includes co-loading of the antigen with an adjuvant, thus delivering both components to the same dendritic cell, which are necessary for Signal 1 and 2 for T-cell activation [76, 80]. These effects were supported by numerous studies and in particular demonstrated by increased CTL responses elicited by delivery of PolyI:C encapsulated within fusogenic liposomes compared to fusogenic liposomes administered together with soluble PolyI:C [54].

In addition, nanoparticles can effectively protect their cargo from degradation in serum conditions and can effectively traffic through the lymphatic making them ideal for *in vivo* antigen delivery thus offering an alternative to labor-intensive and expensive cell-based therapies. Targeting of the antigens to the cytosol of APCs can also be enhanced by variety of nanoparticle systems exhibiting endosomal escape characteristics, thus allowing for effective antigen cross-presentation and induction of CTL responses, which generally fail to be developed by traditional vaccination methods.

These systems generally do not induce immune responses against the vehicle itself due to lack of protein components. This allows for multiple administrations of the same formulation without induction of an immune reaction or loss of potency, providing advantage over viral vectors. Additionally, polyethylene glycol can be incorporated on particle surface leading to decreased aggregation, increased lymph node accumulation, and prolonging antigen exposure due to ease with which nanoparticle surfaces can be functionalized [81]. These also provide potential for enhancing delivery to specific cells (e.g. APCs) by conjugation of receptor ligands or antibodies [82].

Nanoparticles can be composed of variety of materials ranging from metals and synthetic polymers to natural polymers and lipid-based systems, thus their characteristics can be finely

tuned, although risks and benefits must be carefully weighed. In particular, lipid-based nanoparticles offer advantages in material biocompatibility and biodegradability making them safe for use and preventing accumulation in the body [83]. On the other hand, these lipid-based platforms are prone to degradation and early antigen release, which has been a major difficulty and focus of many current studies. As described below, variety of nature-inspired carrier systems and vaccine approaches have also been studied recently including the use of cell membranes for antigen delivery.

Plasma cell membranes, very complex structures composing of lipids and proteins, serve many critical cell functions. Recent focus has shifted onto the generation of exosomes and microvesicles, which can bud off from the cell surface [84, 85]. While these vesicles are continuously produced and shed by cells, they can carry proteins or even RNA molecules promoting cell-to-cell communication. There has been extensive interest in use of red blood cell enucleated "ghosts" for use in drug delivery due to their biodistribution profiles and prolonged half-life. In addition, cell membranes derived from various cell subtypes display surface markers, ligands, or enzymes with very specific function thus prompting their development and use [86-88].

The membrane preparation technology and utilization developed through these studies allowed for the focus on tumor cell membranes and their role in cancer therapies. In particular, utilization of sonicated melanoma cell membranes in combination with encapsulated CpG has resulted in the generation of the therapy termed "reduced cancer cell" (RCC) vaccine [89]. This strategy was characterized using *in vitro* models of T cell responses and demonstrated limited T cell activation *in vivo*. Others focused on PLGA particles loaded with CpG and cloaking them with melanoma membranes to demonstrate effective localization to the draining lymph nodes

displaying detectable level of prophylactic and therapeutic efficacy [90]. Taken together, these studies demonstrate interest in tumor cell membrane-based cancer immunotherapy approaches due to their nanoparticle advantages such as biocompatibility, size-dependent lymph node draining, and prolonged stability. However, limited successes of these studies call for further research. In particular, PEGylation of cancer cell membranes may aid in their ability to effectively traffic to the lymph nodes, while loading of peptides onto immunogenic cell membranes may promote effective antigen-specific responses.

Improvements for nanoparticle-based therapies require effective characterization prior to pre-clinical studies in order to provide efficient throughput for approach validation. Currently, formulations are examined for physiochemical characteristics and cargo loading prior to empirical pre-clinical animal studies. Particle size and surface characteristics have been correlated to their ability to efficiently drain to the local lymph, providing a set of guidelines needed for optimal formulations. However, while the encapsulation amount is necessary for appropriate antigen dosing in immunotherapies, it may not always convert to administration of immunologically active molecules [91]. There is a need for high-throughput technique, which can predict the immunogenic efficiency of nanoparticles displaying antigens on their surface. Flow cytometry approaches have been utilized for assessment of cellular exosomes and microvesicles, providing an opportunity to exploit this approach for use with nanoparticle vaccine formulations.

1.6 Conclusions

Melanoma affects hundreds of thousands of patients every year in the United States, and disease progression to the metastatic grade used to be associated with extremely poor prognosis. Through the introduction of immune checkpoint blockade, the landscape has shifted greatly, resulting in two- to three-fold increase in 5-year survival rate. It has also allowed for new and promising approaches to be further explored and promoted further investigation into neo-antigen vaccination, which has demonstrated tremendous curative capabilities in small-scale clinical trials. As it stands, the outlook on the future is extremely positive, although details must be worked out in order to establish efficacious protocols which also limit short- and long-term safety concerns.

Since melanoma is responsible for less than 2% of cancer deaths in the United States, adapting these approaches to other tumor types is imperative and these efforts have been underway. In fact, it is no coincidence that immunotherapeutic approaches pioneered combating melanoma. Due to extensive time necessary for disease progression, uniqueness of melanocytes, and commonly dysfunctional DNA repair mechanism, melanoma has been characterized by the most extensive mutational burden [92]. This has been regarded as the reason for high number of tumor-infiltrating lymphocytes and responsiveness towards immune therapies. Further work is necessary in order to adapt these approaches for use against less immunogenic tumor types. While tremendous progress has been made with the use of immunotherapies, future approaches are likely to focus on nanoparticle- and membrane-based vaccination to harness their ability to elicit strong responses while limiting adverse effects.

1.7 Motivation

The heterogeneity of cancer across tissues, classifications, persons, and even individual metastases of the same patient has become evident and calls for highly personalized approaches. Recent studies have focused on next generation sequencing in order to identify patient-specific neo-antigens or tumor-reactive T/B cell receptors, allowing for generation of novel vaccine systems and cell engineering approaches. However, while extremely promising, the cost and time-to-treatment of these therapies is high at this moment, thus alternatives must be explored. The above-mentioned sequencing requires tissue biopsy or tumor resection, which provides cellular material that in turn can be used to develop an effective vaccine. Our approach has focused on utilization of the available tumor tissue in order to generate nano-sized tumor cell membrane vesicles. The composition of the vehicle would consist of endogenous plasma membrane and tumor proteins (both self- and tumor-specific antigens), allowing for minimal vehicle-directed immunity, focus on enhancing responses against cancer, and complete biocompatibility and biodegradability. In addition, stabilizing surface modification and potent immunostimulatory molecules would be included in order to provide efficient lymph node delivery and immune activation. This approach demonstrates facile production of vaccines that can be administered without prolonged turnaround time allowing for recruitment of the immune system to fight against cancer as early as possible.

1.7 References

1. Siegel, R., et al., *Cancer statistics, 2014.* CA: A Cancer Journal for Clinicians, 2014. **64**(1): p. 9-29.

2. Siegel, R., et al., *Cancer treatment and survivorship statistics, 2012.* CA: A Cancer Journal for Clinicians, 2012. **62**(4): p. 220-41.

3. Siegel, R.L., K.D. Miller, and A. Jemal, *Cancer Statistics, 2018.* Ca-a Cancer Journal for Clinicians, 2018. **68**(1): p. 7-30.

4. Wolchok, J.D., et al., *Overall Survival with Combined Nivolumab and Ipilimumab in Advanced Melanoma.* New England Journal of Medicine, 2017. **377**(14): p. 1345-1356.

5. Eggermont, A.M.M., A. Spatz, and C. Robert, *Cutaneous melanoma.* Lancet, 2014. **383**(9919): p. 816-827.

6. Pardoll, D.M., *The blockade of immune checkpoints in cancer immunotherapy.* Nature Reviews Cancer, 2012. **12**(4): p. 252-264.

7. Lui, P., et al., *Treatments for metastatic melanoma: Synthesis of evidence from randomized trials.* Cancer Treatment Reviews, 2007. **33**(8): p. 665-680.

8. Middleton, M.R., et al., *Randomized phase III study of temozolomide versus dacarbazine in the treatment of patients with advanced metastatic malignant melanoma.* Journal of Clinical Oncology, 2000. **18**(1): p. 158-166.

9. Jang, S. and M.B. Atkins, *Which drug, and when, for patients with BRAF-mutant melanoma?* The Lancet Oncology, 2013. **14**(2): p. e60-e69.

10. Moreau, S., et al., *Prognostic Value of BRAF (V600) Mutations in Melanoma Patients After Resection of Metastatic Lymph Nodes.* Annals of Surgical Oncology, 2012. **19**(13): p. 4314-4321.

11. Flaherty, K.T., et al., *Combined BRAF and MEK Inhibition in Melanoma with BRAF V600 Mutations.* New England Journal of Medicine, 2012. **367**(18): p. 1694-1703.

12. Sullivan, R.J. and K.T. Flaherty, *Resistance to BRAF-targeted therapy in melanoma.* European Journal of Cancer, 2013. **49**(6): p. 1297-304.

13. Atkins, M.B., et al., *High-dose recombinant interleukin 2 therapy for patients with metastatic melanoma: Analysis of 270 patients treated between 1985 and 1993.* Journal of Clinical Oncology, 1999. **17**(7): p. 2105-2116.

14. Hodi, F.S., et al., *Improved Survival with Ipilimumab in Patients with Metastatic Melanoma.* New England Journal of Medicine, 2010. **363**(8): p. 711-723.

15. Robert, C., et al., *Ipilimumab plus Dacarbazine for Previously Untreated Metastatic Melanoma.* New England Journal of Medicine, 2011. **364**(26): p. 2517-2526.

16. Clemente, C.G., et al., *Prognostic value of tumor infiltrating lymphocytes in the vertical growth phase of primary cutaneous melanoma.* Cancer, 1996. **77**(7): p. 1303-1310.

17. Brahmer, J.R., et al., *Safety and Activity of Anti-PD-L1 Antibody in Patients with Advanced Cancer.* New England Journal of Medicine, 2012. **366**(26): p. 2455-2465.

18. Hamid, O., et al., *Safety and Tumor Responses with Lambrolizumab (Anti-PD-1) in Melanoma.* New England Journal of Medicine, 2013. **369**(2): p. 134-144.

19. Topalian, S.L., et al., *Safety, Activity, and Immune Correlates of Anti-PD-1 Antibody in Cancer.* New England Journal of Medicine, 2012. **366**(26): p. 2443-2454.

20. Wolchok, J.D., et al., *Nivolumab plus Ipilimumab in Advanced Melanoma.* New England Journal of Medicine, 2013. **369**(2): p. 122-133.

21. Chen, L.P. and X. Han, *Anti-PD-1/PD-L1 therapy of human cancer: past, present, and future.* Journal of Clinical Investigation, 2015. **125**(9): p. 3384-3391.

22. Heinzerling, L., et al., *Cardiotoxicity associated with CTLA4 and PD1 blocking immunotherapy.* J Immunother Cancer, 2016. **4**: p. 50.

23. Kumar, H., T. Kawai, and S. Akira, *Pathogen Recognition by the Innate Immune System.* International Reviews of Immunology, 2011. **30**(1): p. 16-34.

24. Grulich, A.E., et al., *Incidence of cancers in people with HIV/AIDS compared with immunosuppressed transplant recipients: a meta-analysis.* Lancet, 2007. **370**(9581): p. 59-67.

25. Banchereau, J. and R.M. Steinman, *Dendritic cells and the control of immunity.* Nature, 1998. **392**(6673): p. 245-252.

26. Palm, N.W. and R. Medzhitov, *Pattern recognition receptors and control of adaptive immunity.* Immunological Reviews, 2009. **227**: p. 221-233.

27. Joffre, O.P., et al., *Cross-presentation by dendritic cells.* Nature Reviews Immunology, 2012. **12**(8): p. 557-569.

28. Barry, M. and R.C. Bleackley, *Cytotoxic T lymphocytes: All roads lead to death.* Nature Reviews Immunology, 2002. **2**(6): p. 401-409.

29. Villadangos, J.A. and P. Schnorrer, *Intrinsic and cooperative antigen-presenting functions of dendritic-cell subsets in vivo.* Nature Reviews Immunology, 2007. **7**(7): p. 543-555.

30. Nakamura, T., et al., *Efficient MHC class I presentation by controlled intracellular trafficking of antigens in octaarginine-modified liposomes.* Molecular Therapy, 2008. **16**(8): p. 1507-14.

31. Yuba, E., et al., *A liposome-based antigen delivery system using pH-sensitive fusogenic polymers for cancer immunotherapy.* Biomaterials, 2013. **34**(12): p. 3042-3052.

32. Andrews, C.D., et al., *Encapsulating immunostimulatory CpG oligonucleotides in listeriolysin O-liposomes promotes a Th1-type response and CTL activity.* Molecular Pharmaceutics, 2012. **9**(5): p. 1118-25.

33. Germain, R.N., *T-cell development and the CD4-CD8 lineage decision.* Nature Reviews Immunology, 2002. **2**(5): p. 309-322.

34. Mescher, M.F., et al., *Signals required for programming effector and memory development by CD8(+) T cells.* Immunological Reviews, 2006. **211**: p. 81-92.

35. Vesely, M.D., et al., *Natural Innate and Adaptive Immunity to Cancer*, in *Annual Review of Immunology, Vol 29*, W.E. Paul, D.R. Littman, and W.M. Yokoyama, Editors. 2011. p. 235-271.

36. Knutson, K.L. and M.L. Disis, *Tumor antigen-specific T helper cells in cancer immunity and immunotherapy.* Cancer Immunology Immunotherapy, 2005. **54**(8): p. 721-728.

37. Kennedy, R. and E. Celis, *Multiple roles for CD4(+) T cells in anti-tumor immune responses.* Immunological Reviews, 2008. **222**: p. 129-144.

38. Schoenberger, S.P., et al., *T-cell help for cytotoxic T lymphocytes is mediated by CD40-CD40L interactions.* Nature, 1998. **393**(6684): p. 480-483.

39. Vacchelli, E., et al., *Trial Watch Dendritic cell-based interventions for cancer therapy.* Oncoimmunology, 2013. **2**(10): p. 15.

40. Dillman, R.O., A.N. Cornforth, and G. Nistor, *Cancer stem cell antigen-based vaccines: the preferred strategy for active specific immunotherapy of metastatic melanoma?* Expert Opinion on Biological Therapy, 2013. **13**(5): p. 643-656.

41. Chapatte, L., et al., *Processing of tumor-associated antigen by the proteasomes of dendritic cells controls in vivo T-cell responses.* Cancer Research, 2006. **66**(10): p. 5461-5468.

42. Schwartzentruber, D.J., et al., *gp100 Peptide Vaccine and Interleukin-2 in Patients with Advanced Melanoma.* New England Journal of Medicine, 2011. **364**(22): p. 2119-2127.

43. Oshita, C., et al., *Dendritic cell-based vaccination in metastatic melanoma patients: Phase II clinical trial.* Oncology Reports, 2012. **28**(4): p. 1131-1138.

44. Schumacher, T.N. and R.D. Schreiber, *Neoantigens in cancer immunotherapy.* Science, 2015. **348**(6230): p. 69-74.

45. Gubin, M.M., et al., *Tumor neoantigens: building a framework for personalized cancer immunotherapy.* J Clin Invest, 2015. **125**(9): p. 3413-21.

46. Kreiter, S., et al., *Mutant MHC class II epitopes drive therapeutic immune responses to cancer.* Nature, 2015. **520**(7549): p. 692-6.

47. Ott, P.A., et al., *An immunogenic personal neoantigen vaccine for patients with melanoma.* Nature, 2017. **547**(7662): p. 217-+.

48. Sahin, U., et al., *Personalized RNA mutanome vaccines mobilize poly-specific therapeutic immunity against cancer.* Nature, 2017. **547**(7662): p. 222-+.

49. Kuai, R., et al., *Designer vaccine nanodiscs for personalized cancer immunotherapy.* Nature Materials, 2017. **16**(4): p. 489-+.

50. Coffman, R.L., A. Sher, and R.A. Seder, *Vaccine Adjuvants: Putting Innate Immunity to Work.* Immunity, 2010. **33**(4): p. 492-503.

51. Mount, A., et al., *Combination of adjuvants: the future of vaccine design.* Expert Review of Vaccines, 2013. **12**(7): p. 733-746.

52. Rosenfeld, M.R., et al., *A multi-institution phase II study of poly-ICLC and radiotherapy with concurrent and adjuvant temozolomide in adults with newly diagnosed glioblastoma(dagger).* Neuro-Oncology, 2010. **12**(10): p. 1071-1077.

53. Li, A.V., et al., *Generation of Effector Memory T Cell-Based Mucosal and Systemic Immunity with Pulmonary Nanoparticle Vaccination.* Science Translational Medicine, 2013. **5**(204).

54. Nakamura, T., et al., *Incorporation of polyinosine-polycytidylic acid enhances cytotoxic T cell activity and antitumor effects by octaarginine-modified liposomes encapsulating antigen, but not by octaarginine-modified antigen complex.* International Journal of Pharmaceutics, 2013. **441**(1-2): p. 476-81.

55. Hoebe, K., E. Janssen, and B. Beutler, *The interface between innate and adaptive immunity.* Nature Immunology, 2004. **5**(10): p. 971-974.

56. Moon, J.J., et al., *Interbilayer-crosslinked multilamellar vesicles as synthetic vaccines for potent humoral and cellular immune responses.* Nature Materials, 2011. **10**(3): p. 243-51.

57. Goldinger, S.M., et al., *Nano-particle vaccination combined with TLR-7 and -9 ligands triggers memory and effector CD8(+) T-cell responses in melanoma patients.* European Journal of Immunology, 2012. **42**(11): p. 3049-3061.

58. Narayan, R., et al., *Immunomodulation by Imiquimod in Patients with High-Risk Primary Melanoma.* Journal of Investigative Dermatology, 2012. **132**(1): p. 163-169.

59. Iwasaki, A. and R. Medzhitov, *Toll-like receptor control of the adaptive immune responses.* Nature Immunology, 2004. **5**(10): p. 987-995.

60. Speiser, D.E., et al., *Rapid and strong human CD8(+) T cell responses to vaccination with peptide, IFA, and CpG oligodeoxynucleotide 7909.* Journal of Clinical Investigation, 2005. **115**(3): p. 739-746.

61. Scheiermann, J. and D.M. Klinman, *Clinical evaluation of CpG oligonucleotides as adjuvants for vaccines targeting infectious diseases and cancer.* Vaccine, 2014. **32**(48): p. 6377-6389.

62. Whitmore, M.M., et al., *Synergistic activation of innate immunity by double-stranded RNA and CpG DNA promotes enhanced antitumor activity.* Cancer Research, 2004. **64**(16): p. 5850-5860.

63. Kantoff, P.W., et al., *Sipuleucel-T Immunotherapy for Castration-Resistant Prostate Cancer.* New England Journal of Medicine, 2010. **363**(5): p. 411-422.

64. Aranda, F., et al., *Trial Watch Peptide vaccines in cancer therapy.* Oncoimmunology, 2013. **2**(12).

65. Vacchelli, E., et al., *Trial Watch Toll-like receptor agonists for cancer therapy.* Oncoimmunology, 2013. **2**(8): p. 14.

66. Palucka, K. and J. Banchereau, *Cancer immunotherapy via dendritic cells.* Nature Reviews Cancer, 2012. **12**(4): p. 265-277.

67. Dillman, R.O., et al., *Phase II Trial of Dendritic Cells Loaded with Antigens from Self-Renewing, Proliferating Autologous Tumor Cells as Patient-Specific Antitumor Vaccines in Patients with Metastatic Melanoma: Final Report.* Cancer Biotherapy and Radiopharmaceuticals, 2009. **24**(3): p. 311-319.

68. Dillman, R.O., et al., *Tumor Stem Cell Antigens as Consolidative Active Specific Immunotherapy: A Randomized Phase II Trial of Dendritic Cells Versus Tumor Cells in Patients With Metastatic Melanoma.* Journal of Immunotherapy, 2012. **35**(8): p. 641-649.

69. Tel, J., et al., *Natural Human Plasmacytoid Dendritic Cells Induce Antigen-Specific T-Cell Responses in Melanoma Patients.* Cancer Research, 2013. **73**(3): p. 1063-1075.

70. Goozner, M., *Concerns About Provenge Simmer as CMS Ponders Coverage.* Journal of the National Cancer Institute, 2011. **103**(4): p. 288-289.

71. Prasad, S., et al., *Polymer nanoparticles containing tumor lysates as antigen delivery vehicles for dendritic cell-based antitumor immunotherapy.* Nanomedicine-Nanotechnology Biology and Medicine, 2011. **7**(1): p. 1-10.

72. Yoshikawa, T., et al., *Vaccine efficacy of fusogenic liposomes containing tumor cell-lysate against murine B16BL6 melanoma.* Biological & Pharmaceutical Bulletin, 2006. **29**(1): p. 100-104.

73. Mueller, M., et al., *Coencapsulation of tumor lysate and CpG-ODN in PLGA-microspheres enables successful immunotherapy of prostate carcinoma in TRAMP mice.* Journal of Controlled Release, 2012. **162**(1): p. 159-166.

74. Liu, S.Y., et al., *Nanoparticles-based multi-adjuvant whole cell tumor vaccine for cancer immunotherapy.* Biomaterials, 2013. **34**(33): p. 8291-8300.

75. Ali, O.A., et al., *Identification of immune factors regulating antitumor immunity using polymeric vaccines with multiple adjuvants.* Cancer Research, 2014. **74**(6): p. 1670-81.

76. Kamath, A.T., et al., *Synchronization of dendritic cell activation and antigen exposure is required for the induction of Th1/Th17 responses.* Journal of Immunology, 2012. **188**(10): p. 4828-37.

77. Zhuang, Y., et al., *PEGylated cationic liposomes robustly augment vaccine-induced immune responses: Role of lymphatic trafficking and biodistribution.* Journal of Controlled Release, 2012. **159**(1): p. 135-42.

78. Nakamura, T., et al., *The nanoparticulation by octaarginine-modified liposome improves alpha-galactosylceramide-mediated antitumor therapy via systemic administration.* Journal of Controlled Release, 2013. **171**(2): p. 216-24.

79. Badiee, A., et al., *The role of liposome size on the type of immune response induced in BALB/c mice against leishmaniasis: rgp63 as a model antigen.* Experimental Parasitology, 2012. **132**(4): p. 403-9.

80. Demento, S.L., et al., *Role of sustained antigen release from nanoparticle vaccines in shaping the T cell memory phenotype.* Biomaterials, 2012. **33**(19): p. 4957-64.

81. Jiang, H., Q. Wang, and X. Sun, *Lymph node targeting strategies to improve vaccination efficacy.* Journal of Controlled Release, 2017. **267**: p. 47-56.

82. Trumpfheller, C., et al., *Dendritic cell-targeted protein vaccines: a novel approach to induce T-cell immunity.* Journal of Internal Medicine, 2012. **271**(2): p. 183-192.

83. Torchilin, V.P., *Recent advances with liposomes as pharmaceutical carriers.* Nature Reviews Drug Discovery, 2005. **4**(2): p. 145-160.

84. van Niel, G., G. D'Angelo, and G. Raposo, *Shedding light on the cell biology of extracellular vesicles.* Nat Rev Mol Cell Biol, 2018.

85. Pucci, F. and M.J. Pittet, *Molecular pathways: tumor-derived microvesicles and their interactions with immune cells in vivo.* Clin Cancer Res, 2013. **19**(10): p. 2598-604.

86. Wei, X., et al., *Nanoparticle Functionalization with Platelet Membrane Enables Multifactored Biological Targeting and Detection of Atherosclerosis.* ACS Nano, 2018. **12**(1): p. 109-116.

87. Zhang, X., et al., *Remote Loading of Small-Molecule Therapeutics into Cholesterol-Enriched Cell-Membrane-Derived Vesicles.* Angew Chem Int Ed Engl, 2017. **56**(45): p. 14075-14079.

88. Tang, J., et al., *Therapeutic microparticles functionalized with biomimetic cardiac stem cell membranes and secretome.* Nat Commun, 2017. **8**: p. 13724.

89. Cheung, A.S., et al., *Adjuvant-Loaded Subcellular Vesicles Derived From Disrupted Cancer Cells for Cancer Vaccination.* Small, 2016. **12**(17): p. 2321-2333.

90. Kroll, A.V., et al., *Nanoparticulate Delivery of Cancer Cell Membrane Elicits Multiantigenic Antitumor Immunity.* Advanced Materials, 2017. **29**(47).

91. Desai, K.G.H. and S.P. Schwendeman, *Active self-healing encapsulation of vaccine antigens in PLGA microspheres.* Journal of Controlled Release, 2013. **165**(1): p. 62-74.

92. Alexandrov, L.B., et al., *Signatures of mutational processes in human cancer.* Nature, 2013. **500**(7463): p. 415-21.

Chapter 2: PEGylated Cancer Cell Membranes for Elicitation of Anti-tumor Cytotoxic T Lymphocyte Responses

2.1 Abstract

Immunotherapy has become a very promising approach against cancer with the clinical approval of immune checkpoint blockade, while vaccination efforts have led to improved anti-tumor responses in clinical trials. In this study, we sought to establish an autologous cancer vaccine utilizing tumor cells for development of antigen and adjuvant delivery vehicle. Cell membranes can be harvested from tissue-culture grown cancer cells, PEGylated. and formed into nano-sized vesicles (PEG-NPs) allowing for enhanced stability and improved draining efficiency to the local lymph nodes. We demonstrate the advantages of this formulation in eliciting 3.7-fold greater cytotoxic T lymphocyte responses against model antigen, OVA, compared to standard freeze-thawed lysates in a therapeutic vaccination against B16F10 OVA melanoma, leading to decreased tumor growth. Importantly, in combination with αPD-1 therapy, PEG-NPs led to 4.2-fold improved T cell responses, decreased tumor growth, and complete tumor regression in 63% of mice, which were further protected from a subsequent tumor rechallenge. These results support previous effort demonstrating that cancer cell membranes can be used as a vaccination platform and elicit strong anti-tumor responses.

2.2 Introduction

Cancer is a continually increasing concern facing the aging population and the rising incidence of melanoma of the skin leads to nearly 100,000 new cases and over 9,000 deaths per year in the US [1]. The immunotherapy breakthroughs over the past decade have recognized the previously suggested role of the immune system in fighting cancer, leading to the clinical approval of checkpoint blockade inhibitors including αCTLA4 and αPD-1 antibodies [2-6]. While tumor regression and complete cures have been seen with these approaches in many patients, the limited response rate to immune checkpoint blockade demonstrate the need for new approaches [7].

One of the drawbacks of PD-1 targeting is the reliance on patients' endogenous tumor-specific cytotoxic T lymphocyte (CTL) responses, which may be low or absent [8]. Therapeutic vaccination may address this issue by eliciting CTL responses, but current cancer vaccine approaches require identification and manufacturing of tumor antigens [9, 10]. Specifically, following tumor exome sequencing, promising peptide-based neo-antigen vaccines can deliver large doses of immunogenic epitopes resulting in strong and durable levels of responses [11, 12]. In comparison tumor cell lysates, containing complete library of self- and tumor-associated antigens, are readily available for processing and vaccine generation without the need for sequencing or peptide synthesis [13]. However, the use of lysates remains challenging because of the limited antigen dose, which can be realistically obtained, thus potent formulations containing strong immunostimulatory adjuvants must be prepared.

In the past, tumor cell lysates have been utilized by incorporation into nanoparticle preparations or administration as *ex vivo* generated dendritic cell-based vaccines, but their efficacy has been quite limited [14-17]. Recently, advances in plasma membrane utilization and

preparation technology yielded impressive results demonstrating *in vivo* stability and targeting [18-20], all the while exosomes and plasma membrane microvesicles were being identified as signaling messengers capable of carrying variety of cargos [21-23]. As a result, reports have shown that membrane vesicles formulated with adjuvants can be used effectively for eliciting immune responses against melanoma, although the therapeutic outcomes have been limited [24, 25].

In this study, we demonstrate a simple method for generation of nano-sized membrane vesicles from B16F10 OVA melanoma cell lysates, which can elicit strong tumor antigen-specific CTL responses (**Fig. 2-1**). Introduction of surface polyethylene glycol layer generates monodisperse vesicles (PEG-NPs), enhancing their stability and promoting trafficking to the local lymph nodes, compared to the traditionally prepared freeze-thawed (FT) lysates or purified plasma membranes. These characteristics led to generation of strong OVA-specific T cell responses demonstrating greater anti-tumor protection in a prophylactic immunization. Additionally, therapeutic immunization with PEG-NPs aimed at combating established tumors led to markedly enhanced T cell responses and decreased tumor growth. Combinatory approach utilizing αPD-1 antibody therapy with PEG-NPs vaccination led to complete tumor regression in 63% of animals and established protective immunity against future tumor re-challenge. These data demonstrate that PEGylated tumor cell membranes can serve as a potent cancer vaccine platform with strong anti-tumor efficacy.

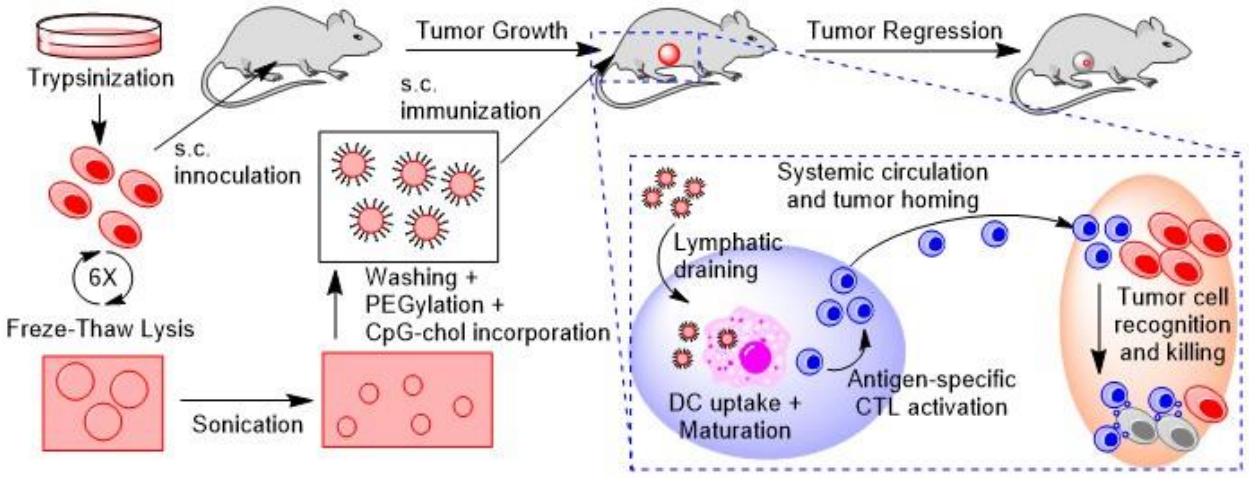

Figure 2-1. Schematic representation of PEG-NPs preparation and therapy.
B16F10 OVA cells are harvested from cell culture plates and used for s.c. inoculation of the tumor in the flank for C57BL/6 mice. Cells are also lysed through freeze-thaw cycling and sonicated to form nano-sized vesicles, aggregated with calcium, and the cytosolic fraction is washed away. PEGylation, removal of calcium with EDTA, and further wash steps are then performed. Finally, cholesterol-linked CpG is incorporated and the vaccine is administered subcutaneously at the tail base. PEG-NPs drain efficiently to the lymph nodes where they are taken up by DCs in order to activate antigen-specific cells, which enter the systemic circulation and home to the tumor. Once there, CTLs can recognize the antigen on tumor surface and kill cancer cells leading to tumor regression.

2.3 Materials and Methods

Cell culture

B16F10 OVA cells, expressing exogenous model antigen ovalbumin with a transmembrane domain, were grown in RPMI 1640 media supplemented with 10% FBS, 100 U/mL penicillin, and 100 μg/ml streptomycin. B16F10 OVA cells were kindly provided by the lab of Dr. Darrel Irvine (Massachusetts Institute of Technology; Cambridge, MA). Bone marrow-derived dendritic cells (BMDCs) were cultured as previously described [26]. Briefly, tibiae and femurs of C57BL/6 mice (Envigo) were harvested and the bone marrow extracted by flushing media through the bones using syringe equipped with a 26 gauge needle. Cells were

passed through a 40 μm strainer to remove debris, washed, and plated. Complete media (RPMI supplemented on 10% FBS, 100 U/mL penicillin, 100 μg/ml streptomycin, 50 μM β-mercaptoethanol, and 20 ng/ml GM-CSF) was supplemented on day 3 and refreshed on days 6, 8, and 10. BMDCs were used on days 8-12 from the suspended and loosely-adhered cell population.

Lysate preparation

Tissue culture-grown B16F10 OVA cells were trypsinized and washed three times with PBS. Cells were resuspended at 1 x 10^8 cells/ml and lysed by freeze-thaw cycling (10 minutes in liquid nitrogen and 10 minutes in 37°C water bath; 6 cycles total). Low-speed centrifugation (100 x g, 10 minutes) was used to remove large debris and generate the Freeze-Thaw (FT) lysates from supernatant. Sonicated lysates were obtained by probe-tip sonicating FT lysates for 2 minutes on ice using 50% intensity setting (QSonica, 125 W/20 kHz sonicator) and collecting the supernatant after centrifugation (10,000 x g, 10 minutes). Cytosol and membrane fractions were generated by ultracentrifugation (200,000 x g; 1 hour) of sonicated lysates and collecting the supernatant and pellet, respectively.

Nanoparticle preparation

To generate PEGylated nanoparticles (PEG-NPs), we first aggregated the membrane fraction of cell lysates by adding 20 mM $CaCl_2$ to sonicated cell lysates (6 mg/ml) in PBS, followed by incubation at 37°C for 1 hour. Particles were washed two times with PBS via centrifugation (20,000 x g; 5 minutes) and resuspended in PBS containing 100 mM EDTA and 10 mg/ml Methoxy-Poly (Ethylene Glycol) - 1, 2-Distearoyl-sn-Glycero-3-

Phosphoethanolamine-N (DSPE-PEG, 5 kDa average molecular weight; Laysan Bio, Inc.). Aggregates were fully dispersed by water-bath sonication (approx. 1 minute for 100 µl solution) and further incubated for 1 hour at 37°C to allow post-insertion of DSPE-PEG. The resulting PEG-NPs were purified by passing through Zeba desalting column (7K molecular weight cut-off, Thermo Fisher Scientific).

Lysate and nanoparticle characterization

Sample concentrations for all assays were standardized by total protein content as measured by MicroBCA Assay Kit (Thermo Scientific). SDS-PAGE was performed, followed by gel staining with Coomassie or transfer to a PVDF membrane for Western Blotting using antibodies against gp100 (Abcam), TRP2 (Santa Cruz), or ovalbumin (Abcam). Transmission electron microscopy images were obtained using JEOL 1400-plus microscope (JOEL USA) following sodium phosphotungstate negative staining. Particle size and zeta potential were measured and analyzed using dynamic light scattering (DLS, Malvern Zetasizer Nano Range) in PBS or ultrapure water, respectively. For stability studies, samples were incubated with PBS or 10% FBS in PBS at 4°C (long term) or at 37°C while shaking (short term) as indicated in the figures.

Protein uptake by dendritic cells

In order to obtain fluorescently labeled lysate, trypsinized B16F10 OVA cells (2 million cells/ml) were incubated with 1 µM Oregon Green 488 carboxylic acid, succinimidyl ester (OG488, Thermo Fisher Scientific) in RPMI at 37°C for 10 minutes. Lysate was prepared as described above and then incubated with BMDCs for 24 hours. Cells were then washed,

trypsinized, and resuspended in FACS buffer (1% BSA in PBS) containing anti-CD16/32 blocking antibodies. Cell were stained with CD11c antibody, washed, and analyzed via flow cytometry for OG488 signal.

T cell expansion

In vitro T cell expansion was examined by pulsing BMDCs (50,000 cells per well) overnight with lysate fractions or PEG-NPs at 1 mg/ml in 96-well plates. As indicated, 5 μg/ml CpG (IDT) or 1 μg/ml MPLA (Avanti Polar Lipids) were used as adjuvants. BMDCs were washed three time with PBS and CFSE-labeled T cells were added. First, OT-I transgenic $CD8^+$ T cells were purified from spleens using a negative selection kit (Stemcell Technologies). T cells were labeled with CFSE (1 μM concentration, 2 million cells/ml, 10 minutes in RPMI), washed, added to BMDC-containing wells, and allowed to expand for three days. Then, cells were collected by pipetting, blocked with FACS buffer containing anti-CD16/32 blocking antibodies, stained with anti-CD8α antibody, washed, and analyzed via flow cytometry for the dilution of the CFSE signal and count of surviving live T cells ($DAPI^-/CD8\alpha^+$). Proliferation Index was calculated using Proliferation Platform in FlowJo.

Lymph node draining

B16F10 OVA cell membranes were labeled with lipophilic DiD dye (1,1'-Dioctadecyl-3,3,3',3'-Tetramethylindodicarbocyanine) by incubating 5 million cells/ml at 37°C for 10 minutes with 1 μg/ml DiD. Cells were washed three times with PBS to remove any unincorporated dye and processed into fractions and NPs as described above. Labeled formulations were normalized by DiD fluorescence and administered subcutaneously at the tail base of C57BL/6 mice (n = 4).

Two days post-injection, animals were euthanized, inguinal lymph nodes harvested, and imaged using *In Vivo* Imaging System (IVIS) to assess radiance efficiency. Then, lymph nodes were processed into single cell suspensions using a 40 μm cell strainer, washed, and blocked with FACS buffer containing anti-CD16/32 blocking antibodies. Next, we stained the cells for markers of macrophages (anti-F4/80 antibody) and DCs (anti-CD11c antibody), washed the cells, and analyzed with flow cytometry.

Animal experiments

All immunizations and tumor studies were performed according to the federal, state, and local guidelines. All work performed on animals was in accordance with and approved by University Committee on Use and Care of Animals (UCUCA) at University of Michigan, Ann Arbor. For all immunizations, cholesterol-modified CpG (IDT) was incubated with vaccine formulations at 37°C for 30 minutes prior to administration. For the prophylactic vaccination studies, 6-8 weeks old, female C57BL/6 mice were immunized subcutaneously at the tail base with 1 mg of total protein and 15 μg of CpG on days 0 and 14, followed by a challenge with 1 x 10^6 B16F10 OVA cells at s.c. flank on day 35. For the therapeutic vaccination studies, 6-8 weeks old, female C57BL/6 mice were inoculated with 2 x 10^5 B16F10 OVA cells at s.c. flank on day 0, and immunized with vaccine formulations (1 mg of total protein and 15 μg of CpG) on days 5 and 12 with or without co-administration of anti-PD-1 IgG (i.p.; 100 μg per mouse per injection) on days 6, 9, 13, and 16. Tumor size was measured every other day and the volume determined using the following formula: length x width x width x 0.50.

Tetramer staining

Cytotoxic T lymphocyte responses were analyzed by tetramer staining one week after each immunization as described before [27]. Briefly, 150 µl of blood was collected and red blood cells were removed with ACK lysis buffer. Washed PBMCs were blocked with FACS buffer containing anti-CD16/32 blocking antibodies and stained with H-2Kb OVA Tetramer-SIINFEKL-PE (MBL International), followed by staining with anti-CD8 antibody. Cells were washed, dead cells were labeled with DAPI, and the final suspension analyzed by flow cytometry.

Statistical analyses

For animal studies, mice were randomized to match similar average volume of the primary tumors, and all procedures were performed in a non-blinded fashion. Statistical analysis was performed with Prism 6.0 software (GraphPad Software) by an unpaired student's t-test and one-way or two-way ANOVA with Tukey's comparisons post-test, as indicated. Statistical significance for survival curve was calculated by the log-rank test. Statistical significance is indicated as *$P < 0.05$, **$P < 0.01$, ***$P < 0.001$, and ****$P < 0.0001$.

2.4 Results and Discussion

Characterization of tumor cell lysate

In this study, we aimed to use tumor cell lysate to generate adaptive anti-tumor immune responses, and we have utilized B16F10 OVA murine melanoma cells expressing the model antigen ovalbumin (OVA) on their plasma membrane. We generated sonicated cell lysate by freeze-thaw cycles, followed by probe-tip sonication and centrifugation to remove large debris.

Examination of cell lysate under transmission electron microscopy (TEM) demonstrated the presence of nano-sized vesicles (**Fig. 2-2A**), which we suspected to be self-assembled remnants of the plasma membrane. Membrane fraction was separated via ultracentrifugation and demonstrated to contain various proteins as shown by gel electrophoresis, followed by Coomassie staining (**Fig. 2-2B**). We performed Western blotting to test for the retention of various tumor-associated antigens in the membrane fraction. Proteins with transmembrane domain, such as endogenous glycoprotein 100 (gp100) and tyrosine-related protein 2 (TRP2) [28, 29], along with the model antigen OVA (with a transmembrane domain in our B16F10 OVA cell line) were detected in varying levels in either the whole cell lysate or the membrane fraction (lane 1 and 2, respectively. **Fig. 2-2B**).

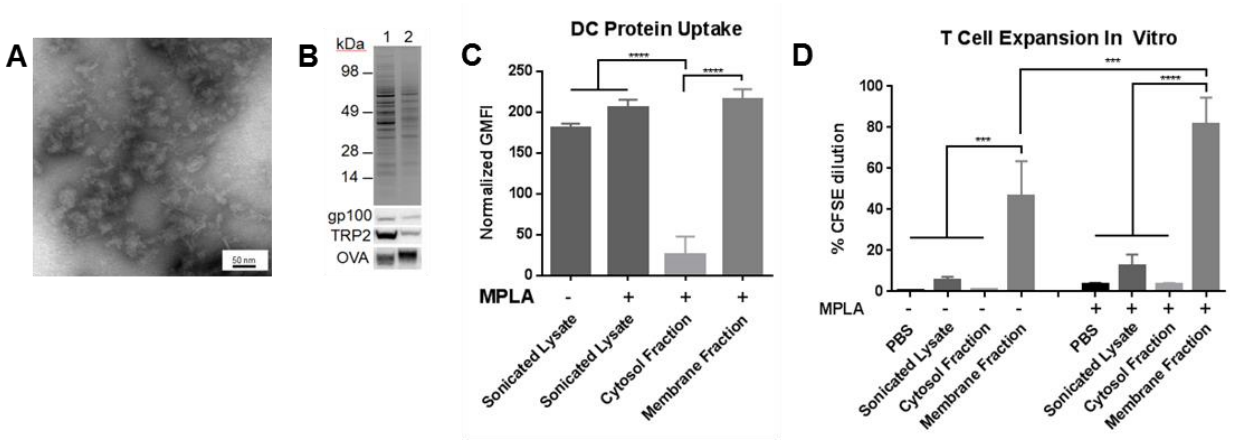

Figure 2-2. Characterization of membrane fraction of cell lysates.
A. TEM image of cell lysates show nano-sized membrane structures. B. Wide protein repertoire from whole cell lysate (lane 1) is retained within the membrane fraction (lane 2) as seen via coomassie staining (top panel). Tumor-associated antigens (gp100 and TRP2) and model antigen (OVA) incorporation was determined by Western Blot analysis (bottom three panels). C. Fluorescently-labeled lysates, cytosol fraction, and membrane fraction were pulsed to dendritic cells and the relative protein uptake analyzed by flow cytometry. D. Dendritic cells were pulsed with lysate fractions with or without MPLA and co-cultured with OT-I OVA-specific T cells. T cell proliferation was measured by the dilution of CFSE dye via flow cytometry. Mean ± SD are shown. Statistical analysis was performed using one-way ANOVA comparison with Tukey's multiple comparison test (*** = $p < 0.001$, **** = $p < 0.0001$).

When incubated with bone-marrow derived dendritic cells (BMDCs) *in vitro*, membrane-associated proteins were preferentially taken up by DCs ($P < 0.0001$, **Fig. 2-2C**), in contrast to inefficient uptake of cytosolic proteins by DCs, suggesting that proteins associated with membrane vesicles have increased interactions with antigen-presenting cells (APCs), leading to enhanced phagocytosis of cellular proteins. We hypothesized that this enhanced uptake and eventual presentation of antigens in the context of major histocompatibility complex-I (MHC-I) would result in activation of antigen-specific cytotoxic T lymphocytes (CTLs). To test this, we isolated OVA-specific CD8α+ T cells from OT-I transgenic mice, co-cultured them with lysate-pulsed BMDCs, and examined proliferation of OT-I CD8α+ T cells. Cell membrane fraction, characterized by enhanced DC uptake and high antigen content, led to significantly increased T cell expansion *in vitro* ($P < 0.001$, **Fig. 2-2D**), compared with the cytosolic or whole lysate fractions. Furthermore, as immunostimulatory agents induce strong T-cell activation and proliferation, we added monophosphoryl lipid A (MPLA), a Toll-like receptor (TLR) 4 agonist. Similar trend of T cell expansion was observed after addition of MPLA, with the membrane fraction containing MPLA generating the greatest extent of CD8α+ T cell proliferation among all the groups ($P < 0.001$, **Fig. 2-2D**). These results showed that the membrane fraction of cell lysate contained vesicular nanostructures with tumor-associated antigens and that DCs pulsed with these membrane vesicles cross-primed antigen-specific CD8α+ T cell responses *in vitro*.

Preparation and characterization of PEG-NPs

Having shown induction of CD8α+ T cells with membrane vesicles *in vitro*, we sought to further characterize them along the preparation procedure and improve their overall stability for the subsequent vaccination studies *in vivo* (see below). When B16F10 OVA cells were

harvested and cycled between liquid nitrogen and 37°C water bath, followed by low speed centrifugation, the resulting supernatant contained large, poly-disperse structures, which we termed freeze-thawed (FT) lysate. Analyses with dynamic light scattering indicated that FT lysate contained vesicles with 610 ± 60 nm hydrodynamic diameter, the polydispersity index (PDI) of 0.67 ± 0.12, and zeta potential of -30 mV ± 1 mV (**Fig. 2-3A**). Further probe-tip sonication and removal of large debris via high speed centrifugation yielded smaller and

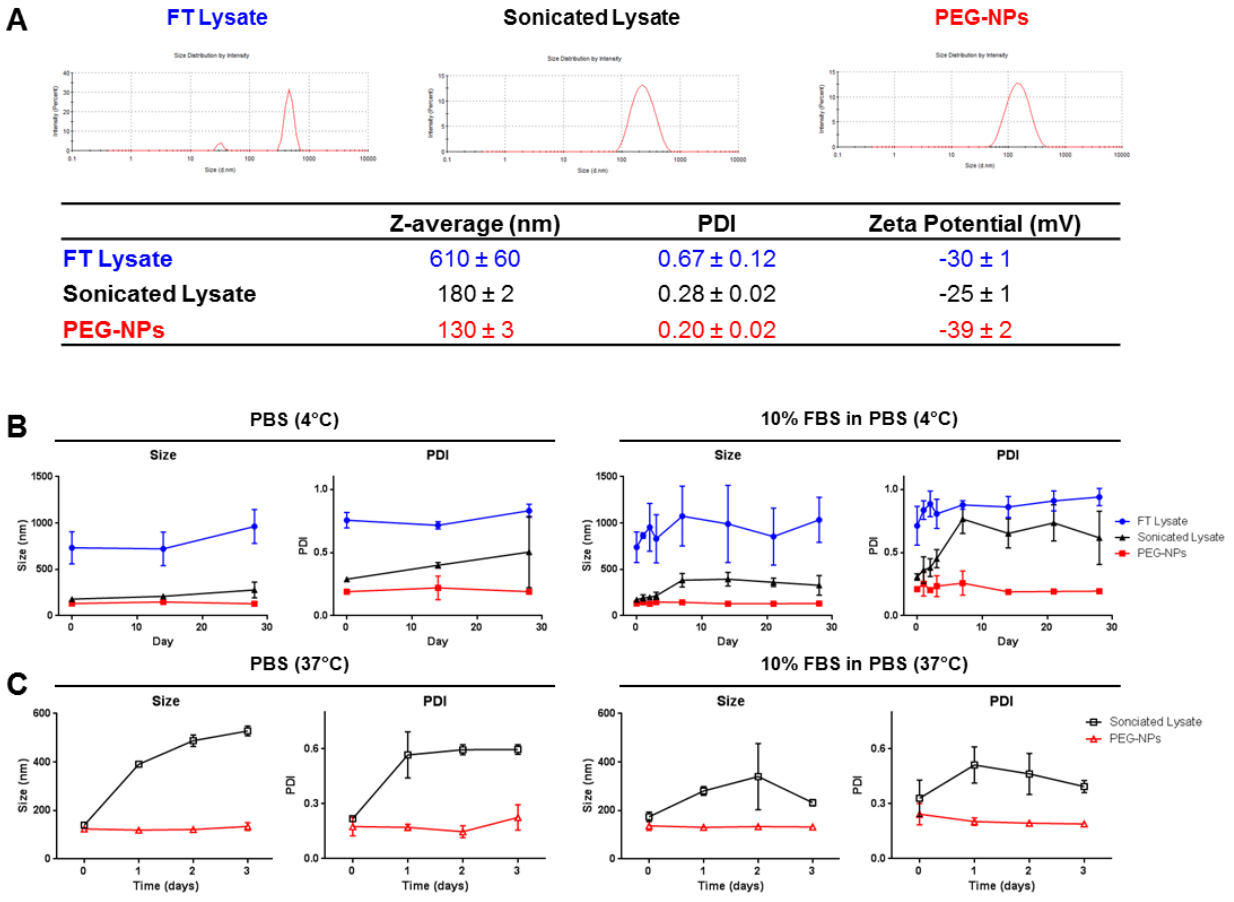

	Z-average (nm)	PDI	Zeta Potential (mV)
FT Lysate	610 ± 60	0.67 ± 0.12	-30 ± 1
Sonicated Lysate	180 ± 2	0.28 ± 0.02	-25 ± 1
PEG-NPs	130 ± 3	0.20 ± 0.02	-39 ± 2

Figure 2-3. Characterization PEG-NPs.
A. Particle size, PDI, and zeta potential were determined by dynamic light scattering analysis. B. Particles were incubated over a period of four weeks in PBS or 10%/90% FBS/PBS at 4°C. Stability was assessed by determining particle sizes and PDIs within that duration. C. Particles were incubated over a period of three days in PBS or 10%/90% FBS/PBS at 37°C. Aggregation was assessed by determining particle sizes and PDIs within the timeframe and mean ± SD are shown.

monodisperse membrane vesicles with 180 ± 2 nm hydrodynamic diameter, PDI of 0.28 ± 0.02, and zeta potential of -25 mV ± 1 mV (**Fig. 2-3A**).

We examined the stability of FT lysate stored at 4°C in PBS or 10% FBS-containing PBS over time. Our data indicated that FT lysate increased in size from 610 nm to approximately 1 micron in both conditions with the PDI values increasing beyond 0.70 (**Fig. 2-3B**). Endogenous nano-vesicles present in the sonicated lysate preparation (without PEGylation) also aggregated over the four-week period in PBS increasing in size from 180 nm to 280 nm and becoming more polydisperse (PDI > 0.5) (**Fig. 2-3B**). Instability of endogenous nano-vesicles was exacerbated in the presence of 10% FBS, causing sonicated lysate to aggregate within just one week (**Fig. 2-3B**).

To address potential aggregation of native cellular membrane vesicles and to promote draining of these vesicles to local lymph nodes (LNs) upon s.c. administration *in vivo*, we have introduced a polyethylene glycol (PEG) layer on these cell membrane vesicles (**Fig 2-1**). First, sonicated lysate containing membrane vesicles was incubated at 37°C with calcium to promote membrane fusion and aggregation, which allowed for facile collection of membrane vesicles via simple table-top centrifugation. Washed particles were then mildly sonicated together in the presence of lipid-conjugated PEG (DSPE-PEG) and EDTA to chelate any remaining calcium. Upon desalting column purification, the resulting PEGylated cell membrane particles (PEG-NPs) exhibited 130 ± 3 nm hydrodynamic diameter, PDI of 0.20 ± 0.02, and zeta potential of -39 mV ± 2 mV (**Fig. 2-3A**).

In sharp contrast to the gradual aggregation of endogenous membrane vesicles during long-term storage as shown above (**Fig. 2-3B**), the size of PEG-NPs stored at 4°C in PBS or 10% FBS-containing PBS was maintained stably at ~130 nm with the PDI remaining below 0.25 for

the course of four week study. Importantly, when we increased the storage temperature to 37°C to better simulate *in vivo* conditions, we observed even bigger differences. Endogenous sonicated nano-vesicles (without PEGylation) rapidly aggregated within 1 day at 37°C in either PBS or 10% FBS-PBS, whereas PEG-NPs maintained their size and monodispersity for at least 3 days (**Fig. 2-3C**). Overall, PEG-NPs outperformed the other lysate preparations during the simulated stability testing as shown by complete lack of aggregation. These results suggested that PEG-NPs may drain efficiently to local LNs following administration, whereas other lysate formulations may aggregate *in vivo*, potentially limiting their draining to LNs upon s.c. administration.

In vitro T cell activation

We next tested the impact of various cell lysate formulations on cross-presentation of antigens by DCs and cross-priming of antigen-specific T cells *in vitro*. We pulsed BMDCs with lysate formulations for 1 day and performed T cell expansion assay with OT-I CD8α+ T cells, using media and OT-I peptide (sequence = SIINFEKL) as negative and positive controls, respectively. Overall, stimulation of DCs with CpG, a potent TLR9 agonist composed of a single stranded DNA containing unmethylated CG motifs, was more effective at expansion of OT-I CD8α+ T cells, compared with the use of MPLA (**Fig. 2-4**). Based on these results, we chose to use CpG as the adjuvant for the remainder of our experiments.

BMDCs pulsed with PEG-NPs effectively induced T cell activation and proliferation, as evidenced by extensive dilution of the CFSE dye within the surviving T cells (**Fig. 2-5A,B**). CFSE dilution induced by the PEG-NPs *in vitro* was on par with the membrane fraction but more effective than that induced by FT lysate ($P < 0.0001$, **Fig. 2-5A,B**). The proliferation index,

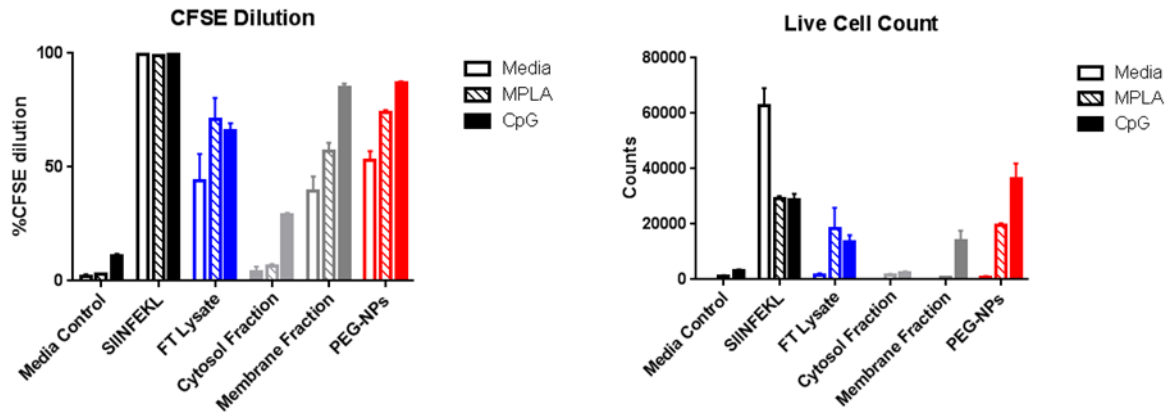

Figure 2-4. CFSE dilution assay.
Dendritic cells were pulsed with controls and lysate formulations overnight and then co-cultured with CFSE-labeled OT-I T cells for three days. Average percentage of proliferated T cells after three days of culture are represented by percentage of cells with diluted CFSE fluorescence. Relative count of live T cells was examined within the CD8α+ population. Mean ± SD are shown.

which reports the average number of divisions that proliferating cells undergo [30], was significantly higher for the PEG-NP group, compared with FT lysate, cytosolic or membrane fractions ($P < 0.001$, **Fig. 2-5C**). Additionally, we have examined the overall number of T cells at the end of experiments, as these data provide context to the CFSE dilution results. The number of live T cells remaining at the end of 3 day co-culture period was at least two-fold greater for the PEG-NP group, compared with the FT lysate or the membrane fraction group ($P < 0.001$, **Fig. 2-5D**). Notably, the PEG-NPs treatment sustained comparable number of live T cells as the SIINFEKL positive control group (**Fig. 2-5D**), indicating strong induction and maintenance of T-cell proliferation supported by the PEG-NPs. Taken together, these results suggest that the PEG-NPs are taken up and processed effectively by DCs, leading to potent cross-priming of antigen-specific CD8α+ T cells.

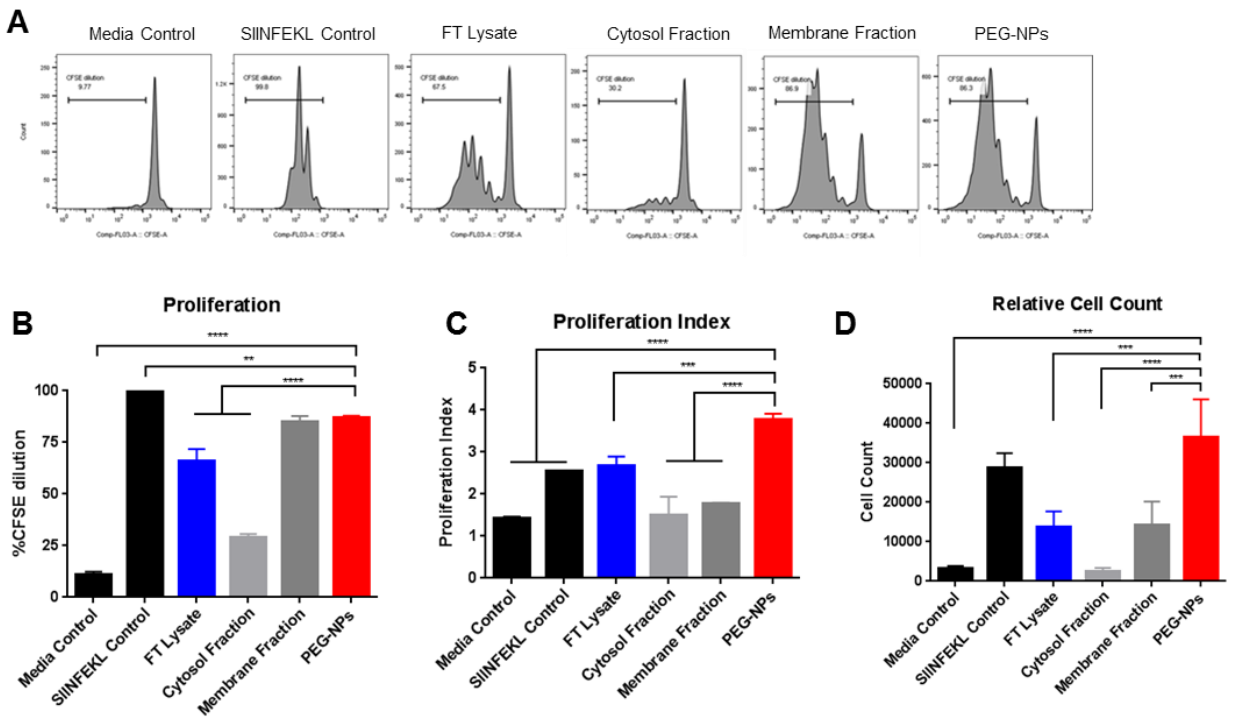

Figure 2-5. T cell expansion *in vitro*.
Dendritic cells were pulsed with controls and lysate formulations overnight and then co-cultured with CFSE-labeled OT-I T cells for three days. A. Representative FACS histograms demonstrating CFSE dilution within proliferating OT-I T cells are shown. B. Average percentage of proliferated T cells after three days of culture are represented by percentage of cells with diluted CFSE fluorescence. C. Proliferation index was determined by FlowJo analysis software. D. Relative count of live T cells was examined within the CD8α+ population. Mean ± SD are shown. Statistical analysis was performed using one-way ANOVA comparison with Tukey's multiple comparison test (** = p< 0.01, *** = p < 0.001, **** = p < 0.0001).

Lymph node draining

PEGylation generally provides an advantage for subcutaneous (s.c.) administration of nano-formulations, by drastically reducing interactions between the formulation and cells or serum proteins, thus promoting their trafficking to draining lymph nodes (dLNs) [31]. To determine the level of particle localization in dLNs at the whole tissue and cellular levels, lysate formulations were labeled with DiD, a lipophilic dye, and administered s.c. at the tail base. After

two days, inguinal dLNs were extracted, and the relative draining efficiency was assessed via whole LN imagining and flow cytometry. PEG-NPs exhibited significantly increased trafficking to dLNs, compared with the membrane fraction ($P < 0.01$, **Fig. 2-6A**). We have also examined subset of APCs that are responsible for lysate uptake. PEG-NPs were efficiently taken up by F4/80+ macrophages as well as DCs (**Fig. 2-6B**). These results demonstrated the ability of PEG-NPs to drain efficiently to dLNs and localize within APCs for potential antigen processing and presentation.

In vivo T cell activation and protective immunization

Next, we performed immunization studies *in vivo* to examine T cell responses induced by FT lysate and PEG-NPs. We immunized C57BL/6 mice on days 0 and 14 with FT lysate or PEG-NPs containing 1 mg of total protein and 15 μg of CpG per mouse (**Fig. 2-6C**). On day 7, 1 week post-prime, we examined peripheral blood mononuclear cells (PBMCs) for OVA-specific CD8α+ T cell responses via tetramer staining. We observed that immunization with PEG-NPs increased the frequency of OVA-specific CD8α+ T cells by 5-fold, compared with FT lysate group although this difference was not statistically significant ($P = 0.25$, **Fig. 2-6D**). We then examined the efficacy of vaccine formulations to induce protective immune responses against tumor challenge. Pre-immunized mice were inoculated at s.c. flank with 10^6 B16F10 OVA cells (10-fold more cells than necessary to establish tumors in naïve animals) (**Fig. 2-6C**). Mice vaccinated with FT lysate exhibited the median survival time of 42 days, compared with 17 days in the PBS control group (**Fig. 2-6E**). Importantly, vaccination with PEG-NPs significantly extended the median survival time to 55 days ($P < 0.01$ versus PBS or FT lysate, **Fig. 2-6E**), and

50% of the animals remained completely free of tumor for at least 80 days, demonstrating the potency of PEG-NPs to elicit protective immune responses against tumor cells.

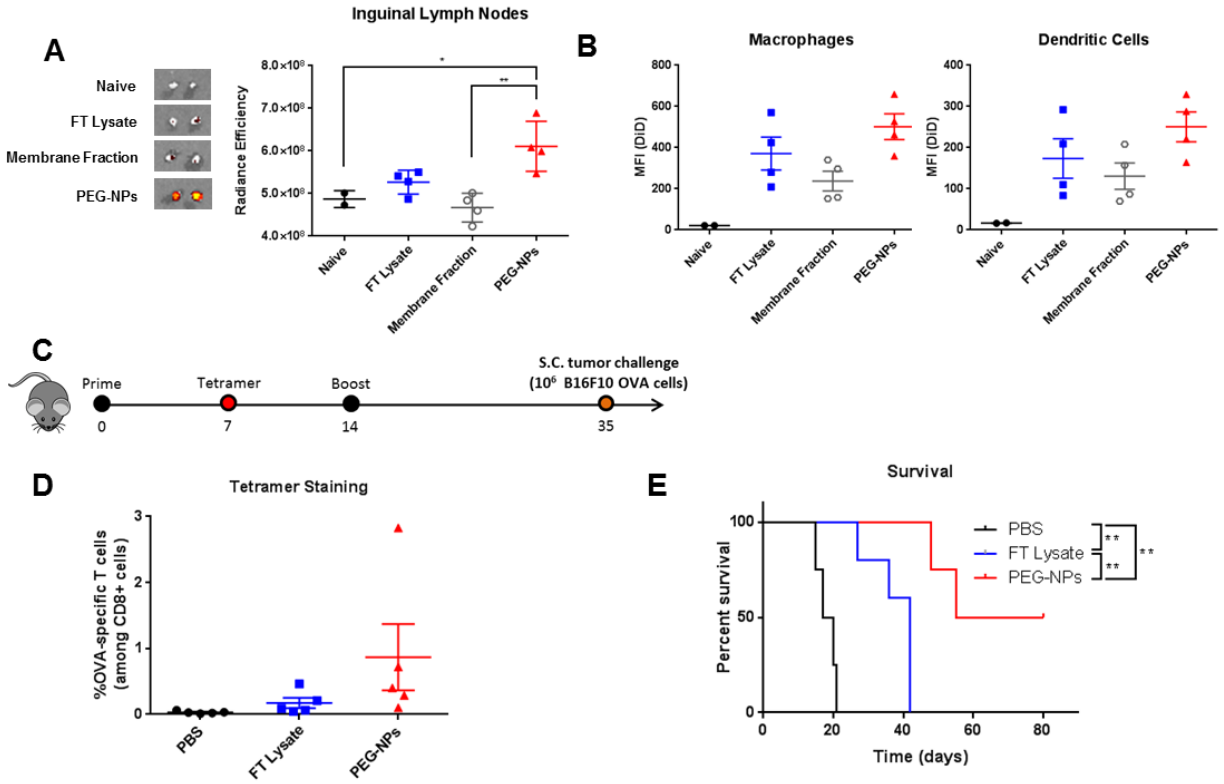

Figure 2-6. *In vivo* lymph node draining and prophylactic immunization.
Cell lysate formulations were labeled with DiD fluorescent lipophilic dye and administered subcutaneously at the tail base. A. Whole lymph node imaging is shown along with analysis of the radiance efficiency measured by IVIS two days after injection. B. Harvested lymph nodes were dissociated into single cell suspension and analyzed for DiD uptake by macrophages and dendritic cells via flow cytometry. C. Mice were immunized twice on day 0 and 14 followed by administration of ten-fold more cells than necessary to ensure tumor engraftment in immunized animals. D. OVA-specific $CD8^+$ T cell population among PBMCs was determined via tetramer staining. E. Overall survival following s.c. tumor challenge on day 35 is shown. Mean ± SEM values are shown. Statistical analysis was performed using (A) one-way ANOVA comparison with Tukey's multiple comparison test; and (E) Log-rank (Mentel-Cox) test (* = $p < 0.05$, ** = $p < 0.01$).

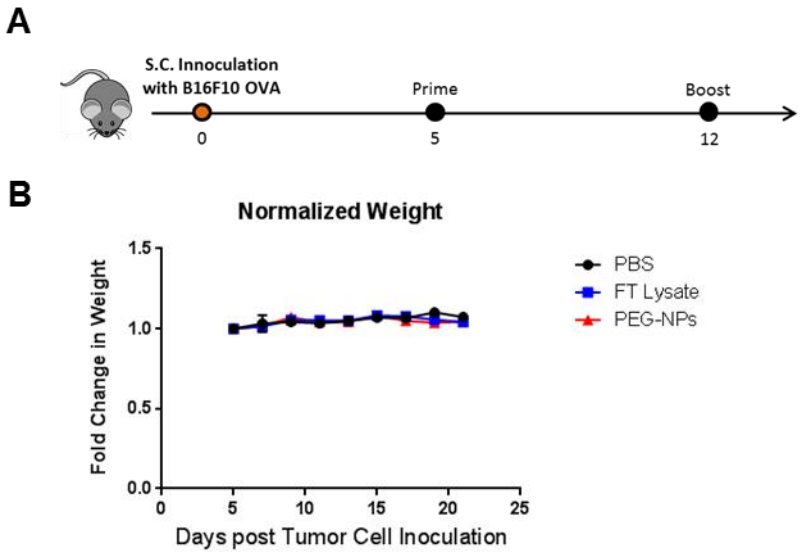

Figure 2-7. Safety of PEG-NPs.
A Mice were inoculated with B16F10 OVA on day 0 and immunized twice on days 5 and 12. B. Weight of the animals was recorder starting on the day of first immunization and mean ± SEM fold change is shown for each group.

Therapeutic immunization

B16F10 OVA tumors were established via s.c. injection of 2 x 10^5 tumor cells on the right flank, and when the tumors were palpable on day 5, we vaccinated animals with either FT lysate or PEG-NPs on days 5 and 12 (**Fig. 2-8A**). Throughout the study, we observed no changes in animal health following administration of our vaccines, as demonstrated by normal behavior and maintained body weight (**Fig. 2-7**). Vaccination with FT lysate slowed the tumor growth, compared with the PBS control ($P < 0.0001$ for days 19 and 21, **Fig. 2-8B,C**). Importantly, PEG-NPs treatment exerted significantly enhanced anti-tumor efficacy, further decreasing tumor growth compared with the FT lysate group ($P < 0.001$ for day 21) (**Fig. 2-8B,C**). Importantly, the PEG-NPs treatment elicited robust antigen-specific CD8α+ T cell responses on day 12, characterized by 7.4-fold and 3.7-fold increases in the frequency of OVA-specific CD8α+ T cells among peripheral blood mononuclear cells (PBMCs), compared with PBS ($P < 0.001$) and FT

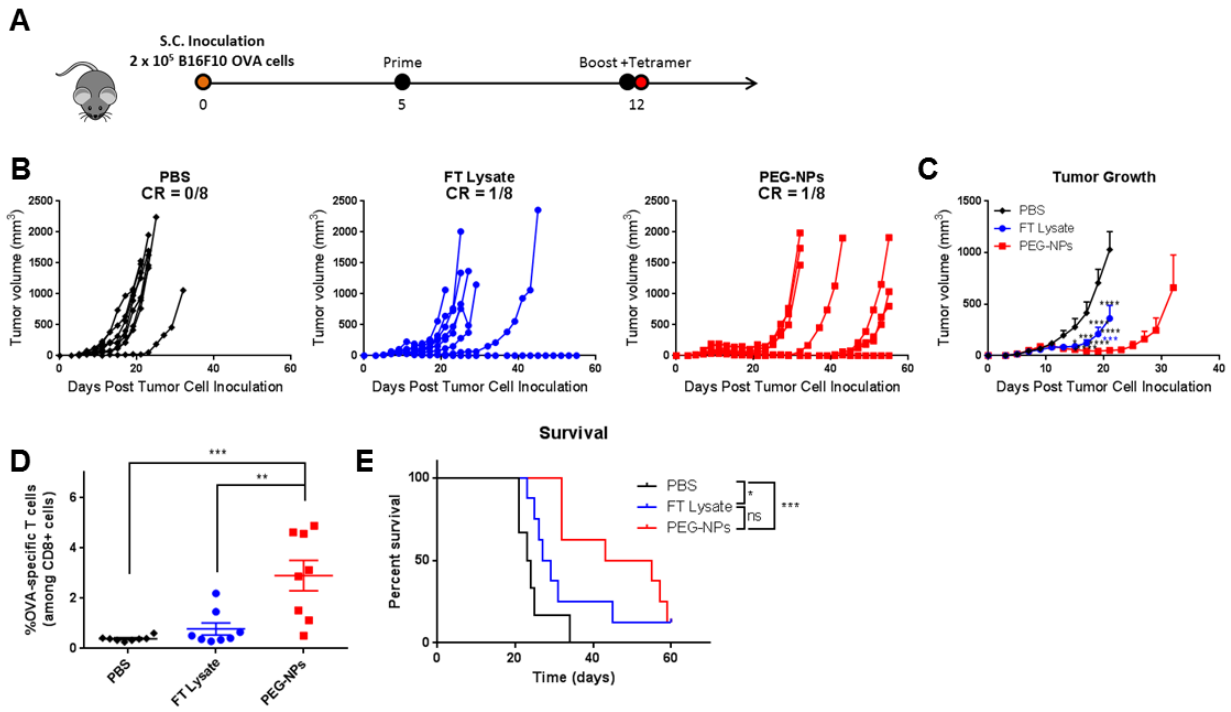

Figure 2-8. Therapeutic treatment against B16F10 OVA.
A. Mice were inoculated with B16F10 OVA tumor s.c. in the flank on day 0 and immunized on days 5 and 12. B-C. Tumor growth curves for individual mice within groups and summary are shown. D. Tetramer staining analysis via flow cytometry was performed to determine OVA-specific CTL responses among PBMCs (day 12; one week post-prime immunization). E. Overall survival is shown. Mean ± SEM are shown for panels C and D. Statistical analysis was performed using (C) two-way ANOVA with Tukey's multiple comparisons test compared to PBS + αPD-1 (black asterisks) and FT Lysate + αPD-1 (blue asterisks); (D) one-way ANOVA comparison with Tukey's multiple comparison test; and (E) Log-rank (Mentel-Cox) test (* = $p < 0.05$, ** = $p < 0.01$, *** = $p < 0.001$ and **** = $p < 0.0001$).

lysate ($P < 0.01$) groups, respectively (**Fig. 2-8D**). These strong T-cell responses induced by PEG-NPs translated to increased animal survival, as mice treated with PEG-NPs exhibited the median survival of 55 days, compared with 22 and 27 days for PBS ($P < 0.001$) and FT lysate groups ($P = 0.12$), respectively (**Fig. 2-8E**). Notably, antigen-specific CD8α+ T cell responses induced by PEG-NPs in these tumor-bearing animals (**Fig. 2-8D**) was greater, compared with those observed in non-tumor bearing animals post PEG-NPs treatments (**Fig. 2-6C**), suggesting that the presence of antigen-expressing tumors boosted the effects of vaccination.

Combination therapy approach with immune checkpoint blockade

Immunosuppressive tumor microenvironment is currently a major challenge in allowing patients' endogenous immune responses from controlling cancer. Blocking the interaction between PD-1 and PD-L1, primarily expressed on T lymphocytes and tumor cells, respectively, allows T cells to engage and kill cancer cells, as demonstrated by recent success of immune checkpoint inhibitors in the clinic [32]. Here, we aimed to further amplify T cell responses induced by PEG-NPs with co-administration of an immune checkpoint inhibitor. Briefly, C57BL/6 mice were inoculated at s.c. right flank with 2 x 10^5 B16F10 OVA tumor cells, and we administered PEG-NPs or FT lysate on days 5 and 12 together with intraperitoneal administration of αPD-1 IgG (100 μg per mouse per dose) on days 1 and 4 after each

immunization (**Fig. 2-9A**). Tumor-bearing mice treated with FT lysate + αPD-1 IgG therapy exhibited similar rate of tumor growth and median survival as animals treated with the αPD-1 IgG monotherapy (**Fig. 2-9B,C**), indicating the aggressive and poorly immunogenic nature of B16F10 OVA tumors. In sharp contrast, the combination of PEG-NPs + αPD-1 IgG therapy markedly decreased tumor growth, compared to αPD-1 monotherapy as well as the FT lysate + αPD-1 treatment ($P < 0.0001$, day 23, **Fig. 2-9B,C**). Analysis of T cell responses in peripheral blood indicated that the PEG-NPs + αPD-1 IgG combination therapy induced 4.2-fold higher frequency of OVA-specific CD8α+ T cell responses, compared with the FT lysate + αPD-1 treatment group ($P < 0.0001$, **Fig 2-9D**). Overall, the PEG-NPs + αPD-1 IgG combination therapy resulted in complete eradication of the tumors in 63% of animals without reaching the median survival for the whole duration of the study. In contrast, animals treated with FT lysate + αPD-1 IgG exhibited only 13% response rate with the median survival of 28 days ($P < 0.01$, **Fig 2-9E**).

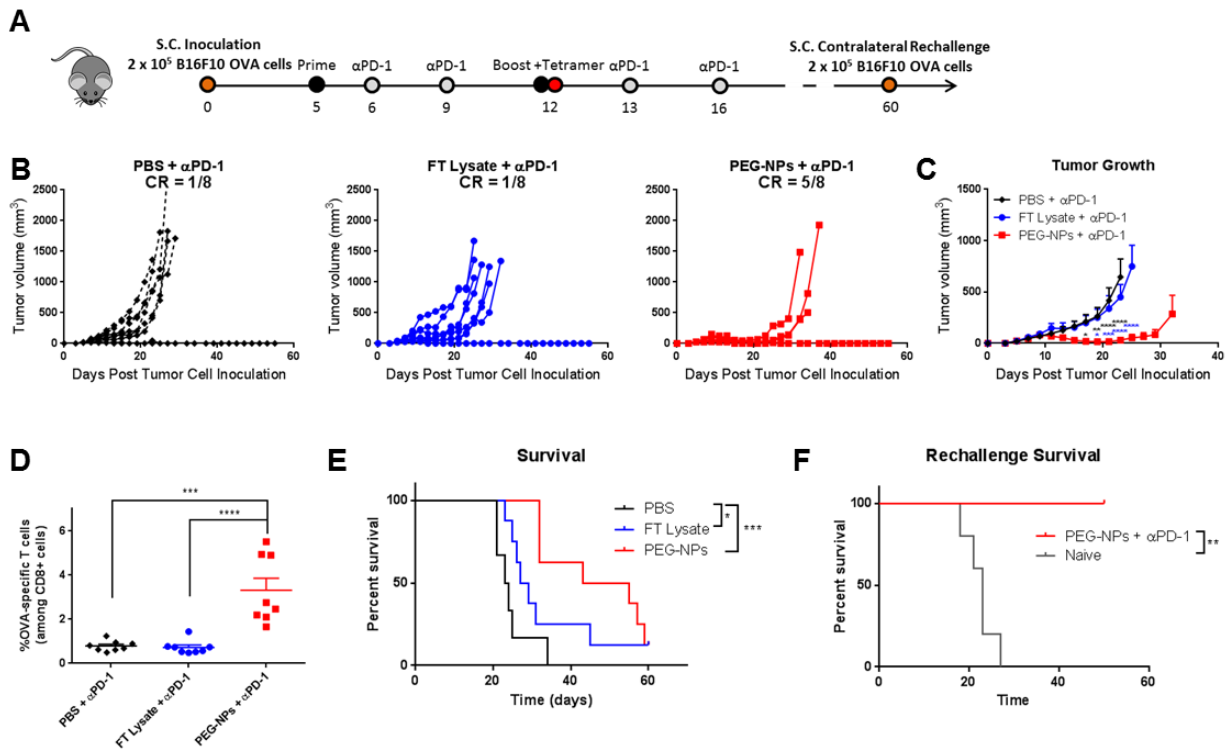

Figure 2-9. Therapeutic treatment against B16F10 OVA.

A. Mice were inoculated with B16F10 OVA tumor s.c. in the flank on day 0 and immunized on days 5 and 12 with anti-PD-1 co-administration. B-C. Tumor growth curves for individual mice within groups and summary are shown. D. Tetramer staining analysis via flow cytometry was performed to determine OVA-specific CTL responses among PBMCs (day 12; one week post-prime immunization). E. Overall survival is shown. F. Mice were rechallenged with B16F10 OVA on day 60 together with a group of naïve mice and the overall survival is shown. Mean ± SEM are shown for panels C and D. Statistical analysis was performed using (C) two-way ANOVA with Tukey's multiple comparisons test compared to PBS + αPD-1 (black asterisks) and FT Lysate + αPD-1 (blue asterisks); (D) one-way ANOVA comparison with Tukey's multiple comparison test; and (E) Log-rank (Mentel-Cox) test (** = $p < 0.01$, *** = $p < 0.001$ and **** = $p < 0.0001$).

We next determined if immune responses induced by the original treatment regimen established long-term systemic immunity against tumor recurrence. The survivors from the previous study (on day 60 of the original study) along with naïve control animals were inoculated with 2 x 10^5 B16F10 OVA tumor cells at the contralateral s.c. flank. None of the re-challenged survivors developed tumors for 50 days, whereas all naïve animals succumbed to

tumor growth with the median survival of 23 days (P < 0.01, **Fig 2-9F**). These results demonstrated that the PEG-NPs + αPD-1 IgG combination therapy elicited long-term protective immunity against the tumor cells.

Therapeutic immunization against large tumors

To determine if our vaccine approach can combat large tumors, we began therapy on day 10 after inoculation, once tumors have reached on average 70 mm^3 in volume (**Fig. 2-10A**). CTL responses after PEG-NPs administration were comparable to the day 5 immunization (3.66% vs 2.90% OVA-specific T cell frequency) and stronger than PBS- and FT-lysate-treated controls (P < 0.0001, **Fig. 2-10D**). There was a significant decrease in the rate of tumor growth resulting in a smaller tumor burden for PEG-NPs compared to the FT-Lysate control (P < 0.05, **Fig. 2-10B,C**). However, due to the persistence of the tumors, there was only a modest increase in the median survival to 35 days, compared to PBS (21 days, P < 0.01) and FT lysate (27 days, P < 0.01) groups (**Fig. 2-8E**).

We hoped that αPD-1 administration will assist with combating the large tumor burden of mice treated starting on da 10. However, even with strong CTL responses (5.17% OVA-specific T cell frequency), there was limited improvement over αPD-1 monotherapy in terms of tumor growth and overall survival (**Fig. 2-10F-J**). We suspect that the large and established tumors may prevent effective T cell infiltration and thus decrease their ability to control further progression. Additionally, the rapid proliferation of great number of tumor cells may outcompete the killing potential of the immune system, indicating the need for tumor debulking approaches, such as surgery or photothermal therapy.

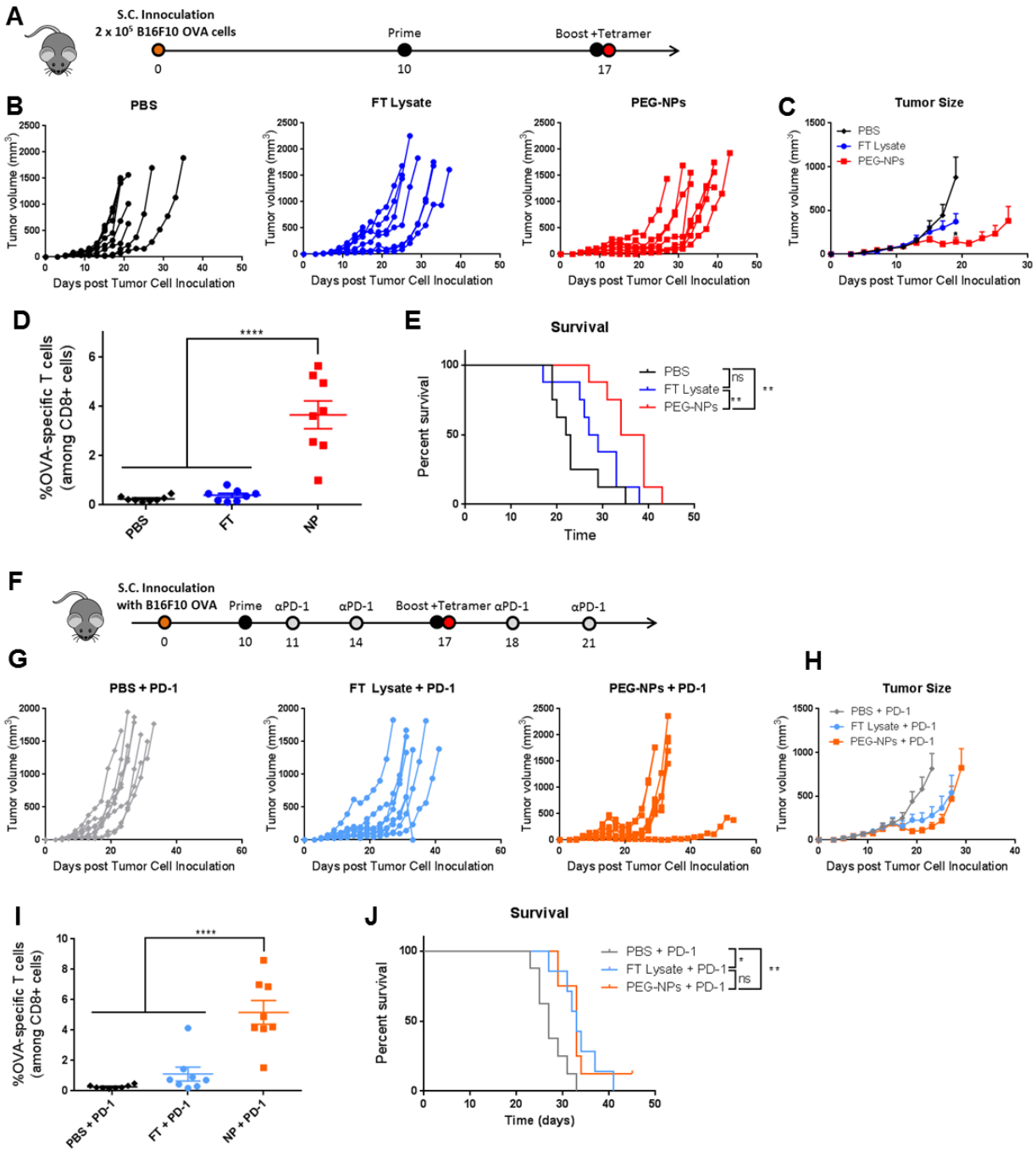

Figure 2-10. Therapeutic treatment against large B16F10 OVA tumors.

A. Mice were inoculated with B16F10 OVA tumor s.c. in the flank on day 0 and immunized on days 10 and 17. B-C. Tumor growth curves for individual mice within groups and summary are shown. D. Tetramer staining analysis via flow cytometry was performed to determine OVA-specific CTL responses among PBMCs (day 17; one week post-prime immunization). E. Overall survival is shown. F. Mice were inoculated with B16F10 OVA tumor s.c. in the flank on day 0 and immunized on days 10 and 17. Anti-PD-1 therapy was administered and 4 days after each

immunization. G-H. Tumor growth curves for individual mice within groups and summary are shown. D. Tetramer staining analysis via flow cytometry was performed to determine OVA-specific CTL responses among PBMCs (day 17; one week post-prime immunization). E. Overall survival is shown. Mean ± SEM are shown for panels C and D. Statistical analysis was performed using (D, I) one-way ANOVA comparison with Tukey's multiple comparison test; and (E, J) Log-rank (Mentel-Cox) test (* = $p < 0.05$, ** = $p < 0.01$, and **** = $p < 0.0001$).

In order to establish if humoral responses contribute to the anti-tumor activity, we examined the antibody and CD4+ T cell responses in tumor-bearing animals. Mice were inoculated with B16F10 OVA cells, immunized on days 10 and 17, treated with αPD-1 as indicated before, and serum and blood samples were collected on day 22 (**Fig. 2-11A**). Incubation of sera from the immunized animals with live tumor cells and staining with secondary anti-mouse IgG showed no differences in the presence of tumor-specific antibodies (**Fig. 2-11B.**) Additionally, PBMCs isolated from the blood sample, were cultured together with OT-II peptide, the MHC-II epitope of ovalbumin, to determine CD4+ T cell reactivity in an ELISpot experimental setting. While the immune responses were elevated in the animals treated with FT lysate, PEG-NPs, αPD-1, or combination of therapies, there were no differences when compared to media control, suggesting presence of nonspecific immune activation (**Fig. 2-11C**).

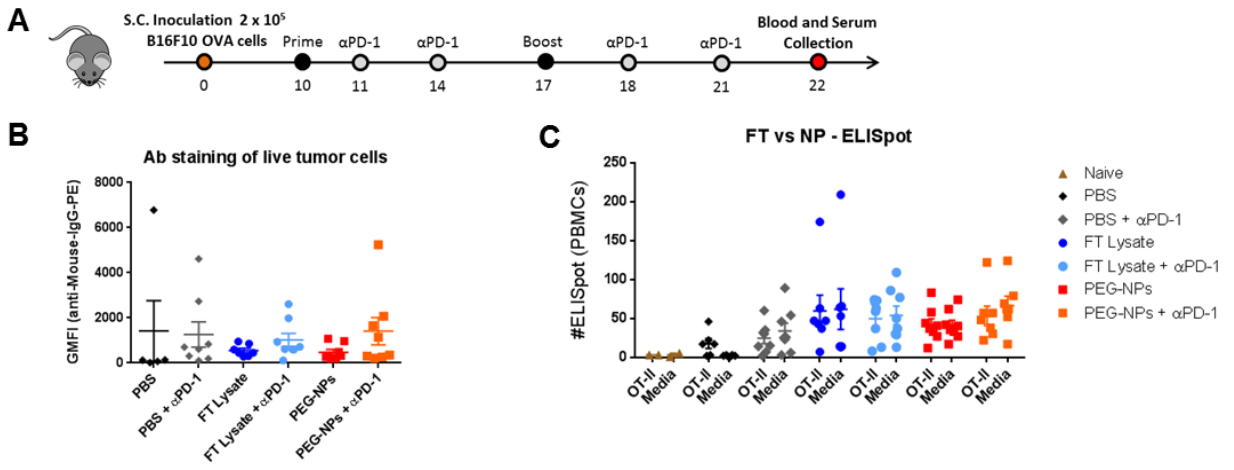

Figure 2-11. Humoral responses against large B16F10 OVA tumors.
A. Mice were inoculated with B16F10 OVA tumor s.c. in the flank on day 0 and immunized on days 10 and 17. Anti-PD-1 therapy was administered and 4 days after each immunization where indicated. B. Sera were collected on day 22 and incubated with live tumor cells followed by anti-mouse-IgG-PE secondary antibody staining. C. PBMCs were obtained from a blood sample and incubated with media control or OT-II peptide to determine CD4 T cell OVA-specific responses. Mean ± SEM are shown. Statistical analysis using one-way and two-way ANOVA comparison with Tukey's multiple comparison test showed no statistical differences between the groups.

2.5 Conclusions

In this study, we have demonstrated that the endogenous liposome-like plasma membrane structures present in cancer cell lysates can be engineered to exhibit stable characteristics and enhanced local lymph node draining via PEGylation. This cancer vaccine approach can elicit strong CTL responses against model antigen OVA, resulting in prophylactic and therapeutic efficacy against murine melanoma. In combination with immune checkpoint blockade, vaccination with engineered membrane nano-vesicles resulted in complete regression in tumors of 63% of the animals and established long-term immunity against tumor cell re-challenge. Overall, we have provided concrete evidence that use of cancer cell membranes for elicitation of anti-tumor immune responses is a feasible and promising approach for cancer immunotherapy.

2.6 References

1. Siegel, R.L., K.D. Miller, and A. Jemal, *Cancer Statistics, 2018.* Ca-a Cancer Journal for Clinicians, 2018. **68**(1): p. 7-30.

2. Pardoll, D.M., *The blockade of immune checkpoints in cancer immunotherapy.* Nature Reviews Cancer, 2012. **12**(4): p. 252-264.

3. Topalian, S.L., et al., *Safety, Activity, and Immune Correlates of Anti-PD-1 Antibody in Cancer.* New England Journal of Medicine, 2012. **366**(26): p. 2443-2454.

4. Wolchok, J.D., et al., *Nivolumab plus Ipilimumab in Advanced Melanoma.* New England Journal of Medicine, 2013. **369**(2): p. 122-133.

5. Robert, C., et al., *Ipilimumab plus Dacarbazine for Previously Untreated Metastatic Melanoma.* New England Journal of Medicine, 2011. **364**(26): p. 2517-2526.

6. Atkins, M.B., et al., *High-dose recombinant interleukin 2 therapy for patients with metastatic melanoma: Analysis of 270 patients treated between 1985 and 1993.* Journal of Clinical Oncology, 1999. **17**(7): p. 2105-2116.

7. Dillman, R.O., *An update on the relevance of vaccine research for the treatment of metastatic melanoma.* Melanoma Management, 2017. **4**(4): p. 203-215.

8. Sznol, M. and L.P. Chen, *Antagonist Antibodies to PD-1 and B7-H1 (PD-L1) in the Treatment of Advanced Human Cancer.* Clinical Cancer Research, 2013. **19**(5): p. 1021-1034.

9. Schumacher, T.N. and R.D. Schreiber, *Neoantigens in cancer immunotherapy.* Science, 2015. **348**(6230): p. 69-74.

10. Gubin, M.M., et al., *Tumor neoantigens: building a framework for personalized cancer immunotherapy.* J Clin Invest, 2015. **125**(9): p. 3413-21.

11. Sahin, U., et al., *Personalized RNA mutanome vaccines mobilize poly-specific therapeutic immunity against cancer.* Nature, 2017. **547**(7662): p. 222-+.

12. Ott, P.A., et al., *An immunogenic personal neoantigen vaccine for patients with melanoma.* Nature, 2017. **547**(7662): p. 217-+.

13. Gonzalez, F.E., et al., *Tumor cell lysates as immunogenic sources for cancer vaccine design.* Hum Vaccin Immunother, 2014. **10**(11): p. 3261-9.

14. Yu, J.S., et al., *Vaccination with tumor lysate-pulsed dendritic cells elicits antigen-specific, cytotoxic T-cells in patients with malignant glioma.* Cancer Research, 2004. **64**(14): p. 4973-4979.

15. Kim, J.H., et al., *Phase I/II study of immunotherapy using autologous tumor lysate-pulsed dendritic cells in patients with metastatic renal cell carcinoma.* Clinical Immunology, 2007. **125**(3): p. 257-267.

16. Ribas, A., et al., *Dendritic Cell Vaccination Combined with CTLA4 Blockade in Patients with Metastatic Melanoma.* Clinical Cancer Research, 2009. **15**(19): p. 6267-6276.

17. Hamdy, S., et al., *Targeting dendritic cells with nano-particulate PLGA cancer vaccine formulations.* Advanced Drug Delivery Reviews, 2011. **63**(10-11): p. 943-955.

18. Wei, X., et al., *Nanoparticle Functionalization with Platelet Membrane Enables Multifactored Biological Targeting and Detection of Atherosclerosis.* ACS Nano, 2018. **12**(1): p. 109-116.

19. Zhang, X., et al., *Remote Loading of Small-Molecule Therapeutics into Cholesterol-Enriched Cell-Membrane-Derived Vesicles.* Angew Chem Int Ed Engl, 2017. **56**(45): p. 14075-14079.

20. Tang, J., et al., *Therapeutic microparticles functionalized with biomimetic cardiac stem cell membranes and secretome.* Nat Commun, 2017. **8**: p. 13724.

21. Pucci, F. and M.J. Pittet, *Molecular pathways: tumor-derived microvesicles and their interactions with immune cells in vivo.* Clin Cancer Res, 2013. **19**(10): p. 2598-604.

22. Raposo, G. and W. Stoorvogel, *Extracellular vesicles: exosomes, microvesicles, and friends.* J Cell Biol, 2013. **200**(4): p. 373-83.

23. van Niel, G., G. D'Angelo, and G. Raposo, *Shedding light on the cell biology of extracellular vesicles.* Nat Rev Mol Cell Biol, 2018.

24. Kroll, A.V., et al., *Nanoparticulate Delivery of Cancer Cell Membrane Elicits Multiantigenic Antitumor Immunity.* Advanced Materials, 2017. **29**(47).

25. Cheung, A.S., et al., *Adjuvant-Loaded Subcellular Vesicles Derived From Disrupted Cancer Cells for Cancer Vaccination.* Small, 2016. **12**(17): p. 2321-2333.

26. Lutz, M.B., et al., *An advanced culture method for generating large quantities of highly pure dendritic cells from mouse bone marrow.* Journal of Immunological Methods, 1999. **223**(1): p. 77-92.

27. Ochyl, L.J. and J.J. Moon, *Whole-animal Imaging and Flow Cytometric Techniques for Analysis of Antigen-specific CD8+T Cell Responses after Nanoparticle Vaccination.* Jove-Journal of Visualized Experiments, 2015(98).

28. Khong, H.T. and S.A. Rosenberg, *Pre-existing immunity to tyrosinase-related protein (TRP)-2, a new TRP-2 isoform, and the NY-ESO-1 melanoma antigen in a patient with a dramatic response to immunotherapy.* J Immunol, 2002. **168**(2): p. 951-6.

29. Theos, A.C., et al., *The Silver locus product Pmel17/gp100/Silv/ME20: controversial in name and in function.* Pigment Cell Res, 2005. **18**(5): p. 322-36.

30. Roederer, M., *Interpretation of Cellular Proliferation Data: Avoid the Panglossian.* Cytometry Part A, 2011. **79A**(2): p. 95-101.

31. Jiang, H., Q. Wang, and X. Sun, *Lymph node targeting strategies to improve vaccination efficacy.* Journal of Controlled Release, 2017. **267**: p. 47-56.

32. Chen, L.P. and X. Han, *Anti-PD-1/PD-L1 therapy of human cancer: past, present, and future.* Journal of Clinical Investigation, 2015. **125**(9): p. 3384-3391.

Chapter 3: Dendritic Cell Membrane Vesicles for Activation and Maintenance of Antigen-specific T Cells

3.1 Abstract

Cancer immunotherapy has undergone a dramatic transformation over the past decade, due to successes of the immune checkpoint blockade and CAR T cell technology, fueling further efforts to enhance these treatments. Vaccination has traditionally been associated with preventing infections, but great progress had been made in the field of cancer vaccines, which can synergize with the existing immune therapies to boost the level of available cytotoxic T cells to fight tumors. In this study, we have developed a nano-sized dendritic cell membrane vesicles (DC-MVs) capable of activating antigen presenting cells as well as delivering peptide antigens. DC-MVs successfully led to maturation of dendritic cells and promoted T cell survival and proliferation *in vitro*. These effects were also observed *in vivo*, where mice adoptively transferred with antigen-specific T cells exhibited greater frequency of those T cells following vaccination with DC-MVs and peptide antigen compared to peptide antigen alone. Additionally, DC-MVs vaccination led to enhanced levels of endogenous T cell responses against model antigen ovalbumin in an OVA-expressing tumor model. These results suggest that DC-MVs are a potentially attractive platform for further development as a peptide-based vaccine for cancer immunotherapy.

3.2 Introduction

Cytotoxic T lymphocyte (CTL) responses have evolved to eliminate virally and bacterially infected cells and have been responsible for keeping tumors at bay as demonstrated by increased cancer rates amongst immunocompromised individuals [1]. In the recent years, cancer immunotherapy focused on the CTL activation and responses has shown great promise by generating efficacious responses and obtaining clinical approval. Immune checkpoint blockade has released the brakes from the immunosuppressive tumor environment allowing for demonstration of therapeutic effects following cancer vaccination [2]. At the same time advances in affordable next generation sequencing and technology necessary for peptide synthesis compliant with current good manufacturing practices (cGMP), allowed for discovery and characterization of neo-antigens in variety of tumor types [3, 4].

Due to the exceptional mutational rate of dividing tumor cells, they are very likely to harbor single amino acid changes or reading frame shifts randomly generating brand new peptide sequences [5]. While these mutations may not necessary drive or even contribute to the cancer growth, they may provide a therapeutic target. The existence of a brand new peptide sequence may lead to alternative proteasomic degradation, association with and affinity for major histocompatibility complex class I (MHC-I), and most importantly recognition by CTLs. All of these characteristics have the ability to change the identity of the peptide from self-antigen to immunogenic neo-antigen, leading to immune responses and antigen-dependent eradication of the tumor cells. These discoveries and tremendous amount of work over the past decade had led to development of effective cancer vaccines evaluated in small scale clinical trials [6, 7].

In this study we had focused on the development of allogenic cell-derived vehicle for antigen peptide delivery in order to promote immune responses, with the goal of generating neo-

antigen-specific T cell immunity in the long run. We had utilized cell membrane preparation technology developed by our lab in order to generate dendritic cell membrane vesicles (DC-MVs) from matured antigen-presenting cell population. We had sought to utilize these to function by delivering peptides to the lymph nodes, as has been seen by our previous utilization of PEGylated cancer cell membranes (unpublished data). Successful uptake and activation of antigen presenting cells (APCs) would allow for antigen presentation and T cell proliferation.

Here, we show that MPLA-activate DC-MVs were able to effectively load model antigenic SIINFEKL peptide onto the particle surface and promote activation of immature DCs and stimulate T cells for enhanced maintenance and proliferation *in vitro* (**Fig 3-1**). In addition, following adoptive cell transfer, OT-I T cell population was activated prompting strong proliferation *in vivo* after immunization with DC-MVs. Finally, tumor-bearing animals exhibiting low levels of endogenous OVA-specific responses were immunized with our formulation and showed enhanced frequency of antigen-specific T cells. Taken together, these results demonstrate that the DC-MV formulation can load peptides onto the particle surface and deliver it to the site of action along with its endogenous immunostimulatory function. This outcome provides promise for this peptide-based vaccination approach for further development in the field of neo-antigen-specific cancer immunotherapy.

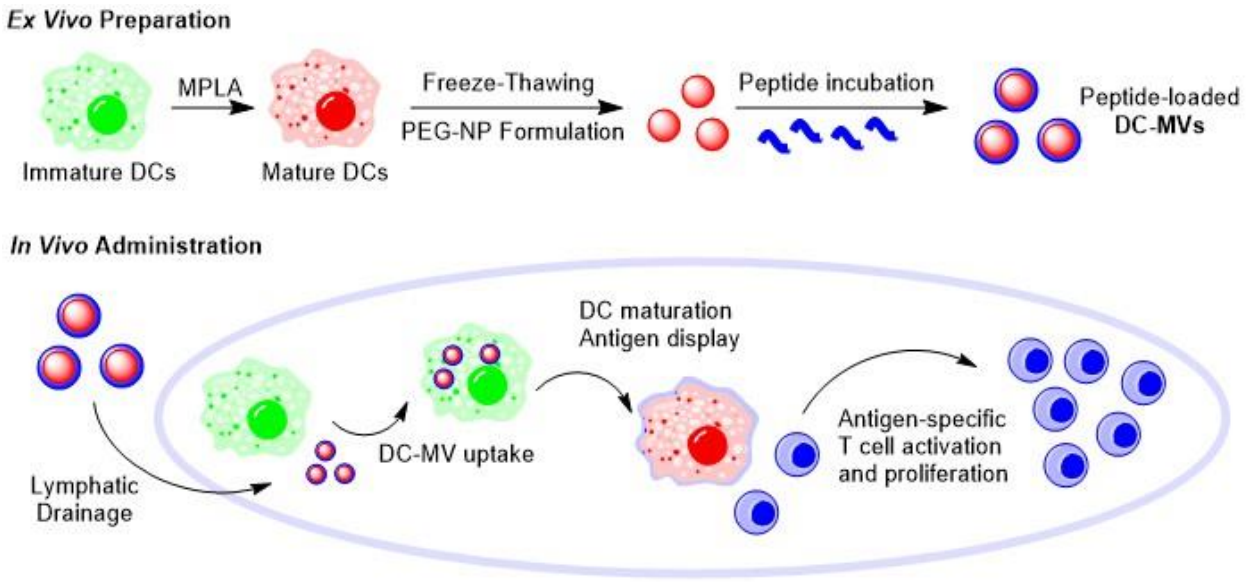

Figure 3-1. Schematic representation of DC-MVs.
Immature DCs are stimulated with MPLA, prepared in PEG-NPs, and loaded with antigen peptide to generate DC-MVs. *In vivo* administration results in lymphatic drainage, uptake by DCs promoting maturation and antigen display, and antigen-specific T cell activation and proliferation.

3.3 Materials and Methods

Cell Culture

Bone marrow-derived dendritic cells (BMDCs) were generated as previously described [8]. Briefly, 6- to 12-week old C57BL/6 or BALB/c mice were euthanized and the tibiae and femurs harvested. The bones were cut on each side and flushed in order to extract the bone marrow, which was then dissociated into single cell suspension and passed through a 40 µm strainer. Cells were spun down, resuspended at 2 x 10^5 cells per ml of complete media (RPMI supplemented with 10% FBS, 100 U/mL penicillin, 100 µg/ml streptomycin, 50 µM β-mercaptoethanol, and 20 ng/ml GM-CSF), and plated in non-treated petri dishes for continuous culture. Media was added on day 3 and replenished on days 6 and 8. Loosely adherent cells

(immature DCs) were collected via gentle pipetting and washed with PBS prior to further use. B16F10 OVA cells were kindly provided by Dr. Darrell Irvine (Massachusetts Institute of Technology; Cambridge, MA) and cultured in RPMI supplemented with 10% FBS, 100 U/mL penicillin, 100 µg/ml streptomycin.

Western Blot Analysis

BMDCs were plated in culture-treated dishes and allowed to adhere overnight followed by stimulation with 1 µg/ml of MPLA for 24 hours. Suspended cells were harvested (MPLA-S population), plates were washed, and Accutase was added to facilitate further cell dissociation from the plates for 30 minutes. The remainder of the cells was removed with a cell scraper (MPLA population). Untreated cells had both of the suspended and strongly adhered populations combined for analysis (NO TX). Harvested cells were lysed through freeze-thaw cycling between liquid nitrogen and 37°C followed by probe-tip sonication to generate whole cell lysates. Fractionation was achieved through consecutive centrifugation of supernatants from previous steps to generate cell debris (pellet after 1000 x g, 10 minutes), mitochondria (pellet from 20,000 x g, 10 minutes), and cytosol and membrane fractions (supernatant and pellet, respectively, from 100,000 x g, 1 hour). Protein content was analyzed by microBCA assay (Thermo), 20 µg of total protein was loaded onto 4-12% gradient gel to perform SDS-PAGE, and transferred to PVDF membrane using the iBlot system (Thermo). Membranes were blocked with 5% milk solution and probed with anti-CD80 (R&D Systems), anti-CD86 (R&D Systems), and cytochrome c (Santa Cruz) primary antibodies overnight at 4°C. After three washes, membranes were incubated with secondary HRP-linked antibodies for 1 hour at room temperature.

Following further washes, ECL reagent was used to develop the Western Blots for imagining with FluorChem M (ProteinSimple).

DC-MV Preparation and Peptide Loading

Dendritic cell membrane vesicles (DC-MVs) were generated from sonicated cell lysates following removal of large debris and organelles via centrifugation (10,000 x g, 10 minutes). Lysates were adjusted to 6 mg/ml concentration and incubated with 20 mM $CaCl_2$ for 1 hour to promote fusion and aggregation of membranes allowing for washes using table-top centrifugation (20,000 x g, 5 minutes). DC-MVs were then resuspended with mild water bath sonication in 10 mg/ml DSPE-PEG 100 mM EDTA solution prompting calcium chelation and surface coating with polyethylene glycol. Finally, vesicles were passed through PBS-equilibrated Zeba desalting column to remove excess EDTA, calcium, and DSPE-PEG to generate DC-MVs.

SIINFEKL or fluorescently labeled SIINFEK(FITC)L peptides (Genscript) were loaded at 100 µg/ml onto the DC-MV surface via incubation at 37°C at varying DC membrane concentrations (10.0, 2.5, and 1.0 mg/ml in PBS). Loading efficiency was determined after samples were passed two times through 40 kDa Zeba desalting column via plate-based fluorescence assay.

BMDC Maturation

Day 10 differentiated dendritic cells were added to 96-well plates at 1 x 10^5 cells per well and allowed to adhere overnight. MPLA (1 µg/ml), unstimulated DC-MVs, and (MPLA)DC-MVs were incubated with DCs for 24 hours and then washed away with PBS. Cells were trypsinized and lifted off of the plate, washed twice with FACS buffer (1% bovine serum

albumin in PBS), and resuspended with anti-CD16/32 antibody to promote blocking of the Fc receptor. Then, cells were stained with anti-CD40 and anti-CD80 fluorescently-labeled antibodies, incubated for 30 minutes on ice, and washed twice more with FACS buffer. Finally, samples were resuspended in FACS buffer containing 1 µg/ml DAPI and analyzed with ZE5 Cell Analyzer (Bio Rad). Gating and analysis was performed using FlowJo software.

T Cell Proliferation *In vitro*

In vitro T cell proliferation was performed using OVA-specific primary T cells. Briefly, 6- to 12-week old OT-I transgenic mouse was euthanized and its spleen harvested and processed into single cell suspension. Red blood cells were removed by three-minute incubation with ACK lysis buffer (Gibco) and CD8α+ T cells were separated using negative selection kit (StemCell Technologies). Cells were then adjusted to a concentration of 4 million cells / ml in RPMI and combined with equivalent volume of 2 µM CFSE solution to be incubated at 37°C for ten minutes allowing fluorescent labeling. Reaction was quenched with FBS-containing media and the cells were washed prior to counting and resuspending in complete T cell media (RPMI supplemented with 10% FBS, 100 U/mL penicillin, 100 µg/ml streptomycin, 50 µM β-mercaptoethanol, 1 mM HEPES buffer, and 1X non-essential amino acid solution (Gibco)). Cells were then plated in 96-well plates at 50,000 or 10,000 cells / well concentration and treated with 0.01 to 10 ng/ml SIINFEKL peptide with or without 50 µg/ml of DC-MVs (as determined by protein content). After three days of culture, T cells were collected, washed, and stained with anti-CD8α, anti-CD25, and DAPI similarly to the procedure outlined above.

Adoptive Cell Transfer

OVA-specific, Thy1.1+ OT-I CD8α+ T cells were obtained as described above using the negative selection kit and adoptively transferred into naïve C57BL/6 mice via tail vein injection of 5 x 10^5 cells. One day after transfer mice were immunized with SIINFEKL peptide (10 µg per mouse) with or without DC-MVs (250 µg protein per mouse). After 5 days, blood samples were obtained using submandibular bleeds and red blood cells removed via ACK lysis to yield peripheral blood mononuclear cells (PBMCs). Samples were processed for flow cytometry by washing, blocking CD16/32 Fc receptor, and staining with anti-CD8α, anti-Thy1.1, and in some cases anti-PD-1 fluorescently-labeled antibodies. Cells were then resuspended in FACS DAPI solution and examined via flow cytometry. In order to examine memory recall, mice were boosted with 100 µg OVA on day 26 after primary immunization and responses analyzed once more by analyzing frequency of Thy1.1+ CD8 T cells among PBMCs on day 33.

Therapeutic Tumor Study

2 x 10^5 B16F10 OVA melanoma cells were inoculated subcutaneously into the flank of 6- to 8-week old C57BL/6 mice and allowed to establish tumors. Prime immunization was performed with 10 µg of SIINFEKL with or without 250 µg of (MPLA)DC-MVs on day 10 and compared to PBS control. On day 17, PBMCs were stained with H2-K^b-SIINFEKL tetramer (MBL International) and anti-CD8α and analyzed via flow cytometry for frequency of OVA-specific T cells. Study endpoints (tumor diameter > 15 mm, large ulceration, or moribund state) were used to establish overall survival.

Statistical analyses

For animal studies, mice were randomized to match similar average volume of the primary tumors and all procedures were performed in a non-blinded fashion. Statistical analysis was performed with Prism 6.0 software (GraphPad Software) by one-way or two-way ANOVA with Tukey's multiple comparisons post-test. Statistical significance is indicated as *P < 0.05, **P < 0.01, ***P < 0.001, and ****P < 0.0001.

3.4 Results and Discussion

Generation of DC-MVs

Dendritic cell surface proteins interact with T cells promoting their activation and proliferation, but the use of *ex vivo* generated DC vaccines is laborious and expensive [9]. We aimed to utilize the membrane preparation techniques developed in our lab to generate dendritic cell membrane vesicles (DC-MV), which could be prepared more easily and utilized as an off-the-shelf product. Our studies focused on the use of murine bone marrow, extracted from the tibiae and femurs of C57BL/6 mice and differentiated into dendritic cells through the use of granulocyte-macrophage colony-stimulating factor (GM-CSF) as described before [8]. Immature dendritic cells were collected from the supernatant of the culture and placed in separate dishes to be further activated. Similar cell preparation can be achieved by isolating monocytes from human patients and differentiating and activating the *ex vivo* [10].

Monophosphoryl Lipid A (MPLA) has been proven to be a strong dendritic cell activator in the past, thus it was chosen as the immunostimulant for DC maturation [11]. Cells were cultured overnight in the presence of MPLA along with untreated cells to be used as a negative

control. Two MPLA-treated populations were prepared based on their adherence to treated flasks: suspended or loosely attached cells dissociated via pipetting (MPLA-S) and fully attached cells further treated with Accutase and removed with a cell scraper (MPLA). Untreated cells consisted mostly of the suspended and loosely adherent cells so the two populations were combined (NO TX). Next, the harvested cells underwent freeze-thaw lysis and mild probe-tip sonication. Fractionation was achieved through centrifugation and individual fractions (whole cell, debris, mitochondria, cytosol, and membrane) were analyzed via Western Blot analysis for the level of expression and enrichment of T-cell-activation ligands CD80 and CD86 (**Fig. 3-2A**, top and middle panels). Specifically, CD86 expression increased within the plasma membrane preparations following MPLA treatment (lanes 10 and 11) compared to the untreated controls (lane 9). Additionally, the higher intensity of the CD86 band and the lower intensity of the cytochrome c band within the membrane fraction compared to the whole cell lane (lane 1) demonstrate proper isolation of mature dendritic cell plasma membranes for further use (**Fig. 3-2A**, bottom panel).

DC-MVs can bind antigen peptide

Our lab has shown in the past that tumor cell membranes can be prepared into nanoparticles coated with polyethylene glycol (PEG) layer, which exhibited efficient lymph node draining, dendritic cell uptake, and T cell activation capabilities. To utilize this technology further, we have prepared DC-MVs in a similar manner through the freeze-thaw and sonication-based cell lysis, calcium-driven membrane aggregation and separation, and finally PEGylation through the post-preparation DSPE-PEG insertion. These DC-MVs were then ready for loading of the antigen of interest onto the particle surface and use in subsequent studies (**Fig. 3-1**).

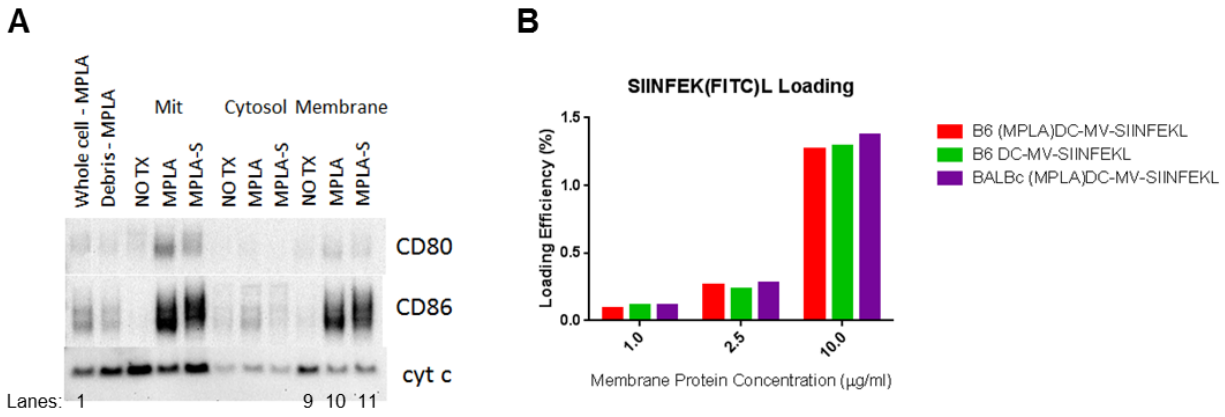

Figure 3-2. DC-MV characterization.
A. Dendritic cells were left untreated or pulsed with MPLA to promote maturation. Loosely adherent cells were harvested via pipetting (MPLA-S), while adherent cells were detached with Accutase and scraped (MPLA). For untreated cells, the two preparations were combined for analysis (NO TX). Cell were fractionated and analyzed via Western Blot for expression of CD80, CD86, or cytochrome c (cyt c). B. DC-MVs were prepared and incubated with SIINFEK(FITC)L peptide to promote loading. After purification, peptide retention was analyzed by fluorescence.

We focused on the use of peptide with the amino acid sequence SIINFEKL, which is a CD8α+ T cell immunogenic epitope from model antigen ovalbumin (OVA). First, we examined the ability to load SIINFEKL peptide onto DC-MVs by utilizing LC/MS, but extraction of the peptide from this complex formulation proved difficult (data not shown). Back-up approach involved the use of labeled peptide with covalently bound fluorophore (FITC) to the lysine amino acid of the peptide (SIINFEK(FITC)L), which has been shown in the past to effectively bind to MHC-I [12]. We generated (MPLA)DC-MVs and unstimulated DC-MVs and incubated them with SINFEK(FITC)L at various membrane protein concentrations followed by desalting column washing capable of removal of 99.98% of free peptide (data not shown). Importantly, different mouse strains express varying MHC-I alleles, prompting us to generate (MPLA)DC-MVs from C57BL/6 (H-2K^{b}, H-2D^{b}) and BALB/c (H-2K^{d}, H-2D^{d}, H-2L^{d}), where only H-2K^{b} is capable of binding SIINFEKL [13]. The results demonstrate that SIINFEKL loading onto DC-

MVs is dependent only on the vesicle concentration and independent on the state of activation (MPLA-treated vs immature) and the MHC-I haplotype (**Fig. 3-2B**). This outcome suggests that the peptide is loaded onto the particle through electrostatic interactions indicating that DC-MVs may function as effective delivery vehicles.

DC-MVs active live DCs *in vitro*

Exosomes and naturally-produced membrane vesicles had been known to carry secondary messengers and transduce cell-to-cell signals [14, 15]. We sought to determine if the artificially produced DC-MVs can serve to activate live dendritic cells *in vitro*. We employed commonly used maturation assay, where cultured BMDCs are pulsed with various formulations and analyzed for expression of activation markers, CD40 and CD80, via flow cytometry. Importantly, (MPLA)DC-MVs but not immature DC-MVs have led to upregulation of both activation markers, suggesting a potential role of this platform as not only a vehicle for peptide delivery, but also as an immunostimulatory adjuvant (**Fig. 3-3A,B**). Interestingly, (MPLA)DC-MVs but not MPLA alone served to upregulate CD80, which can directly bind to CD28 on T cells leading to enhanced proliferation (**Fig. 3-3B**).

These data support a hypothesis where DC-MVs may bind peptides non-specifically through electrostatic interactions and efficiently deliver them to the lymph nodes while providing a vehicle and adjuvant function. We had also considered another mechanism through which DC-MVs may activate and promote T cell proliferation: antigen peptides may bind directly to the MHC-I surface protein providing binding site for antigen-specific T-cell receptor (TCR) and together with activation surface receptors CD80 and CD86 may function as a nano-sized antigen presenting platform analogous to fully mature dendritic cells. These approaches had been studied

in the past and provide attractive alternative methods to standard vaccination [16, 17]. The next set of studies was used to tease out the appropriate mode of action of our DC-MV therapy.

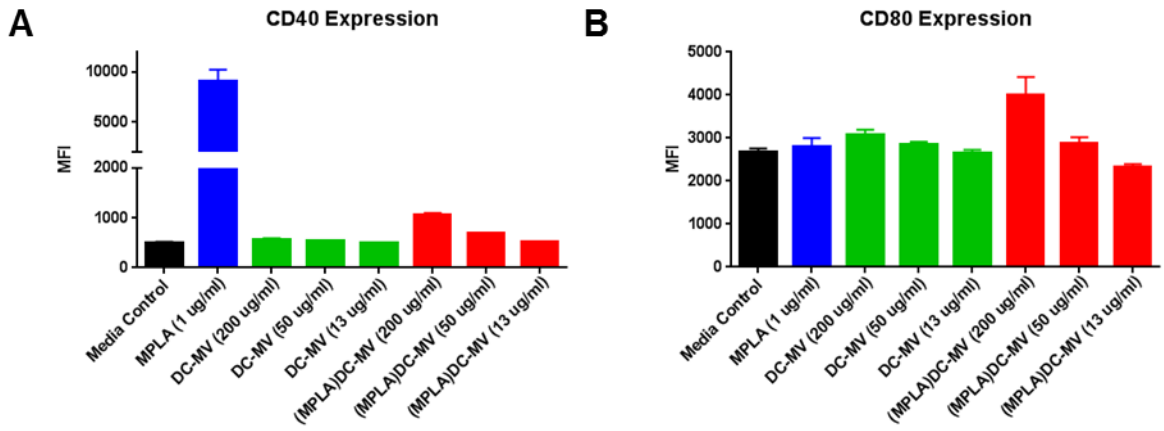

Figure 3-3. BMDC activation using DC-MVs.
BMDCs were cultured with non-activated DC-MVs and (MPLA)DC-MVs and examined for expression maturation markers CD40 (A) and CD80 (B) via flow cytometry

In vitro T cell proliferation

To examine the ability of the DC-MVs to directly interact with T cells and promote their activation and proliferation through TCR and CD28 engagement, we focused on the commonly used CFSE dilution assay [18]. Briefly, OVA-specific CD8α+ T cells were isolated from the spleens of OT-I transgenic mice, labeled with the CFSE fluorescent dye, and co-cultured with the MPLA-treated or unstimulated DC-MVs in the presence of SIINFEKL. Using the standard 50,000 cells/well seeding density, we observed that SIINFEKL alone led to strong proliferation across the 10 to 0.1 ng/ml peptide concentration range, while DC-MVs or (MPLA)DC-MVs had no additional effect (**Fig. 3-4A**). However, looking at the relative number of cells surviving through the three day culture, (MPLA)DC-MVs followed by DC-MVs performed better than the SIINFEKL control (**Fig. 3-4B**). Finally, we examined the proliferating T cells for the expression

of CD25, a subunit of the IL-2 receptor and a late marker of TCR-dependent T cell activation. At 10 to 1 ng/ml peptide concentration over 50% of proliferating T cells were expressing CD25 after co-culture with DC-MVs compared to approximately 15% when stimulated with SIINFEKL alone (**Fig. 3-4C**). Importantly, at the highest concentration, (MPLA)DC-MVs outperformed immature DC-MVs suggesting increased efficacy following adjuvant treatment.

Taken together, these results have led us to speculate that the introduction of SIINFEKL peptide alone to the OT-I T cell culture leads to peptide binding and presentation in the context of MHC-I on the T cell surface itself. This causes swift T cell cross-priming and eventual cross-killing, which is demonstrated by low surviving cell counts and low CD25 expression suggesting lack of prolonged activation. To test this hypothesis, we performed the CFSE dilution assay again, but this time utilizing lower seeding OT-I T cell density (10,000 cells/well; or 5-fold decrease from before) in order to minimize cell-to-cell interactions. (MPLA)DC-MVs have led to enhanced T cell proliferation at 10 and 1 ng/ml peptide concentrations compared to the SIINFEKL alone (**Fig. 3-4D**). Importantly, the number of surviving T cells and surface expression of CD25 was markedly increased due to the presence of (MPLA)DC-MVs (**Fig. 3-4E,F**). Based on these results, we suspect that the activation markers present on DC membranes can effectively engage and enhance T cell proliferation *in vitro*, prompting us to test this formulation *in vivo*.

Characterization of DC-MV mechanism of action

The previous *in vitro* data indicated that DC-MVs may directly interact with T cells and promote their healthy proliferation. While this may be possible in the controlled and simple cell culture conditions, it may be difficult to achieve within the physiological complexity of the body.

As a result, we set out to determine if DC-MVs can deliver cargo and then directly activate antigen presenting cells by screening this effect *in vivo*. Considering potential low immunogenicity of our platform and controlling for mouse to mouse variability, we set off to utilize adoptive cell transfer of OT-I T cells to provide a basal, equivalent antigen-specific T cell population within each animal.

Immunization was administered one day after adoptive cell transfer of 5 x 10^5 OT-I CD8α+ T cells and blood samples were analyzed for Thy1.1+ T cells on day 5. Formulations were prepared as before, by incubating antigen peptides with DC-MVs at 37°C allowing for surface loading, but this time no column purification was performed in order to allow equivalent 10 µg of peptide to be delivered across all groups. Taking previous results into consideration, we

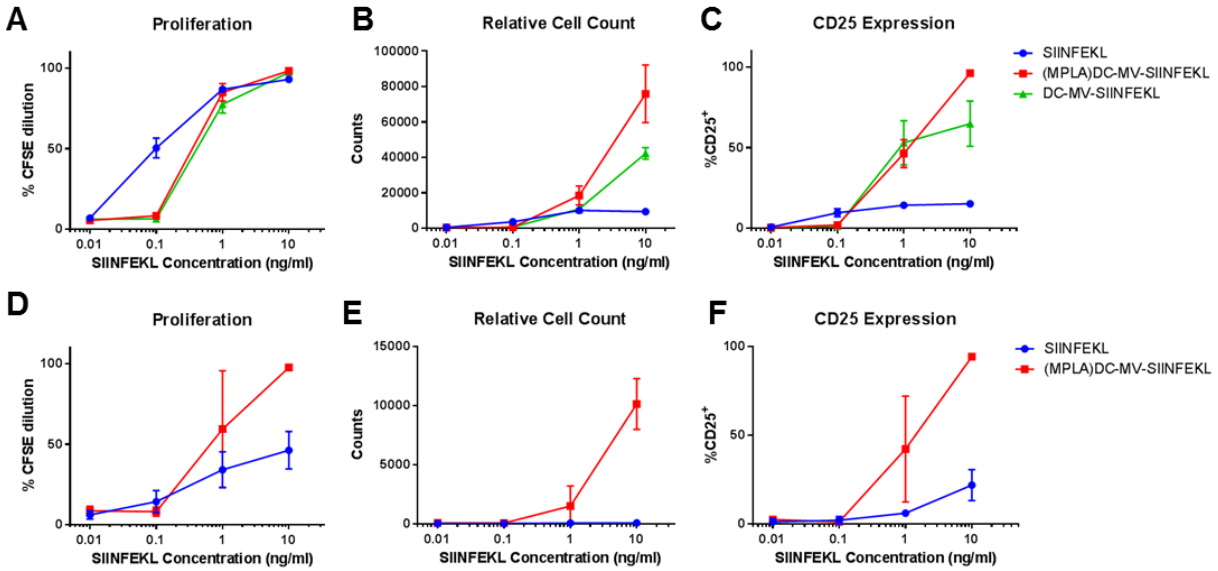

Figure 3-4. T cell proliferation in presence of DC-MVs.
OT-I T cells were incubated with SIINFEKL peptide alone or in the presence of non-activated and (MPLA)DC-MVs at two cell amounts of 50,000 cells/well (panels A-C) or 10,000 cells/well (panels D-F) for three days and analyzed via flow cytometry. A and D. Average percentage of proliferated T cells is shown. B. and E. Relative count of live T cells was determined within the CD8α+ population. D and F. Percentage of T cells expressing CD25 activation marker is shown.

suspected that only ~1.3% or ~130 ng of peptide would be associated with the particles and aided with trafficking to the lymph node, while the remainder was free to interact with serum proteins and cell surfaces. However, the (MPLA)DC-MVs efficiently delivered the peptide and led to OT-I T cell expansion improvement over the soluble SIINFEKL controls regardless of the mouse strain used, reinforcing lack of necessity for matched MHC-I alleles (**Fig. 3-5**). Importantly, C57BL/6- and BALB/c-sourced MPLA-activated MVs have demonstrated improvements in T cell activation compared to unstimulated DC-MVs (P = 0.035 and P = 0.0002, respectively), verifying previous results suggesting that the maturation state of BMDCs prior to harvesting their membranes plays a role in their function. These experiments suggest that the initial hypothesis of LN delivery along with immunostimulatory functions may be correct and that DC-MVs may serve as potential peptide vaccine vehicles for cancer immunotherapy.

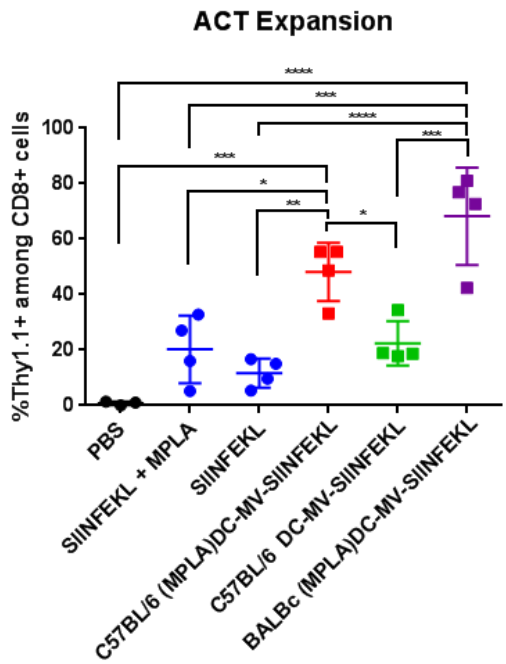

Figure 3-5. T cell proliferation *in vivo* following ACT.
Mice were adoptively transferred with 500,000 OT-I Thy1.1+ CD8α+ T cells and immunized the following day with SIINFEKL peptide with or without the DC-MVs. After 5 days, PBMCs were collected and examined for the fraction of CD8α+ T cells expressing Thy1.1.

Therapeutic immunization against melanoma

The aim of this vaccination platform focused on enhancement of T cell activation and proliferation *in vivo* using peptide-based approaches. We examined this function by employing murine B16F10 OVA melanoma, expressing model antigen ovalbumin. In previous studies, we observed that low levels of endogenous, OVA-specific responses are generated upon tumor inoculation and that they can be boosted through vaccination approaches (data not shown). B16F10 OVA tumors were established through subcutaneous injection of 2 x 10^5 cells in the flank of mice, immunized on day 10, and examined for CTL responses on day 17 (**Fig. 3-6A**).

OVA-specific T cell responses were analyzed via tetramer staining assay focusing on antigen-specific CD8α+ T cell population among peripheral blood mononuclear cells (PBMCs) (**Fig. 3-6B**). Naïve animals were used to establish the staining background, while tumor-bearing PBS-treated mice showed low level of baseline responses against ovalbumin. SIINFEKL alone treatment had no effect on increasing the endogenous responses. Importantly, co-administration of SIINFEKL with (MPLA)DC-MVs has led to generation of strong T cell responses in two of the five animals, and while not statistically significant (P = 0.08 vs PBS and P = 0.22 vs SIINFEKL), suggests an overall trend in enhanced efficacy. However, we did not observe any improvement in terms of decreasing tumor growth or enhancing overall survival (**Fig. 3-6C**).

The parental B16F10 melanoma model is difficult to treat due to quick progression and often requires combination therapy approaches, thus administration of DC-MVs on day 10 may not have been sufficient, even with the presence of foreign antigen OVA [19, 20]. Additionally, based on the response rate to the DC-MV therapy that we have observed, we speculate that this approach may not be suitable for initial activation of CTLs, but rather boosting the responses which are already present. Specifically, we suspect that the two mice that have had high levels of

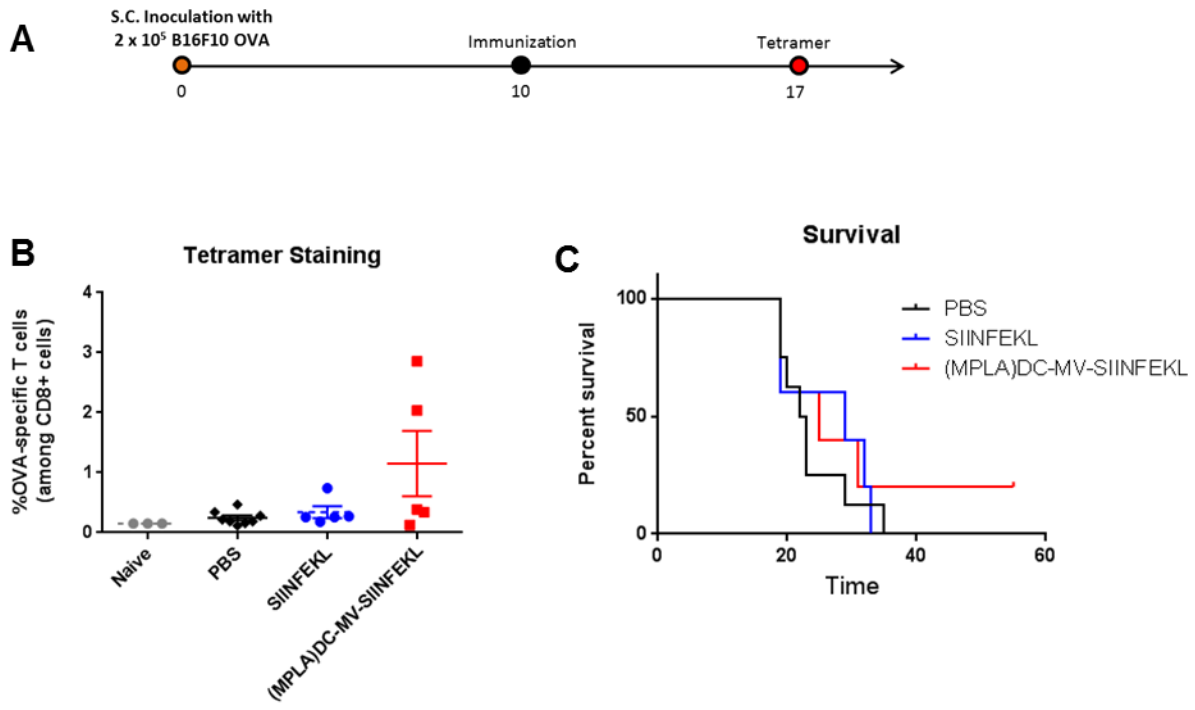

Figure 3-6. T cell proliferation in tumor-bearing mice.
A. Mice were inoculated with B16F10 OVA melanoma and immunized 10 days later with SIINFEKL or (MPLA)DC-MV-SIINFEKL. B. OVA-specific T cell population was analyzed among CD8α+ PBMCs 7 days after immunization. C. The overall survival of the mice is shown.

OVA-specific T cells were most likely to already have elevated responses at the time of vaccination due to the presence of the OVA-expressing tumor. Further pursuit of this therapy would have to focus on prior examination of existing T cell responses with the goal to engage and activate them prompting expansion to therapeutic levels.

Memory recall response of ACT T cells

Up and coming therapies had focused on adoptive cell transfer (ACT) of antigen-specific T cells and range from the isolation and expansion of tumor infiltrating lymphocytes (TILs) to genetically engineering chimeric antigen receptor (CAR) T cells [21-23]. While providing strong responses and therapeutic effects against cancer in early clinical trials, these approaches are

associated with potential safety concerns, which prevent administration of high doses of T cells. Importantly, efficacy and long-term remission in cancer patients is associated with maintenance and survival of the adoptively transferred T cells and, in cases of relapse, patients will sometimes undergo reinfusion of antigen-specific CTLs [24]. As demonstrated in our melanoma tumor model, DC-MV approach may be capable of expansion and maintenance of tumor-specific T cells, prompting us to test if it can be used together with ACT therapy.

Mice were adoptively transferred with 5 x 10^5 OT-I T cells and immunized the following day with SIINFEKL peptide (10 μg) with or without CpG adjuvant or in the context of DC-MVs and varying concentrations of (MPLA)DC-MVs (**Fig. 3-7A**). We observed strong level of T cell proliferation at all (MPLA)DC-MV doses measured by assessing presence of Thy1.1 marker on CD8α+ T cells among PBMCs, suggesting effective activation of OVA-specific CTLs (**Fig. 3-7B**). In comparison, immature DC-MVs and SIINFEKL peptide alone failed to promote T cell maintenance over the five day period. SIINFEKL combined with immunostimulatory molecule, CpG, was effective at increasing T cell proliferation and served as a positive control. We have also focused on examining Programmed Death 1 (PD-1) receptor expression on the activated OVA-specific T cells. (MPLA)DC-MVs led to PD-1 upregulation in a dose-dependent manner suggesting strong levels of activation at high doses (**Fig. 3-7C**). In order to examine the level of T cell maintenance over time and the formation of memory T cell responses, we administered a boost immunization using 100 μg of soluble OVA. We observed that while SIINFEKL + CpG generated a consistent recall response resulting in approximately 40% of OVA-specific T cells, (MPLA)DC-MVs showed a broad range of memory recall characterized by a few very strong (~60%) but predominantly low (~15%) T cell expansion across the varying doses (**Fig. 3-7D**). Importantly, these responses showed correlation to the results from the primary immunization,

where well-expanding, PD-1^{low} responders demonstrated greatest level of proliferation following the boost. These data suggest that the level of T cell activation by the DC-MV formulation requires further optimization and fine-tuning to prevent over-activation of ACT CTLs and the potential for anergy, while at the same time demonstrating promise for prominent activation and maintenance of the antigen-specific T cell population.

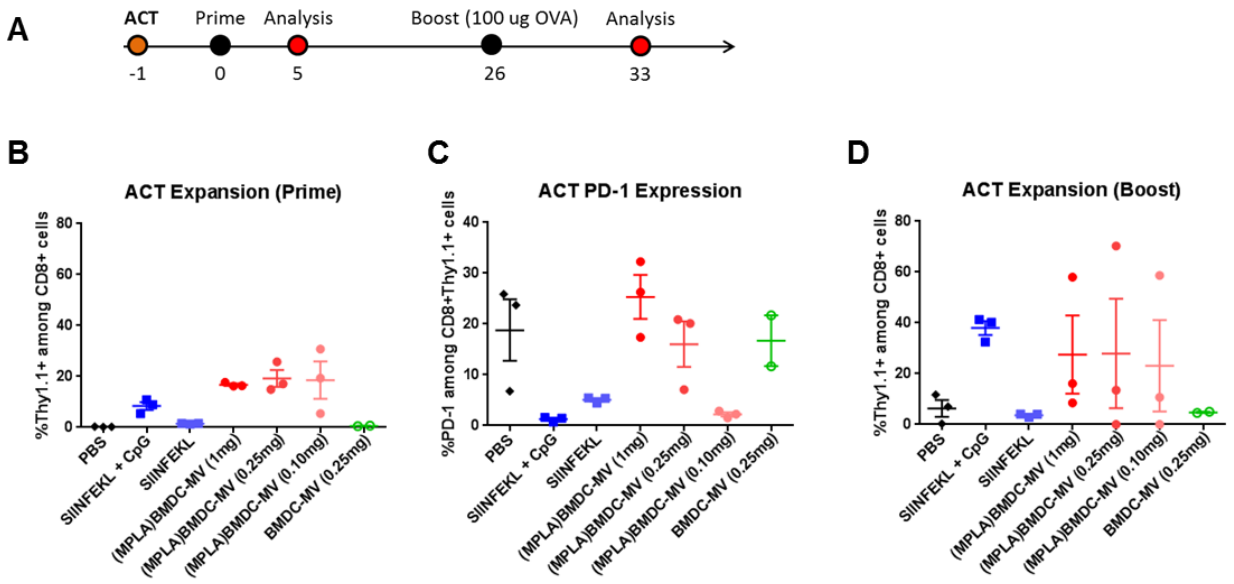

Figure 3-7. Memory recall responses.
A. Mice were immunized were adoptively transferred on day -1 and immunized on day 0 with SIINFEKL with or without DC-MVs. Boost immunization of 100 µg soluble OVA was used to determine memory response. B. ACT T cell expansion was determined 5 days post-treatment via %Thy1,1+ CD8α+ T cells among PBMCs. C. PD-1 expression was examined on OVA-specific T cells. D. Memory responses of expanded OT-I ACT T cells after 100 µg OVA administration are shown. Mean ± SEM are shown.

3.5 Conclusions

This study has focused on generation and characterization of cell membrane vesicles from activated dendritic cells to function as peptide-based vaccine vehicles. We have demonstrated that (MPLA)DC-MVs have strong dendritic cell maturation capabilities and that they can effectively interact with peptide-pulsed OT-I T cells leading to strong proliferation and maintenance *in vitro*. In addition, *in vivo* administration of the SIINFEKL peptide along with (MPLA)DC-MVs allowed for expansion of adoptively transferred OT-I T cells and in some cases generation of strong memory T cell responses. Finally, mice bearing OVA-expressing tumors were immunized with SIINFEKL and (MPLA)DC-MVs leading to expansion of antigen-specific T cells, but therapeutic effect has not been shown. Further studies will focus on determining optimal *in vivo* T cell activation and proliferation in order to generate therapeutic level of responses. The potential use for this technology would revolve around promoting T cell memory in adoptive cell transfer therapies or boosting existing self- and neo-antigen approaches to combat cancer.

3.6 References

1. Grulich, A.E., et al., *Incidence of cancers in people with HIV/AIDS compared with immunosuppressed transplant recipients: a meta-analysis.* Lancet, 2007. **370**(9581): p. 59-67.

2. Chen, L.P. and X. Han, *Anti-PD-1/PD-L1 therapy of human cancer: past, present, and future.* Journal of Clinical Investigation, 2015. **125**(9): p. 3384-3391.

3. Schumacher, T.N. and R.D. Schreiber, *Neoantigens in cancer immunotherapy.* Science, 2015. **348**(6230): p. 69-74.

4. Gubin, M.M., et al., *Tumor neoantigens: building a framework for personalized cancer immunotherapy.* J Clin Invest, 2015. **125**(9): p. 3413-21.

5. Alexandrov, L.B., et al., *Signatures of mutational processes in human cancer.* Nature, 2013. **500**(7463): p. 415-21.

6. Ott, P.A., et al., *An immunogenic personal neoantigen vaccine for patients with melanoma.* Nature, 2017. **547**(7662): p. 217-+.

7. Sahin, U., et al., *Personalized RNA mutanome vaccines mobilize poly-specific therapeutic immunity against cancer.* Nature, 2017. **547**(7662): p. 222-+.

8. Lutz, M.B., et al., *An advanced culture method for generating large quantities of highly pure dendritic cells from mouse bone marrow.* Journal of Immunological Methods, 1999. **223**(1): p. 77-92.

9. Goozner, M., *Concerns About Provenge Simmer as CMS Ponders Coverage.* Journal of the National Cancer Institute, 2011. **103**(4): p. 288-289.

10. Chapuis, F., et al., *Differentiation of human dendritic cells from monocytes in vitro.* European Journal of Immunology, 1997. **27**(2): p. 431-441.

11. Mata-Haro, V., et al., *The vaccine adjuvant monophosphoryl lipid A as a TRIF-biased agonist of TLR4.* Science, 2007. **316**(5831): p. 1628-1632.

12. Saini, S.K., et al., *Dipeptides promote folding and peptide binding of MHC class I molecules.* Proc Natl Acad Sci U S A, 2013. **110**(38): p. 15383-8.

13. Falk, K., et al., *Both Human and Mouse Cells Expressing H-2k(B) and Ovalbumin Process the Same Peptide, Siinfekl.* Cellular Immunology, 1993. **150**(2): p. 447-452.

14. Pucci, F. and M.J. Pittet, *Molecular pathways: tumor-derived microvesicles and their interactions with immune cells in vivo.* Clin Cancer Res, 2013. **19**(10): p. 2598-604.

15. Raposo, G. and W. Stoorvogel, *Extracellular vesicles: exosomes, microvesicles, and friends.* J Cell Biol, 2013. **200**(4): p. 373-83.

16. Kovar, M., et al., *Direct stimulation of T cells by membrane vesicles from antigen-presenting cells.* Proceedings of the National Academy of Sciences of the United States of America, 2006. **103**(31): p. 11671-11676.

17. Hwang, I.Y., X.F. Shen, and J. Sprent, *Direct stimulation of naive T cells by membrane vesicles from antigen-presenting cells: Distinct roles for CD54 and B7 molecules.* Proceedings of the National Academy of Sciences of the United States of America, 2003. **100**(11): p. 6670-6675.

18. Quah, B.J.C., H.S. Warren, and C.R. Parish, *Monitoring lymphocyte proliferation in vitro and in vivo with the intracellular fluorescent dye carboxyfluorescein diacetate succinimidyl ester.* Nature Protocols, 2007. **2**(9): p. 2049-2056.

19. Kuai, R., et al., *Designer vaccine nanodiscs for personalized cancer immunotherapy.* Nature Materials, 2017. **16**(4): p. 489-+.

20. Moynihan, K.D., et al., *Eradication of large established tumors in mice by combination immunotherapy that engages innate and adaptive immune responses.* Nat Med, 2016. **22**(12): p. 1402-1410.

21. Tran, E., D.L. Longo, and W.J. Urba, *A Milestone for CAR T Cells.* New England Journal of Medicine, 2017. **377**(26): p. 2593-2596.

22. Wu, R., et al., *Adoptive T-Cell Therapy Using Autologous Tumor-Infiltrating Lymphocytes for Metastatic Melanoma Current Status and Future Outlook.* Cancer Journal, 2012. **18**(2): p. 160-175.

23. Foppen, M.H.G., et al., *Tumor-infiltrating lymphocytes for the treatment of metastatic cancer*. Molecular Oncology, 2015. **9**(10): p. 1918-1935.

24. Hurton, L.V., et al., *Tethered IL-15 augments antitumor activity and promotes a stem-cell memory subset in tumor-specific T cells.* Proceedings of the National Academy of Sciences of the United States of America, 2016. **113**(48): p. E7788-E7797.

Chapter 4: Nanoparticle Analysis by Flow Cytometry for Characterization and Prediction of Responses *In vivo*

4.1 Abstract

Nanoparticles had been utilized since the advent of liposomes several decades ago due to their favorable pharmacokinetic properties. While great advances had been made in the characterization of these formulations, most of them focused on bulk analysis without closely examining features of each particle. Recent advances in flow cytometric analysis allow for the examination of individual nano-sized particles prompting us to adopt and further develop this technique. In these studies, we demonstrate setup of the MoFlo Astrios cytometer for the characterization lipid-based nanoparticles by analyzing incorporated fluorophores as well as probing the surface display of antigens with antibodies. Ultimately, thorough analysis of cell membrane vesicles derived from cancer and dendritic cells will assist in understanding and proper optimization of these formulations for further use in cancer immunotherapy. Meanwhile, additional studies utilized hepatitis C virus antigen E2 incorporation into varying nanoparticle formulations and examined correlation with murine immune responses following vaccination. The results showing similar broadly neutralizing antibody binding to E2-his and E2c-his nanoparticle constructs via flow cytometry provided explanation for activity shown via *in vitro* neutralization assay. Taken together, we have demonstrated effective adaptation of nanoparticle

flow cytometry methodology and analysis of lipid-based nanoparticle vaccine formulations establishing foundation for further work with cell membrane vesicles.

4.2. Introduction

Nanoparticles have been widely utilized for various therapeutic approaches by providing major benefits such as limiting the systemic drug availability, providing controlled release, or enhancing drug accumulation at the site of action [1, 2]. Specifically, the use of nanoparticles for vaccination has been greatly exploited in recent years, as they can effectively encapsulate antigens and adjuvants, protect the cargo from degradation, and, due to their size, efficiently traffic to the local lymph nodes [3]. As these formulations may often mimic pathogenic architecture, the surface presentation and appropriate density of antigens may direct generation of potent antibody responses due to cross-linking of B cell receptors conveying strong activation [4, 5].

Standard formulation characterization includes determination of particle size, surface charge (zeta potential), and polydispersity [6]. Recently, nanoparticle tracking analysis (NTA) technology has allowed for further insight into size as well as fluorescence features of formulations by characterizing individual particles [7]. In addition, various types of electron microscopy (EM) may be used to explore detailed surface structure (scanning EM) or even visualize individual protein antigens (cryo-EM) [8]. Determining encapsulation amount of antigens and adjuvants within simple nanoparticle formulations with limited number of components can be achieved using multiple techniques such as bicinchoninic acid assay (BCA), Coomassie staining, or high-pressure liquid chromatography (HPLC). While quantification of absolute amount of antigen present within the formulation is necessary, it is also important to

determine the amount of biologically active, or in the case of vaccines, immunogenic protein cargo [9, 10]. Many biologic-based nanoparticle approaches utilizing exosomes or plasma membrane preparations may be quite difficult to analyze due to sample variability and presence of strong background in these highly complex structures. Due to recent technological advances, flow cytometry has been adapted to be used for high throughput and effective analysis of these types of nano-sized formulations [11-14]. These studies had focused on enumeration of nanoparticles within various biological samples and detecting expression of activation markers on cell-secreted exosomes

Exosomes can effectively be isolated from patients or tissue culture and examined for surface presence of particular markers, such as MHC-I, with the use of antibody staining [15]. We sought to establish this technique to allow for close analysis of membrane vesicles generated in our lab from tumor cells and dendritic cells for cancer vaccination. Expression of specific cell-surface proteins on the outside of the particles would assist in their designated function and the use of nanoparticle flow cytometry would provide the necessary confirmation and aid in protocol optimization. For the tumor cell membrane vaccine, surface presence of ovalbumin (OVA, model exogenous antigen) would confirm its incorporation and hint at potential ability of these particles to elicit OVA-specific humoral responses. Recent reports demonstrate that Fas ligand and PD-L1 expression on membrane vesicles shed by the tumor cells may lead to decreased T cell function, thus assessing our formulations for presence of these molecules would provide further insight [16-18]. In terms of the dendritic cell platform, expression of co-stimulatory markers, CD80/86, would allow to screen for optimal DC activation, harvest, and particle preparation protocol. At the same time, we had hoped to utilize this approach to aid other research avenues, thus we focused on analysis of lipid nanoparticle-based vaccine formulations.

In particular, broadly neutralizing antiviral antibodies, providing protection against different strains of one virus, have been sought after for a long time, and while their identification and characterization have been achieved, inducing production of these antibodies has been challenging [19]. Lack of effective vaccines against prevalent viruses, such as Hepatitis C Virus (HCV), Human Immunodeficiency Virus (HIV), and even influenza, stems from the highly mutagenic nature and presence of numerous variable regions on the surfaces of these pathogens. We hypothesized that proper preparation and orientation of the antigen on the particle surface, demonstrated by the ability of binding known broadly neutralizing antibodies *in vitro*, will allow for the recognition and production of broadly neutralizing antibodies against those epitopes *in vivo*.

In this study, we demonstrate the flow cytometry setup, which has allowed for single particle analysis and examination of antigen loading efficiency in model experiments. Importantly, the use of this technique has allowed us to confirm antigen presence on the surface of tumor membrane vesicles. Finally, we were able to examine different lipid-based nanoparticle vaccines against HCV and screened them with a panel of monoclonal antibodies with broadly and non-broadly neutralizing capabilities. To our knowledge, this is the first time that flow cytometry approach has been use to examine antigen presentation and configuration on synthetically generated nanoparticles as opposed to exosomes shed by cells. Correlation of this data with responses *in vivo* would provide the possible use of this technique for screening of future vaccine formulations prior to *in vivo* administration saving on labor, costs, and animal use.

4.3. Materials and Methods

Nanoparticle preparation

Multilamellar vesicles (MLVs) and interbilayer cross-linked multilamellar vesicles (ICMVs), the lipid-based formulations utilized in these studies, were prepared as previously reported [20]. In short, lipid film generated by drying 1,2-dioleoyl-sn-glycero-3-phosphocholine (DOPC) and 1,2-dioleoyl-sn-glycero-3-phosphoethanolamine-N-[4-(p-maleimidophenyl) butyramide] (MPB) in a 1:1 ratio was rehydrated with aqueous 10 mM bis-tris propane buffer by vortexing for 10 seconds every 10 minutes for 1 hour. Next, particles were probe-tip sonicated (40% intensity setting on 125W/20kHz sonicator) to generate unilamellar vesicles. Addition of 33 mM $CaCl_2$ and 2.4 mM dithiothreitol (DTT) allowed for fusion and molecular stapling of the lipid bilayers during 1 hour incubation at 37°C. Next, particles were washed twice with ddH_2O and incubated with 10 mg/ml polyethylene glycol-thiol (PEG(2K)-SH) to allow surface PEGylation for 30 minutes at 37°C. Finally, particles were washed twice more with ddH_2O and resuspended in PBS.

For the HCV formulations, ICMVs were produced as described above whereas NTA ICMV synthesis was performed by incorporation of 2% 1,2-dioleoyl-sn-glycero-3-[(N-(5-amino-1-carboxypentyl)iminodiacetic acid)succinyl] nickel salt (DOGS NTA) lipid within the lipid film. HCV E2 constructs were kindly provided by Dr. Mansun Law from The Scripps Research Institute.

Cell membrane nanoparticles were generated from cancer cell lines (B16F10 OVA or CT26 cell line) by freeze-thaw cycling, sonicating, and removing large debris via centrifugation. Then, 20 mM calcium chloride was used to aggregate membrane fractions (adjusted to 6 mg/ml of total protein), followed by tabletop centrifugation for washing, and post-preparation insertion

of DPSE-linked polyethylene glycol (5kDa, Laysan Bio) and removal of calcium via EDTA treatment. Particles were passed through Zeba desalting column in order to remove any free DSPE-PEG and calcium-bound EDTA.

Fluorophores and antibodies

Nanoparticles were labeled with a Di family of dyes including 3,3'-Dioctadecyloxacarbocyanine Perchlorate (DiO, excitation/emission = 488/520 nm), 1,1'-Dioctadecyl-3,3,3',3'-Tetramethylindocarbocyanine Perchlorate (DiI, excitation/emission = 530/580), 1,1'-Dioctadecyl-3,3,3',3'-Tetramethylindodicarbocyanine, 4-Chlorobenzenesulfonate Salt (DiD, excitation/emission = 600/660 nm), and (1,1'-Dioctadecyl-3,3,3',3'-Tetramethylindotricarbocyanine Iodide (DiR, excitation/emission = 600/780 nm). AlexaFluor647-NHS was utilized to fluorescently label ovalbumin (Worthington). Allophycocyanin (APC) and Phycoerythrin (PE) were prioritized as the fluorophore conjugates for the secondary antibodies due to their strong fluorescence output, or brightness.

Rabbit anti-OVA primary IgG (Abcam) and anti-rabbit IgG secondary antibody linked to APC (Thermo) were used for studies focused on ovalbumin surface presentation. Monoclonal human HCV specific primary antibodies were kindly provided by Dr. Mansun Law. Secondary antibody utilized was anti-human IgG linked with PE (eBioscience).

Antibody staining

Particles were freshly prepared and resuspended in FACS buffer (1% bovine serum albumin in PBS, w/v) to allow for blocking of nonspecific interaction. Then primary antibody was added to the solution of each particle and incubated over night at 4°C. Samples were washed

once with FACS buffer by centrifugation at 20,000 x g for 45 minutes with a 4°C temperature setting. Particles were then resuspended in a secondary antibody FACS buffer solution and incubated for 1 hour on ice. Samples were then washed two more times with FACS buffer. For bulk analysis, samples were transferred to 96-well black opaque plates and read using a plate reader (BioTek). Finally, samples were transferred to individual 5 ml round-bottom tubes and refrigerated prior to analysis by flow cytometry.

Flow cytometry

Flow cytometric analysis was performed using MoFlo Astrios EQ (Beckman Coulter) equipped with the Dual-PMT (Photomultiplier Tube) Forward Scatter Upgrade with M1 and M2 masks. 488 nm laser forward scatter detector was used for triggering events and relatively low, but noise-eliminating, threshold level was utilized (0.002% off of 300 voltage with 100% laser power). Further side scatter gating was utilized to eliminate aggregates within samples to generate monodisperse single-particle populations within the fluorescence plots. Results were analyzed by FlowJo software.

Animal Studies

6- to 8-week old female C57BL/6 mice were immunized with E2-his and E2c-his NTA ICMV formulations using a prime / boost / boost approach with 10 / 5 / 5 µg of antigen and 1.0 / 0.5 / 0.5 µg MPLA, respectively, and were administered subcutaneously at the tail base. Each immunization was given three weeks apart (days 1, 21, 42), whereas sera samples were also collected three weeks apart starting one day prior to first boost immunization (days 20, 41, 62). Sera titers were examined via ELISA assay, where E2 antigen adhering to lectin-coated plate

was utilized to capture antigen-specific murine antibodies. After washing, samples were stained with anti-mouse IgG HRP-linked secondary antibody, washed further, and then developed to determine overall antibody titers. Neutralization assay was performed as described before [21], but this time incubating cells with viral pseudo particles with or without immunized murine sera for 6 hours and allowed for infection to take place over 72 hours.

Stability Studies

ICMV samples tagged with DiO and encapsulating AF647-OVA were centrifuged (20,000 x g, 45 minutes) and resuspended in plain RPMI or RPMI containing 10%, 50%, or 90% of FBS. Samples were then incubated while shaking at 37°C for 24 hours and diluted with FACS buffer to be directly run on the flow cytometer with the appropriate media controls.

4.4. Results and Discussion

Nanoparticle flow cytometry setup

Flow cytometry has been utilized for surface and intracellular marker analysis allowing for high-throughput characterization of mixed cell populations. Utilization of this technique for nanoparticle characterization would provide new information and allow for increased work efficiency. However, due to the difference in size between cells and nanoparticles spanning a few orders of magnitude, a few considerations must take place. Most importantly, triggering the instrument to record an event taking place becomes challenging due to the particle size (~200 nm compared to the 488 nm laser) and the low light-scattering characteristics of tiny lipid-based structures.

In order to address these issues, we utilized MoFlo Astrios cytometer equipped with particle analysis module and started off by greatly decreasing the trigger threshold until the detection of non-specific noise occurred even when no sample was being analyzed (**Fig. 4-1A**). Next, running filtered PBS has shown low levels of background noise, which could be distinguished from the strong machine noise by plotting the signal from two forward scatter detectors against each other (**Fig 4-1A**). By next raising the threshold, the machine noise was eliminated and running nanoparticle sample generated a distinctly grouped population (**Fig. 4-1B**). In addition, the inability to detect very small particles within the sample may skew our overall results, but considering the high monodisperisity of our formulation (data not shown), we expected to obtain a proper representation.

Detection of fluorescence signal

Once the particles were effectively detected by the flow cytometer we sought to detect the fluorescence signal within our formulation and determine the analytic dynamic range. Throughout all of our experiments we focused on the use of lipid-based nanoparticle formulations generated by previously-reported methods from our lab [20, 22]. Briefly, particles were prepared through hydrating lipid films to generate multi-lamellar vesicles (MLVs), sonicated, and then fused in a controlled manner through the addition of calcium chloride. Addition of dithiol linker allowed for stapling of the multiple lipid bilayers due to presence of maleimide-functionalized lipids and stabilizing post-synthesis PEGylation generated interbilayer cross-linked multilamellar vesicles (ICMVs).

First, ICMVs were formulated with the addition of a lipid-based dye (DiO, excitation/emission = 488/520) into the lipid film prior to hydration, capable of incorporation

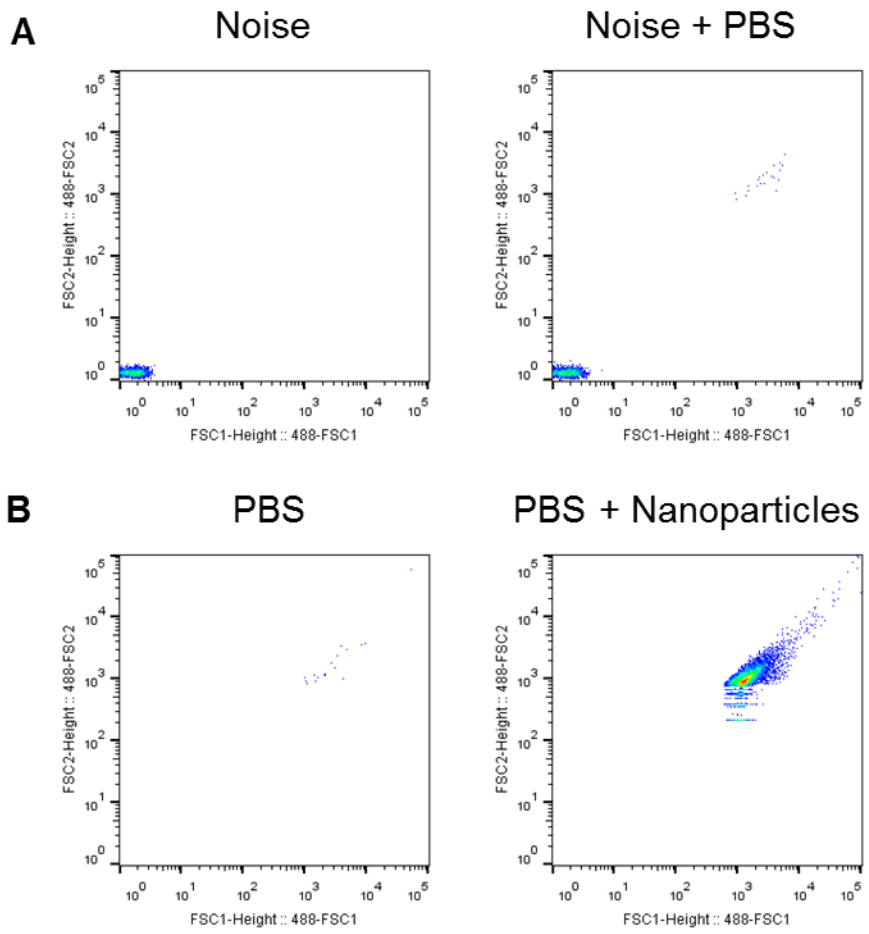

Figure 4-1. Forward vs side scatter FACS plots showing nanoparticle detection.
A. Machine noise can be eliminated by increasing the threshold on the forward scatter detector. B. Nanoparticles can be detected with reasonably low background in the PBS control alone.

into the bilayer. Analysis of these particles via flow cytometry has demonstrated a clear separation from the unlabeled, blank ICMVs (**Fig. 4-2A**). Importantly, the DiO-labeled particles generated a single peak with no events registering near the unlabeled population. Because of this, we feel confident that addition of the DiO tag to all of our future analyses will provide a critical quality control step, ensuring that the events that we analyze represent true single-particle populations and exclude any potential particulate contamination.

The next step was to demonstrate that the fluorescence signal is dependent on the amount of fluorophore present, thus ensuring a dose-dependent dynamic range. ICMVs were hydrated with aqueous solution containing 0, 25, or 100 µg of ovalbumin fluorescently labeled with AlexaFluor647 (AF647, excitation/emission = 600/660). Cytometric analysis demonstrated discernable peaks with median fluorescence intensity dependent on the amount of dye encapsulated (**Fig. 4-2B**). Taken together, these results have shown that nanoparticles can be labeled with lipophilic dyes and fluorescently-tagged cargo and analyzed within the dynamic range.

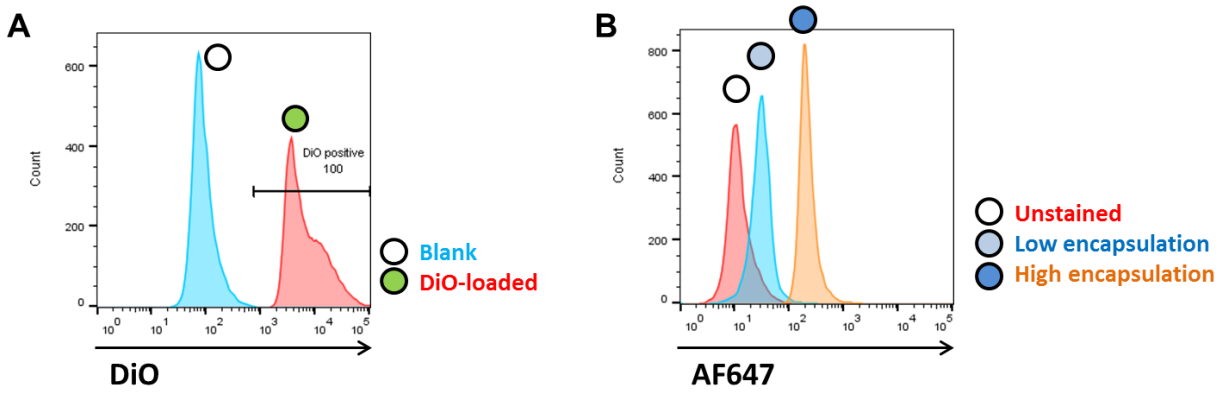

Figure 4-2. Fluorescence detection in nanoparticles.
A. Particles can be separated based on fluorescence from DiO loaded into lipid layers. B. Particles can be separated based on the amount of fluorescently-labeled protein encapsulated within the formulation.

Detection of separate populations

Previous analysis has focused on comparing separate samples analyzed via flow cytometry, whereas we have aimed to utilize this technique for distinguishing and characterizing various populations within mixed samples. In order to establish our capacity to achieve that, we

have prepared MLVs labeled with previously utilized DiO, a different lipophilic dye (DiR, excitation/emission = 600/780), combination of both dyes (DiO and DiR), or no fluorophores at all (blank). As shown, separately ran samples have resulted in distinct populations present in four quadrants on the DiO vs DiR mean fluorescence intensity (MFI) FACS plots (**Fig 4-3A**). As noted in the far-right panel, there is a linear trend suggesting that particles incorporating greater levels of DiO also encapsulate greater amounts of DiR. Considering their multilamellar nature, it is expected for particles of various sizes and with various numbers of bilayers to incorporate varying amounts of the lipophilic dye. However, the amount of incorporation for both dyes should be proportional, which is what is seen in the last panel.

Most importantly, the bottom panel demonstrates that the mixture of the nanoparticle preparations within one sample can be easily separated (**Fig 4-3B**). As shown, the double DiO- and DiR-labeled particles retain the above-described pattern, but the level of fluorescence of individual dyes remains constant. These data strongly support the ability of this technique to identify and analyze fluorescence exhibited by individual nanoparticles.

Nanoparticle FRET

Fluroescence Resonance Energy Transfer (FRET) is a valuable technique utilized to determine the proximity of two fluorophores: donor and acceptor [23]. Samples are excited at a wavelength which can be absorbed by the donor and then emitted at a higher wavelength or directly transferred to the acceptor, which will then emit a photon at an even greater wavelength. Due to requirement for sub 10 nm distances, this technique has been used for examining protein-protein interactions, protein folding, as well as lipid membrane fusion and association. We had decided to determine if our flow cytometry method would be able to detect and analyze the

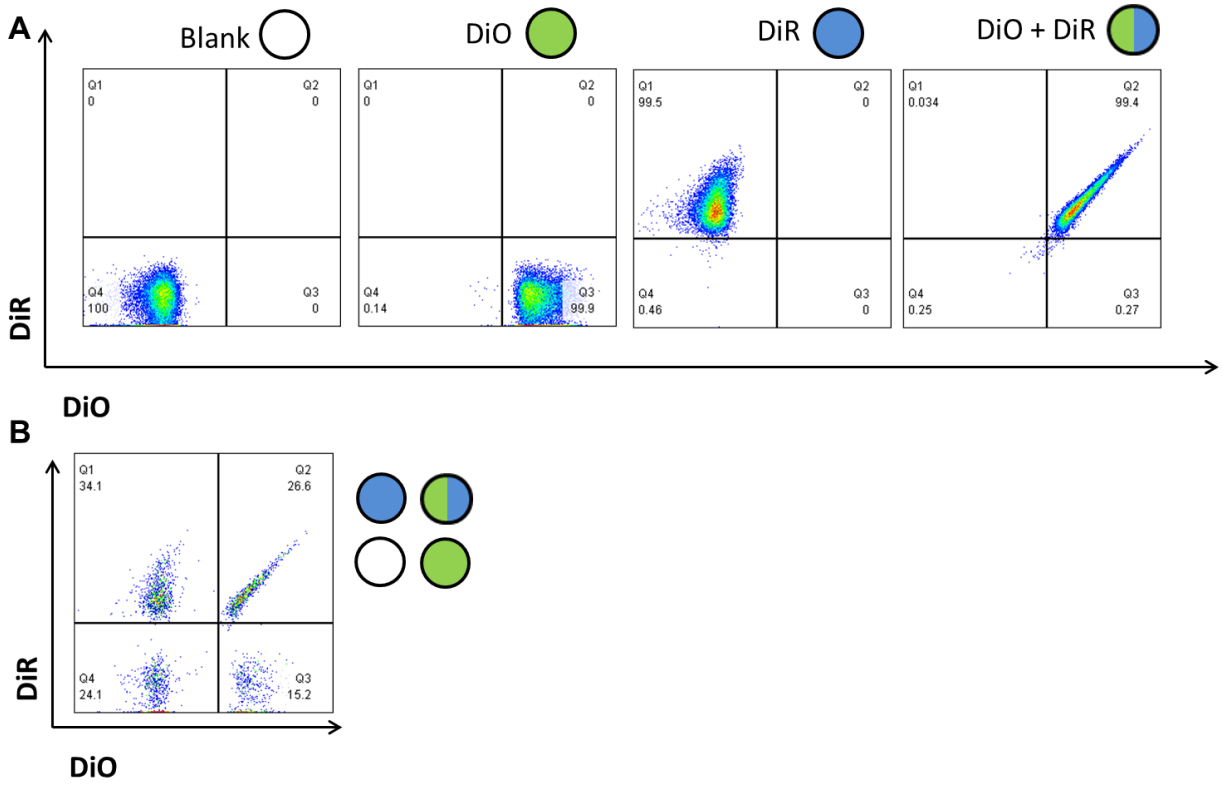

Figure 4-3. Detection of individual nanoparticles.
A. Various fluorophores and fluorophore combinations can be used to label nanoparticle preparations. B. Physical mixture of fluorophore-labeled particles can be separated into distinct populations.

FRET phenomenon providing insight into lipid membrane fusion and association on a single-particle basis rather than with previously utilized bulk analysis [24].

We utilized DiO and DiI dyes, which act as donor and acceptor respectively and sought to determine if the physical mixture of the particles exhibits can be distinguished from one another (**Fig. 4-4A**). While it becomes very apparent that there are two distinct populations of DiO and DiI nanoparticles, incorporation of both dyes within the same formulation does not lead to detection of the signal within quadrant two of the scatter blot as seen before with DiO and DiR. In fact, the DiO + DiI particles exhibit decreased DiO fluorescence and enhanced DiI

signal. The FRET ratio, suggesting the relative amount of fluorescence transfer that takes place, was calculated, where ratio approaching 1 indicates complete transfer and ratio of approaching 0 indicates lack of the FRET effect (**Fig. 4-4B**). We sought to establish the FRET efficiency (the FRET ratio expressed in percent form) via plate- and FACS-based assays, which led to somewhat consistent results (**Fig. 4-4C**). Taken together, the results indicate that fluorophore incorporation into the film or into the unilamellar vesicles prior to fusion allows for complete mixing and efficient fluorescence transfer. Further studies utilizing this technique could focus on the plasma membrane or endosomal membrane fusion events, which had been analyzed via bulk-based approaches, but not via single-particle analysis to our knowledge.

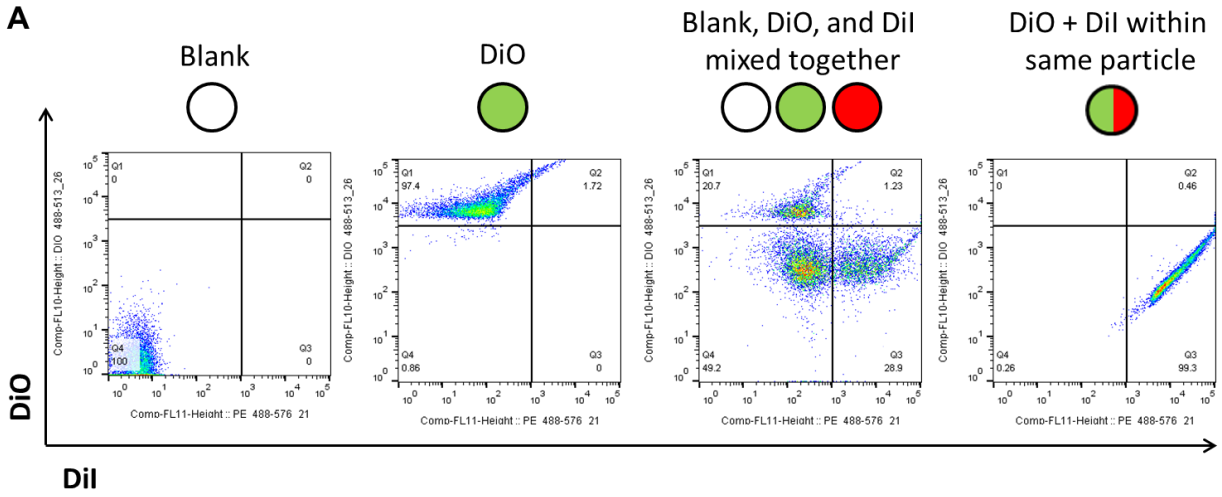

FRET Efficiency	Plate Assay	FACS
DiO particles only	15.8	0.8
Physical mixture of particles	26.0	48.1
Mixed prior to fusion	96.1	94.9
Mixed on film	98.4	98.1

Figure 4-4. Analysis of FRET signal.
A. Individual FACS plots demonstrate individual populations within particle mixtures. B. FRET ratio equation is shown. C. FRET efficiencies were calculated based on fluorophore incorporation method.

Antibody labeling of nanoparticles

As discussed above, establishing a dynamic range in which the signal can be detected, not saturated, and correlated to the dye encapsulation efficiency is important for appropriate characterization. We generated nanoparticles incorporating six different amounts of OVA-AF647, which demonstrated an increasing amount of fluorescence detected by the flow cytometric method (**Fig. 4-5A**).

The downstream goal of this study focuses on the antibody-based approach of this technique on probing the surface antigen amount and configuration (**Fig. 4-5B**). To demonstrate this, DiO-tagged ICMVs were generated containing varying amounts of unlabeled OVA (50, 100, 200, and 400 µg initial hydration). As shown, the DiO content per particle remained quite consistent among the different formulations suggesting lack of aggregation and similar particle size (**Fig. 4-5C**). Analysis of the antibody binding capability, has demonstrated an increasing level of APC signal plateauing past the 200 µg formulation (**Fig 4-5D**). We suspect the binding to be limited due to increased incorporation of OVA on the inside of the particle, considering that the surface may already be protein-saturated at the 200 µg level. In addition, as the surface OVA protein increases in density, it may sterically hinder further antibody binding, resulting in the APC signal to become level.

Finally, as we sought to correlate these results to the bulk analysis, we utilized a plate reader approach for fluorescence detection. It was important to take into consideration that the nanoparticle preparation and the antibody staining process are quite extensive and may lead to unexpected loss through numerous centrifugation and pipetting steps. DiO incorporation was used to serve as a basis for the particle recovery from the overall protocol and thus utilized for normalization of the APC signal. The results demonstrate very similar trends, with the plateauing

effect seen at 200 µg of loaded OVA (**Fig. 4-5E**). Based on this data, the nanoparticle flow cytometry can effectively be correlated with the bulk plate reader-based analysis, while retaining the particle-by-particle measurement capacity.

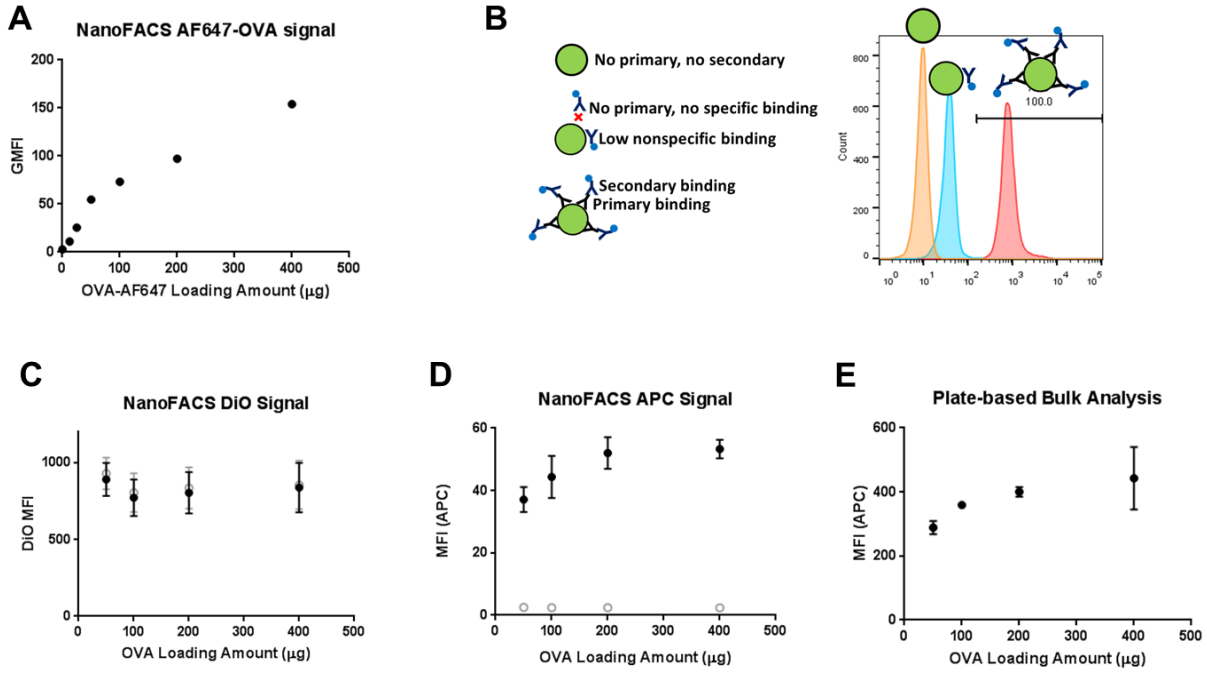

Figure 4-5. Nanoparticle surface antibody binding.
A. NanoFACS analysis of AF647 signal from ICMVs loaded with various amounts of OVA-AF647. B. Schematic and histogram sample results depicting primary and secondary antibody nanoparticle staining. C. DiO MFI for particles loaded with various amounts of OVA. D. Antibody binding intensities analyzed by NanoFACS. E. Antibody binding intensities analyzed by plate-based approach. C and D depict particles that have (black filled circles) and have not (gray open circles) undergone the antibody staining protocol.

Detection of antigens on surface of tumor membrane vesicles

Tumor membrane nanoparticles can be used effectively for elicitation of immune responses as they can effectively traffic to the lymph nodes and be processed by the antigen-presenting cells. In order to enhance the structural understanding of the membrane nanoparticles, we sought to determine surface display of a model antigen, OVA, constructed to contain a transmembrane domain. Additionally, successful binding of anti-OVA antibodies on the particle surface would suggest potential for B cell receptor activation *in vivo*. We have previously observed this effect following B16F10 OVA lysate immunization, where anti-OVA IgG responses were detected in mouse sera (data not shown).

We generated two species of nanoparticles from the lysates of two separate cell lines, B16F10 OVA and CT26. For the purpose of these studies, sonicated lysates contained nano-sized (approx. 180 nm) vesicles with unmodified surface, whereas the PEG-NPs, were slightly smaller (approx. 130 nm) and were modified with surface 5 kDa polyethylene glycol (PEG) chains (data not shown). B16F10 OVA lysates and PEG-NPs were expected to express ovalbumin on the surface, while CT26 served as a negative control.

B16F10 OVA lysate vesicles bound more anti-OVA antibody compared to the CT26 lysate, suggesting antigen-specificity-driven results (**Fig. 4-6**). In addition, PEG-NPs generated from B16F10 OVA cell membranes had higher percentage of OVA-positive vesicles and greater overall MFI compared to CT26 PEG-NPs. However, the drastic difference between B16F10 OVA lysates and the PEG-NPs, suggests a markedly decreased OVA accessibility on PEG-NPs surface. Rather than antigen loss, we expect the PEG layer to play an important role in generating unfavorable interactions with antibodies and provide steric hindrance for the access to the binding site. These results correlate with our observations that PEG-NPs may not be ideal

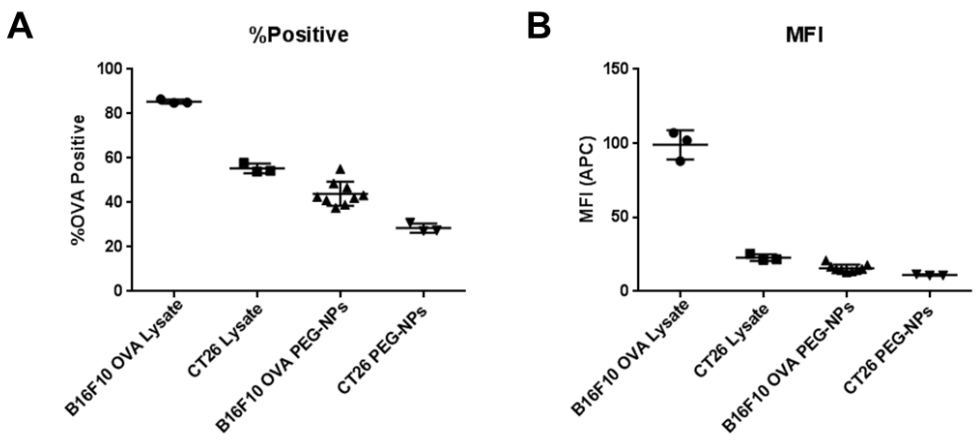

Figure 4-6. NanoFACS analysis of OVA-expressing B16F10 land control CT26 lysates and PEG-NPs.
A. Percentage of OVA-positive vesicles in the membrane preparations. B. Mean fluorescence intensity of OVA in membrane preparations.

candidates for eliciting humoral responses against surface antigens in tumor-bearing mice immunized with this formulation, although they can lead to efficient CTL activation (data not shown). Taking all of these data together, we have demonstrated that antigen on the surface of membrane nano-vesicles can be detected by antibody binding and flow cytometric analysis on a particle-by-particle basis. Further focus can take into account expression of immunosuppressive ligands such as FasL and PD-L1 on tumor membrane vesicles or analysis of membranes sourced from other types of cells, such as dendritic cells.

HCV E2 Antibody Screen

Demonstrating appropriate antigen surface display *in vitro* can allow for examination of potential antibody-generating responses *in vivo*. If done in a high-throughput manner, as in the case of flow cytometry, various formulations can be tested and optimized saving on the costs,

labor, and animal use involved with pre-clinical studies. To establish, whether our nanoparticle flow cytometry can be utilized for this purpose, we employed the use of two different particle systems: ICMV and NTA ICMV. ICMV platform was chosen for its ability to display antigen on their surface and stability, whereas the experimental NTA ICMV variant preparation method, exploiting NTA-tagged lipid interaction with his-tagged protein, allowed for enhanced loading capacity and directed surface display.

Hepatitis C virus (HCV) contains rapidly mutating variable regions, which act to generate antibody responses lacking broadly neutralizing characteristics. Removal of variable regions as well as proper antigen display is believed to direct antibody responses against constant regions, thus allowing for cross-strain activity. In order to test this approach and validate the ability of our nanoparticle formulations to bind to broadly neutralizing antibodies, we generated formulations displaying E2 viral membrane protein. Two constructs with or without the variable regions were utilized (E2 and E2c, respectively) in two variant forms each to contain or exclude the poly-histidine tag. E2 and E2c were encapsulated in standard ICMVs, while his-E2 and his-E2c were incorporated into NTA ICMVs to allow for NTA-his interaction to promote surface binding. Once the particles were generated with the use of fluorescent dye (DiD), they underwent antibody staining process utilizing several conditions summarized in **Table 1**. Primary stain was set overnight at 4°C followed by washing, 1 hour secondary staining, further washing, and incubation on ice prior to sample analysis.

Overall, we did not see extensive differences in the binding of antibodies to the particle surface (**Fig. 4-7A**). Surprisingly, NTA ICMVs, which had greater overall encapsulation efficiency as well as higher surface protein display (data not shown), did not exhibit greater antibody binding compared to standard ICMVs. We suspect that the potential tight packing of

Condition	Primary	Secondary	Role
DiD+	None	None	Negative Control
Isotype	Isotype	anti-Human IgG-PE	Isotype Control
AR3A	AR3A	anti-Human IgG-PE	Broadly Neutralizing
AR2A	AR2A	anti-Human IgG-PE	Non-broadly Neutralizing
AR1B	AR1B	anti-Human IgG-PE	Non-broadly Neutralizing
HCV1	HCV1	anti-Human IgG-PE	Broadly Neutralizing

Table 1. Antibody panel used for characterization of E2 protein-loaded ICMVs and NTA-ICMVs.

the protein may produce steric hindrance and prevent effective antibody binding. In addition, NTA-his interaction, which is expected to be the driving force for the antigen retention on the particle surface, is not particularly strong, thus prolonged incubation and multiple washes may lead to overall antigen loss during the staining process.

E2-his and E2c-his NTA ICMVs were tested *in vivo* by administration of prime immunization and two boost doses three weeks apart. Antibody responses were measured using standard ELISA approach demonstrating that E2-his had generated slightly increased overall humoral responses in weeks 6 and 9 (**Fig. 4-7B**). In addition sera obtained from both groups during week 9 were utilized in an *in vitro* neutralization assay, where HCV pseudo particles were incubated in cell culture with or without the sera antibodies. E2-his NTA ICMVs led to increased neutralization of the autologous H77 HCV strain compared to E2c-his, whereas both led to immune responses with mild neutralization activity against the heterologous UKN1b12.6 strain (**Fig. 4-7C**).

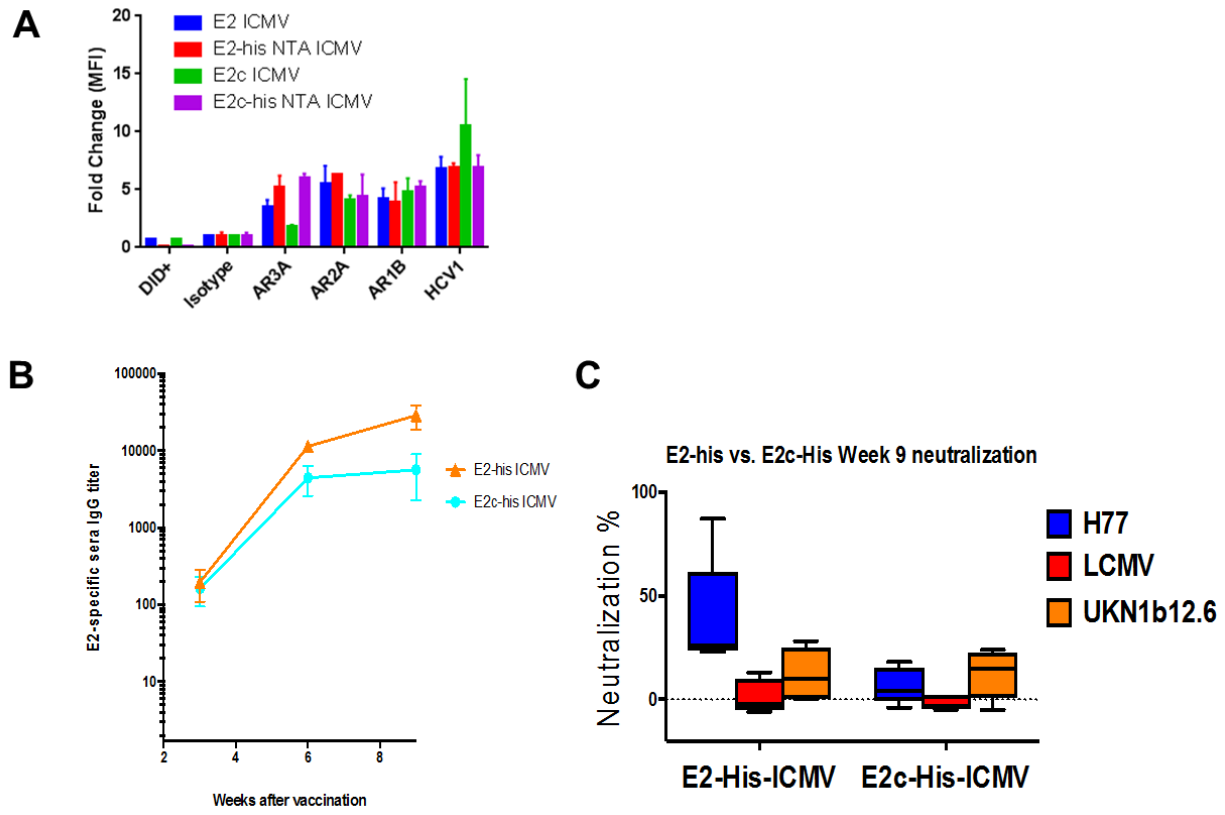

Figure 4-7. HCV NTA ICMV flow cytometry analysis.
A. Fold-change in MFI over isotype antibody binding for ICMVs and NTA ICMVs is shown. B. E2-specific antibody titers for E2-his and E2c-his NTA ICMVs at weeks 3, 6, and 9 post-immunization were measured from sera. C. Week 9 neutralization assay against autologous HCV strain (H77), irrelevant control (LCMV), or heterologous HCV strain (UKN1b12.6) was performed *in vitro*.

The animal data alone provides insight into the types of responses that are generated by these formulations. While both E2-his and E2c-his led to strong humoral responses, the presence of greatly immunogenic variable regions 1 and 2 on the E2-his construct may account for increased antibody titers and more effective autologous virus neutralization. We had expected that the lack of the variable regions on E2c would direct the responses towards more effective broadly neutralizing antibody production, but similar neutralization efficacy was seen. The

nanoparticle flow cytometry data supports these results, by demonstrating that both E2-his and E2c-his are capable of binding the broadly neutralizing antibodies AR3A and HCV1 to the same degree, thus validating the similar level of broadly neutralizing responses. Further work is currently underway to examine E2c ICMVs (**Fig. 4-7A**, green bars), which show promising display of the HCV1 epitope. We hope that these methodologies can be utilized in the future to demonstrate correlation with the *in vivo* immunizations, thus allowing for this to become a predictive tool saving on costs, labor, and use of animals.

Nanoparticle aggregation in FBS

Controlled release is a major appeal to the use of nanoparticles in the delivery of therapeutics, as it may reduce the necessity for frequent administrations reducing costs and patient discomfort (in the case of injectables) [25, 26]. Standard release studies are commonly performed with the use of media containing fetal bovine serum (FBS) to mimic the *in vivo* conditions. We aimed to tease out the kinetics of antigen release from ICMVs as well as to determine if antigen loss occurs through loss of lipid bilayers or complete degradation of the particles.

Unfortunately, the analysis has demonstrated that while particles may remain quite stable in PBS, they aggregate rapidly and to a great extent in the presence of FBS or even RPMI. This behavior can be inferred from the markedly increased level of DiO and AF647 fluorescence and change in the SSC properties of the particles (**Fig 4-8**), whereas it was expected to exhibit a decrease as the particles were degraded and antigen was released. Considering that no noticeable aggregation or precipitation was observed visually, these large particulates may go unseen during standard stability and release studies, resulting in potentially skewed results. Further work with

other types of formulations and other approaches for aggregation determination is required to fully characterize and validate these methods.

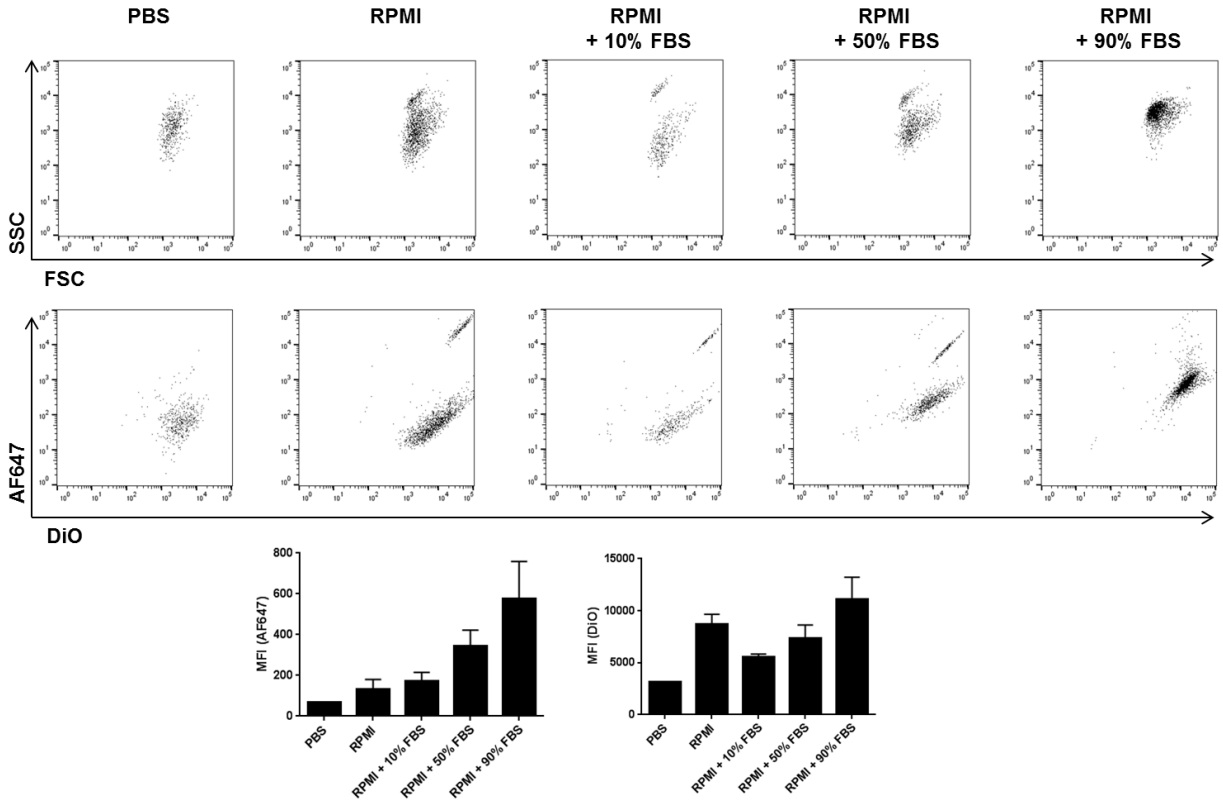

Figure 4-8. Particle stability testing.
Particles were incubated with RPMI with or without any FBS content and demonstrate nanoparticle aggregation *in vitro* via increased SSC as well as AF647 and DiO signals. Individual FACS scatter plots are shown as well as the summary mean ± SD.

4.5. Conclusions

This study has focused on the development of methods necessary for analysis of surface antigen display of nanoparticles and membrane-based biologic vesicles. Our work allowed for detecting antigens presented on synthetic lipid-based nanoparticles across a dynamic range by utilizing fluorophore-tagged proteins or through an antibody-staining procedures. In addition, these methods allowed for probing of model antigen presentation on B16F10 OVA melanoma membrane vesicles, confirming their expression, compared to negative control CT26. Finally, we examined a library of antibodies with a panel of nanoparticles displaying two antigen variants. Utilizing the high-throughput capabilities of flow cytometry, we were able to demonstrate small differences within antigens, which led to more complete interpretation and understanding of neutralization capabilities of *in vivo*-generated antibody responses. With the increased use of nanoparticles for therapeutic use and in particular preparation of vaccine, there is a growing need for appropriate tools necessary for characterization and optimization. We believe that, while there may be a lot of room for improvement, nanoparticle flow cytometry can provide important information about the amount, display, and antibody-binding capabilities of antigens on particle surface.

4.6. References

1. Jiang, H., Q. Wang, and X. Sun, *Lymph node targeting strategies to improve vaccination efficacy.* Journal of Controlled Release, 2017. **267**: p. 47-56.

2. Sahdev, P., L. Ochyl, and J. Moon, *Biomaterials for Nanoparticle Vaccine Delivery Systems.* Pharmaceutical Research, 2014: p. 1-20.

3. Moon, J.J., B. Huang, and D.J. Irvine, *Engineering nano- and microparticles to tune immunity.* Adv Mater, 2012. **24**(28): p. 3724-46.

4. Moon, J.J., et al., *Antigen-Displaying Lipid-Enveloped PLGA Nanoparticles as Delivery Agents for a Plasmodium vivax Malaria Vaccine.* Plos One, 2012. **7**(2).

5. Moon, J.J., et al., *Enhancing humoral responses to a malaria antigen with nanoparticle vaccines that expand T-fh cells and promote germinal center induction.* Proceedings of the National Academy of Sciences of the United States of America, 2012. **109**(4): p. 1080-1085.

6. Murdock, R.C., et al., *Characterization of nanomaterial dispersion in solution prior to In vitro exposure using dynamic light scattering technique.* Toxicological Sciences, 2008. **101**(2): p. 239-253.

7. Filipe, V., A. Hawe, and W. Jiskoot, *Critical Evaluation of Nanoparticle Tracking Analysis (NTA) by NanoSight for the Measurement of Nanoparticles and Protein Aggregates.* Pharmaceutical Research, 2010. **27**(5): p. 796-810.

8. Crawford, R., et al., *Analysis of lipid nanoparticles by Cryo-EM for characterizing siRNA delivery vehicles.* International Journal of Pharmaceutics, 2011. **403**(1-2): p. 237-244.

9. Bilati, U., E. Allemann, and E. Doelker, *Nanoprecipitation versus emulsion-based techniques for the encapsulation of proteins into biodegradable nanoparticles and process-related stability issues.* Aaps Pharmscitech, 2005. **6**(4).

10. Desai, K.G.H. and S.P. Schwendeman, *Active self-healing encapsulation of vaccine antigens in PLGA microspheres.* Journal of Controlled Release, 2013. **165**(1): p. 62-74.

11. van der Pol, E., et al., *Particle size distribution of exosomes and microvesicles determined by transmission electron microscopy, flow cytometry, nanoparticle tracking analysis, and resistive pulse sensing.* Journal of Thrombosis and Haemostasis, 2014. **12**(7): p. 1182-1192.

12. Pasalic, L., et al., *Enumeration of extracellular vesicles by a new improved flow cytometric method is comparable to fluorescence mode nanoparticle tracking analysis.* Nanomedicine-Nanotechnology Biology and Medicine, 2016. **12**(4): p. 977-986.

13. Danielson, K.M., et al., *Diurnal Variations of Circulating Extracellular Vesicles Measured by Nano Flow Cytometry.* Plos One, 2016. **11**(1).

14. van der Vlist, E.J., et al., *Fluorescent labeling of nano-sized vesicles released by cells and subsequent quantitative and qualitative analysis by high-resolution flow cytometry.* Nature Protocols, 2012. **7**(7): p. 1311-1326.

15. Nolte-'t Hoen, E.N.M., et al., *Quantitative and qualitative flow cytometric analysis of nanosized cell-derived membrane vesicles.* Nanomedicine-Nanotechnology Biology and Medicine, 2012. **8**(5): p. 712-720.

16. Abusamra, A.J., et al., *Tumor exosomes expressing Fas ligand mediate CD8(+) T-cell apoptosis.* Blood Cells Molecules and Diseases, 2005. **35**(2): p. 169-173.

17. Ricklefs, F.L., et al., *Immune Evasion Mediate by PD-1 on Glioblastoma Derived Extracelullar Vesicles.* Neuro-Oncology, 2017. **19**: p. 50-50.

18. Kosaka, N., et al., *Versatile roles of extracellular vesicles in cancer.* Journal of Clinical Investigation, 2016. **126**(4): p. 1163-1172.

19. Corti, D. and A. Lanzavecchia, *Broadly Neutralizing Antiviral Antibodies*, in *Annual Review of Immunology, Vol 31*, D.R. Littman and W.M. Yokoyama, Editors. 2013. p. 705-742.

20. Moon, J.J., et al., *Interbilayer-crosslinked multilamellar vesicles as synthetic vaccines for potent humoral and cellular immune responses.* Nature Materials, 2011. **10**(3): p. 243-51.

21. Prentoe, J., et al., *Hypervariable region 1 shielding of hepatitis C virus is a main contributor to genotypic differences in neutralization sensitivity.* Hepatology, 2016. **64**(6): p. 1881-1892.

22. Ochyl, L.J. and J.J. Moon, *Whole-animal Imaging and Flow Cytometric Techniques for Analysis of Antigen-specific CD8+T Cell Responses after Nanoparticle Vaccination.* Jove-Journal of Visualized Experiments, 2015(98).

23. Jares-Erijman, E.A. and T.M. Jovin, *FRET imaging.* Nature Biotechnology, 2003. **21**(11): p. 1387-1395.

24. Marsden, H.R., I. Tomatsu, and A. Kros, *Model systems for membrane fusion.* Chemical Society Reviews, 2011. **40**(3): p. 1572-1585.

25. Elzoghby, A.O., W.M. Samy, and N.A. Elgindy, *Albumin-based nanoparticles as potential controlled release drug delivery systems.* Journal of Controlled Release, 2012. **157**(2): p. 168-182.

26. Cheng, R., et al., *Dual and multi-stimuli responsive polymeric nanoparticles for programmed site-specific drug delivery.* Biomaterials, 2013. **34**(14): p. 3647-3657.

Chapter 5: Conclusions and Future Directions

This thesis presents efficacious use of cell membranes for elicitation of immune responses directed against model antigen, ovalbumin, in a therapeutic cancer vaccination and adoptive cell transfer settings. Additionally, nanoparticle flow cytometry methodology has been developed for use with synthetic vaccine vehicles, but has also been shown to be applied for simple cell membrane vesicle analysis. Taken together, these data support previous progress and further advancements in the field of immunotherapy. However, there is room for improvement and more work is necessary in order to fully validate these results and establish working mechanisms for our methodology.

Cell lysate-based approaches to cancer immunotherapy had been studies for decades with limited successes in the clinic and the work demonstrated here provides a feasible therapy for translation and elicitation of cytotoxic T lymphocyte responses. PEG-NPs formulated using our protocol were able to efficiently traffic to the secondary lymphoid organs, which is the site of action for vaccines, and promote antigen-specific T cell expansion. We had shown that combination with PD-1 immune checkpoint blockade led to synergistic effects and promoted survival and rechallenge protection in 63% of mice compared to 13% efficacy with control therapies.

Future direction for the tumor cell membrane vaccination focuses on the use of more clinically relevant models outside of OVA-expressing cancers. One of the primary examples

would be CT26, colorectal murine tumor cell line, which expresses membrane viral antigen gp70 with an immunogenic CD8 T cell epitope, AH-1. While still not ideal, further development in this model would allow for optimization and potential combination with other immunotherapeutic approaches such as anti-CTLA4 inhibition, which is another subset of immune check point blockade, working through a different mechanism [1, 2]. While PD-1 allows for existing T cell immunity to target and kills cancerous cells in the immunosuppressive tumor microenvironment, CTLA4 blockade allows for targeting of new epitopes and expansion of another subset of T cell clones, prompting fresh responses [3].

Another aspect of targeted T cell responses focuses on tumor-associated antigens (TAAs), which had been extensively identified and characterized in melanoma. The use of the parental B16F10 cell line (lacking the model antigen OVA) would allow for studying responses against endogenous proteins. Interestingly, common melanoma antigens, against which endogenous CTLs had been identified, are often associated with the plasma or the melanosome membrane including gp100, NY-ESO-1, TRP2, Melan-A/MART1, and tyrosinase [4-8]. This observation has prompted our hypothesis, in which naturally dying or plasma membrane-shedding tumor cells can elicit endogenous responses against TAAs, which could potentially be boosted through PEG-NPs or other vaccination approaches. However, the tetramer staining method examining peripheral blood lymphocytes we have utilized in these studies may not provide sufficient response detection. Further studies would focus on analysis of T cells within the tumor or tumor-draining lymph nodes with more sensitive techniques, such as ELISpot following expansion of antigen-specific T cells via peptide stimulation. These would be of particular importance for current work and progress being made in the field of neo-antigens [9]. Demonstrating endogenous responses toward membrane-associated neo-antigens may provide

vaccine targets for peptide-based therapies, as expanding existing cell populations rather than generating new clones, may yield more rapid and effective immune response, quickly halting further tumor progression and eliminating metastases.

At the same time, focus on cancer stem cell (CSC) populations and generating immune responses towards them would be of great benefit, as it would allow targeting the highly-proliferative, chemotherapy-resistant, and metastasis-prone cell subset [10]. Overall debulking of tumors can be achieved through radiation or surgery, but further eradication of microscopic metastases or relapsing tumors proves quite challenging. In the past, CSC-directed DC-based vaccine was shown to be more efficacious at decreasing tumor burden and number of metastases in head and neck cancer and melanoma murine models, respectively [11]. Thus, eliciting of strong immune responses *in situ* against CSCs may provide an additional avenue for cancer therapy.

Similar direction can be utilized for the use of dendritic cell membranes for vaccination purposes. We had demonstrated that DC-MVs work very efficiently at expanding T cells as well as activating immature dendritic cells *in vitro*. In addition, they were capable of expanding and maintaining adoptively transferred antigen-specific T cells and boosting endogenous responses in tumor-bearing animals. While very promising, further work is necessary in order to determine dosing regiments necessary for optimal T cell stimulation, thus preventing over-activation, and characterization of differentiation into long term memory T cells. Other approaches focusing on the use of DC-MVs purely as adjuvants or supportive platform for T cell therapies could also be explored. For example, administration of DC-MVs intratumorally may provide stimulation via CD80/86-CD28 signaling similar to what was seen in the *in vitro* T cell experiments, leading to

breaking of the immunosuppressive microenvironment and enhancement of endogenous T cell responses.

Characterization of nanoparticles through flow cytometry provides a very attractive, high-throughput approach to screening and development of various therapies. Our studies focused primarily on the characterization of lipid-based vehicle system, NTA ICMV, and allowed for probing of antigenic epitopes on the surface-bound proteins with the use of monoclonal antibodies. These results allowed for better understanding of the humoral responses that were observed *in vivo* following immunization. We also suggest that in the future, this technique may be utilized as a screening and predictive tool for selection of optimal formulations, thus limiting the amount of empirical experiments utilizing large number of animals and extensive costs and labor. Additionally, we would like to focus on characterization of other nanoparticle-based approaches, such as simple liposomes and PLGA particles in order to further expand the scope of this technique. Finally, referring back to the cell membrane-based therapies, we had done limited characterization that has focused on the detection of antigen on the membrane surface. Further work could examine presence of various ligands (especially integrins) that had been linked in the past to localization and association with specific cell targets [12, 13]. In addition, functional exosomal ligands had been recently detected and reported on, such as FasL and PD-1L on exosomes and cell membrane vesicles shed by tumor cells resulting in decreased T cell function, thus providing another set of targets that could be identified via high-throughput flow cytometric analysis [14, 15].

While the proposed studies provide an ambitious set of goals, the work demonstrated in this thesis had established a solid foundation for further research. Methodology developed through these experiments in generating and characterizing cell membrane vesicles can be

utilized for a variety of different studies. At the same time, the therapeutic responses that we had seen, add further evidence to the current notion that biologic- and immunotherapy-based approaches may bring in a new era of treatments against cancer, which has plagued the developed world for the past couple of decades.

References

1. Chambers, C.A., et al., *CTLA-4-mediated inhibition in regulation of T cell responses: Mechanisms and manipulation in tumor immunotherapy.* Annual Review of Immunology, 2001. **19**: p. 565-594.

2. Egen, J.G., M.S. Kuhns, and J.P. Allison, *CTLA-4: new insights into its biological function and use in tumor immunotherapy.* Nature Immunology, 2002. **3**(7): p. 611-618.

3. Chen, L.P. and X. Han, *Anti-PD-1/PD-L1 therapy of human cancer: past, present, and future.* Journal of Clinical Investigation, 2015. **125**(9): p. 3384-3391.

4. Gnjatic, S., et al., *NY-ESO-1: review of an immunogenic tumor antigen.* Adv Cancer Res, 2006. **95**: p. 1-30.

5. Khong, H.T. and S.A. Rosenberg, *Pre-existing immunity to tyrosinase-related protein (TRP)-2, a new TRP-2 isoform, and the NY-ESO-1 melanoma antigen in a patient with a dramatic response to immunotherapy.* J Immunol, 2002. **168**(2): p. 951-6.

6. Liu, G.T., et al., *Molecular and functional analysis of tyrosinase-related protein (TRP)-2 as a cytotoxic T lymphocyte target in patients with malignant glioma.* Journal of Immunotherapy, 2003. **26**(4): p. 301-312.

7. Kwon, B.S., et al., *ISOLATION AND SEQUENCE OF A CDNA CLONE FOR HUMAN TYROSINASE THAT MAPS AT THE MOUSE C-ALBINO LOCUS.* Proceedings of the National Academy of Sciences of the United States of America, 1987. **84**(21): p. 7473-7477.

8. Kawakami, Y., et al., *IDENTIFICATION OF A HUMAN-MELANOMA ANTIGEN RECOGNIZED BY TUMOR-INFILTRATING LYMPHOCYTES ASSOCIATED WITH IN-VIVO TUMOR REJECTION.* Proceedings of the National Academy of Sciences of the United States of America, 1994. **91**(14): p. 6458-6462.

9. Schumacher, T.N. and R.D. Schreiber, *Neoantigens in cancer immunotherapy.* Science, 2015. **348**(6230): p. 69-74.

10. Clevers, H., *The cancer stem cell: premises, promises and challenges.* Nature Medicine, 2011. **17**(3): p. 313-9.

11. Ning, N., et al., *Cancer Stem Cell Vaccination Confers Significant Antitumor Immunity.* Cancer Research, 2012. **72**(7): p. 1853-1864.

12. Ha, D., N. Yang, and V. Nadithe, *Exosomes as therapeutic drug carriers and delivery vehicles across biological membranes: current perspectives and future challenges.* Acta Pharm Sin B, 2016. **6**(4): p. 287-96.

13. Hoshino, A., et al., *Tumour exosome integrins determine organotropic metastasis.* Nature, 2015. **527**(7578): p. 329-35.

14. Abusamra, A.J., et al., *Tumor exosomes expressing Fas ligand mediate CD8(+) T-cell apoptosis.* Blood Cells Molecules and Diseases, 2005. **35**(2): p. 169-173.

15. Ricklefs, F.L., et al., *Immune Evasion Mediate by PD-1 on Glioblastoma Derived Extracelullar Vesicles.* Neuro-Oncology, 2017. **19**: p. 50-50.

Appendix: Whole-animal imaging and flow cytometric techniques for analysis of antigen-specific CD8+ T cell responses after nanoparticle vaccination

A.1 Introduction

Traditional vaccine development mainly employed the empirical approach of trial-and-error. However, with the recent development of a wide array of biomaterials and discovery of molecular determinants of immune activation, it is now possible to rationally design vaccine formulations with biophysical and biochemical cues derived from pathogens [1, 2]. In particular, various particulate drug delivery platforms have been examined as vaccine carriers as they can be co-loaded with subunit antigens and immunostimulatory agents, protect vaccine components from degradation, and enhance their co-delivery to antigen presenting cells (APCs) residing in lymph nodes (LNs), thus maximizing immune stimulation and activation[3-5]. In this report, we describe the synthesis of a "pathogen-mimicking" nanoparticle system, termed interbilayer-crosslinked multilamellar vesicles (ICMVs), which have been previously demonstrated as a potent vaccine platform for elicitation of robust cytotoxic T lymphocyte (CTL) and humoral immune responses in both systemic and mucosal tissue compartments [6-9]. Here, using ICMVs

This chapter has been adapted with permission from JoVE: Whole-animal imaging and flow cytometric techniques for analysis of antigen-specific CD8+ T cell responses after nanoparticle vaccination by Ochyl LJ and Moon JJ

as a model vaccine nanoparticle system, we describe methods for characterization of vaccine nano-formulations, such as particle size and zeta potential measurements, and tracking of particle draining to LNs utilizing confocal imaging of cryosectioned tissues[7]. In addition, we present a whole-animal imaging-based method of analyzing expansion of CTL responses in mice after adoptive transfer of luciferase-expressing antigen-specific CD8+ T cells [9, 10]. Finally, we describe tetramer staining of peripheral blood mononuclear cells (PBMCs) for longitudinal quantification of endogenous T cell responses in mice vaccinated with nanoparticles [6, 9].

ICMVs are a lipid-based nanoparticle formulation synthesized by controlled fusion of simple liposomes into multilamellar structures, which are then chemically stabilized by cross-linking maleimide-functionalized phospholipid head groups within lipid layers with dithiol crosslinkers [6]. Once ICMVs are synthesized, a small fraction of nanoparticles can be used to determine particle size and zeta potential (i.e. surface charge of particles) with a dynamic light scattering (DLS) system and a zeta potential analyzer. DLS measures changes in light scattering in particle suspension, which allows determination of the diffusion coefficient and the hydrodynamic size of particles [11]. Achieving consistent particle size from batch to batch synthesis is critical since particle size is one of the major factors influencing lymphatic draining of vaccine particles to draining lymph nodes (dLNs) and subsequent cellular uptake by APCs[12, 13]. In addition, zeta potential can be obtained by measuring the particle velocity when an electric current is applied, which allows determination of the electrophoretic mobility of particles and particle surface charge [11]. Ensuring consistent zeta potential measurement of particles is important since surface charge of particles determines colloidal stability, which has direct impact on particle dispersion during storage and after *in vivo* administration [14, 15]. In order to track the particle localization to dLNs, ICMVs can be labeled with desired fluorophores including

lipophilic dyes and covalently-tagged antigens. Following immunization, mice can be euthanized at various time points, dLNs resected, cryosectioned, and analyzed with confocal microscopy. This technique allows for visualization of lymphatic draining of both the nanoparticle vaccine carriers and the antigen to dLNs. The tissue sections can additionally be stained with fluorescently labeled antibodies and utilized to obtain more information, such as types of cells associated with the antigen and formation of germinal centers as we have shown previously [7].

Once the particle synthesis is optimized and trafficking to the dLNs confirmed, it is important to validate elicitation of *in vivo* CTL expansion. In order to analyze elicitation of antigen-specific CD8+ T cells in response to nanoparticle vaccination, we have utilized a model antigen, ovalbumin (OVA), with $OVA_{257-264}$ peptide (SIIFNEKL) immunodominant CD8+ T cell epitope, which allows detailed immunological analyses of antigen-specific T cell responses for initial vaccine development[16, 17]. In particular, to interrogate the dynamics of expansion and migration of antigen-specific CD8+ T cells, we have generated a double-transgenic mouse model by crossing firefly luciferase-expressing transgenic mice (Luc) with OT-I transgenic mice with T-cell receptor (TCR) specific for SIINFEKL on CD8+ T cells. From these OT-I/Luc mice, luciferase-expressing, OT-I CD8+ T cells can be isolated and prepared for adoptive transfer into naïve C57BL/6 mice. Once seeded, successful immunization with OVA-containing nanoparticles will result in expansion of the transferred T cells, which can be tracked by monitoring bioluminescence signal with an *in vivo* imaging system (IVIS) [9, 10]. This non-invasive whole-body imaging technique have been used with other viral or tumor antigens in the past [18-20], revealing processes involved in T cell expansion in lymphoid tissues and dissemination to peripheral tissues in a longitudinal manner over an extended period.

Complementary to analysis of adoptively transferred antigen-specific CD8+ T cells, endogenous T cell responses post vaccination can be examined with a major histocompatibility complex (MHC) tetramer assay [21], in which peptide-MHC tetramer molecule, consisting of four fluorophore-tagged MHC-class I (MHC-I) loaded with peptide epitope, is employed to bind TCR and label CD8+ T cells in an antigen-specific manner. MHC tetramer assay can be performed either in terminal necropsy studies to identify antigen-specific CD8+ T cells in lymphoid and peripheral tissues or in longitudinal studies with peripheral blood mononuclear cells (PBMCs) obtained from serial blood draws. After staining lymphocytes with peptide-MHC tetramer, flow cytometry analysis is performed for detailed analyses on the phenotype of CTLs or quantification of their frequency among CD8+ T cells.

A.2 Protocol

All experiments described in this protocol were approved by the University Committee on Use and Care of Animals (UCUCA) at University of Michigan and performed according to the established policies and guidelines.

1. Synthesis and characterization of ICMVs co-loaded with protein antigen and adjuvant molecules.

1.1. Mix 1:1 molar ratio of 1,2-dioleoyl-*sn*-glycero-3-phosphocholine (DOPC) and 1,2-dioleoyl-sn-glycero-3-phosphoethanolamine-N-[4-(p-maleimidophenyl) butyramide] (MPB) in chloroform, keeping the total lipid amount at 1.26 μmol per batch (i.e. 500 μg of DOPC and 630 μg of MPB) in a 20 ml glass vial.

1.2. Lipophilic drugs, such as monophosphoryl lipid A (MPLA) or lipophilic dyes (*e.g.* DiD), can be added to the lipid solution at desired concentration. Thoroughly remove the organic solvent by purging with extra dry nitrogen gas or by placing the samples under vacuum overnight.

1.3. Hydrate the lipid film using 200 µl of 10 mM bis-trip propane (BTP, pH 7.0) containing water-soluble drugs (e.g. protein antigens). Vortex for 10 sec every 10 min for 1 hr at RT.

1.4. Transfer the contents from the glass vial into a 1.5 ml microcentrifuge tube, place samples in an ice-water bath, and sonicate continuously for 5 min using 40% intensity setting on a 125 W/20 kHz probe-tip sonicator.

1.5. Add 4 µl of 150 mM dithiothreitol (DTT) to each batch (working concentration 2.4 mM), vortex, and briefly centrifuge using a tabletop microcentrifuge.

1.6. Add 40 µl of 200 mM $CaCl_2$ and mix with the pipette (working concentration 33 mM). Incubate samples at 37 °C for 1 hr to allow crosslinking of MPB-containing lipid layers with DTT.

1.7. Centrifuge samples at 20,000 x g for 15 min, remove the supernatant, and resuspend in 200 µl of ddiH_2O.

1.8. Repeat step 1.7 and centrifuge again after the second ddiH_2O wash.

1.9. Prepare 10 mg/ml of 2 kDa polyethylene glycol-thiol (PEG-SH) in ddiH_2O. Resuspend each ICMV sample in 100 µl of PEG-SH solution and incubate at 37 °C for 30 min.

1.10. Perform two ddiH_2O washes (step 1.7) and resuspend the final ICMV pellet in PBS and store at 4 °C. Prior to use, mix the ICMV suspension, as particles may settle to the bottom after prolonged storage.

1.11. For characterization of particles, remove a small aliquot (~10%) of ICMVs from each batch and dilute individually in a total volume of 1 ml of ddiH_2O. Place a single sample in a zetasizer cell and measure particle size, polydispersity index, and zeta potential of the samples using dynamic light scattering and zeta potential measuring system (according to manufacturer's protocol).

2. Examination of lymph node draining of fluorescence-tagged ICMVs with confocal microscopy

2.1. Preparation of ICMVs loaded with fluorophore-tagged antigen and lipophilic fluorescent dye

2.1.1. Prepare fluorophore-tagged protein, such as ovalbumin reacted with Alexa Fluor 555-succinimidyl ester according to the manufacturer's instruction.

2.1.2 To prepare ICMVs tagged with fluorophore in the lipid shell, add lipophilic fluorescent dye, (e.g. 1, 1′ Dioctadecyl 3,3,3′,3′ Tetramethylindodicarbocyanine, (DiD)) during preparation of the lipid film (Step 1.2) at 0.05% molar lipid amount. For lipid film hydration (Step 1.3), use buffer containing fluorophore-tagged antigen, and complete ICMV synthesis as outlined in steps 1.4.-1.11.

2.2. Subcutaneous administration of nanoparticles at tail base

2.2.1. Anesthetize mouse using a controlled flow vaporizer equipped with an induction chamber utilizing 3% isoflurane and 1.5 L/min of oxygen flow according to an IACUC approved animal protocol. Once the mouse is unconscious, perform the following steps quickly prior to the anesthesia wearing off to allow optimal access to the site of the injection and minimize discomfort to the animal. Alternatively, use a proper fitting nose cone to maintain anesthesia. If mice are anesthetized for longer than 5 min, apply eye lube necessary to minimize irritation after the procedure.

2.2.2. Spray the base of the tail with 70% ethanol to sterilize and wet the fur. Part the wet hair to expose a small patch of visible skin, which can be used to visualize the needle under the skin.

2.2.3. Prepare particle injection suspension containing desired amount of antigen and adjuvant per 100 μl of vaccination dose in PBS (e.g. 10 μg OVA and 0.3 μg MPLA per 100 μl of injection dose has been used in the past[6, 9]).

2.2.4. Draw the particle suspension into a syringe with a 27-29G needle and insert the needle at the base of the tail with the bevel facing up (assuring to avoid the tail vein) and inject 50 μl of the particle suspension[22].

2.2.5. Wait a few seconds for pressure to equalize to prevent excessive back-flow and pull the needle out. Repeat the injection on the other side of the tail base to target both draining inguinal LNs.

2.3. Preparation of lymph node cryosections and examination with confocal microscopy.

2.3.1. Euthanize the mouse with CO_2 asphyxiation, followed by induced pneumothorax according to an IACUC approved animal protocol. Extract inguinal LNs according to protocol demonstrated in Bedoya, et al.[23] and wash out the blood by placing the tissues in 1 ml of 4°C PBS.

2.3.2. Absorb the PBS from the tissues with Kimwipes and place tissue in tissue cryomolds (10 x 10 x 5 mm) pre-filled to the top with OCT freezing medium[24]. Snap freeze the tissue block in liquid nitrogen for 30 seconds. Alternatively, place tissue block on dry ice for 30 min. Store frozen tissue in -80 °C freezer.

2.3.3. Cut tissue sections 5-10 μm thick in a cryostat set at -20 °C[24].

2.3.4. If necessary, perform immunofluorescence labeling, and examine the tissue with confocal microscopy as previously demonstrated[24].

3. Monitoring expansion of antigen-specific, luciferase-expressing CD8+ T cells after nanoparticle vaccination with whole animal imaging.

3.1. Isolation of $OVA_{257-264}$-specific, luciferase-expressing CD8+ T cells from OT-I/Luc transgenic mice

3.1.1. Euthanize an OT-I/Luc transgenic mouse with CO_2 asphyxiation and induce a pneumothorax according to an IACUC approved animal protocol. Harvest the spleen in a sterile

manner by accessing the peritoneal cavity and carefully detaching the tissue from the pancreas[23], and place in 5 ml of 4°C PBS + 2% FBS for transfer to tissue culture hood.

3.1.2. Place the spleen on a 70 μm nylon strainer over a 50 ml conical centrifuge tube (up to 3 spleens at a time). Using a plunger from a 3 ml syringe, grind the cells through the strainer.

3.1.3. Wash the plunger and the strainer with PBS + 2% FBS and discard. Bring the total volume to 10 ml/spleen in the 50 ml tube, take a small sample of the cell suspension to count with hemacytometer, and centrifuge for 10 minutes at 300 x g.

3.1.4. Using a commercially available magnetic negative selection kit, isolate the CD8+ T cell population by following the manufacturer's instructions.

3.1.5. After washing cells with PBS, count the number of isolated CD8+ T cells. To assess purity of isolated CD8+ T cells, incubate ~20,000-30,000 cells in 20 μl of mouse CD16/32 antibody (0.025 mg/ml) for 10 minutes, then add 20 μl αCD8-APC antibody (0.005 mg/ml) and incubate for 30 minutes. Perform all incubations at 4 °C in PBS + 1% w/v BSA. Perform flow cytometric analysis[25].

3.2. Adoptive transfer of isolated CD8+ T cells and visualization of their expansion post vaccination

3.2.1. Perform adoptive transfer of isolated OT-I/Luc CD8+ T cells into naïve C57BL/6 mice by administering 1-10 × 10^5 cells in a 200 μl volume of PBS via intravenous tail vein injection[22] (day -1). Considering that fur and black skin patches in C57BL/6 mice may interfere with the bioluminescent signal, shaved albino C57BL/6 mice are ideal for these studies.

3.2.2. After one day (day 0), administer the vaccine as described previously (section 2.2).

3.2.3. Administer 150 mg luciferin per kg mouse body weight intraperitoneally in 300 µl volume in PBS. After 10 minutes, anesthetize the mice with isoflurane (as in step 2.2.1) and visualize OT-I/Luc CD8+ T cells by acquiring bioluminescence signal for 5-10 min with a whole animal imaging system (IVIS; refer to Wilson, et al.[26] for detailed instruction). Repeat as necessary for longitudinal studies.

4. Peptide-MHC tetramer staining of PBMCs for analysis of antigen-specific CD8+ T cells.

Note: The following protocol procedure can be performed using either C57BL/6 mice adoptively transferred with OT-I/Luc CD8+ T cells or C57BL/6 mice without the adoptive transfer.

4.1. On a desire time point after vaccination, collect approximately 100 µl of blood from mice via submandibular bleeding technique[27] into a tube coated with K_2EDTA and invert several times to prevent clotting.

4.2. Transfer 100 µl of blood to a microcentrifuge tube, add 1 ml of ACK lysis buffer, and incubate for 2 to 3 minutes in order to remove red blood cells (RBCs). Centrifuge samples for 5 minutes at 1500 x g and remove the supernatant. If the pellet still appears red (indicating incomplete removal of RBCs), repeat the lysis step with a brief incubation (< 1 min) of ACK lysis buffer.

4.3. Wash the remaining PBMCs with 1 ml of FACS buffer (PBS + 1% w/v BSA) and centrifuge at 1500 x g for 5 minutes.

4.4. Aspirate the supernatant and resuspend the sample in 20 µl of mouse CD16/32 antibody (0.025 mg/ml) to block nonspecific and FcR-mediated antibody binding. Incubate for 10 minutes at room temperature.

4.5. Transfer cells from microcentrifuge tubes into 4 ml round bottom FACS tubes. Add 20 µl of H-2K^{b} OVA Tetramer-SIINFEKL-PE solution according to manufacturer's specifications to each sample and incubate for 30 minutes on ice.

4.6. Prepare the antibody cocktail (e.g. αCD8-APC, αCD44-FITC, and αCD62L-PECy7 antibodies (0.005, 0.005, and 0.002 mg/ml concentration, respectively)). Add 20 µl to each experimental sample, and incubate for 20 minutes on ice. Prepare single fluorophore controls by labeling cells with each fluorophore-tagged tetramer or antibody at the concentration indicated above.

4.7. Wash 2 times with FACS buffer and resuspend the final pellet in FACS buffer containing 2 µg/ml of DAPI. The cells are now ready for flow cytometry analysis (details and examples can be found in Scheffold, et al.[25]).

A.3 Representative Results

The steps involved in the synthesis of ICMVs are illustrated in Figure 1[6]. Briefly, a lipid film containing any lipophilic drugs or fluorescent dyes is hydrated in the presence of hydrophilic drugs. Divalent cations, such as Ca^{2+}, are added to drive fusion of anionic liposomes into multilamellar vesicles. Dithiol crosslinker, such as DTT, is added to "staple" maleimide-

functionalized lipids on apposing lipid layers, and finally remaining external maleimide groups are quenched in a reaction with thiolated-PEG moieties. A small fraction of each batch can be readily subjected to quality control measurements by determining particle size, polydispersity index, and zeta potential with dynamic light scattering and zeta potential analyzer. The resulting particles are relatively homogenous with an average size of 130 ± 24 nm, polydispersity index of 0.22 ± 0.022, and zeta potential of -54 ± 2.6 mV for OVA-encapsulating particles (**Fig. A-1B and A-1C**). Typical yield of particles, measured in dry weight of particles, is ~ 50%[6].

Using the protocol described above, ICMVs can be co-loaded with fluorophore-tagged protein antigen and fluorescent lipophilic dye, allowing visualization of antigen and nanoparticle delivery *in vivo*. To compare the patterns of antigen delivery in soluble form versus in ICMVs, C57BL/6 mice were administered s.c. at tail base with 100 μg of AlexaFluor555-tagged OVA either in soluble or DiD-labeled ICMV formulations, and draining inguinal LNs were excised on various time points for preparation of dLN tissue sections. Visualization with confocal microscopy indicated that soluble antigen quickly reached the dLNs within 4 h, but was also cleared very rapidly with 24 h (**Fig. A-2**)[7]. In contrast, OVA-loaded ICMVs were detected at the periphery of dLNs by 24 h, with continued accumulation as examined on day 4, depositing a large amount of OVA-ICMVs in dLNs (**Fig. A-2**). Confocal micrographs also showed co-localization of AlexaFluor555-tagged OVA and DiD-labeled ICMVs within dLNs, suggesting that ICMVs permit stable co-delivery of protein antigen and other immunostimulatory agents encapsulated within ICMVs[7].

Isolation of CD8+ T cells from OT-I/Luc transgenic mouse can be readily performed with the commercially available magnetic negative selection kit, yielding ~ 8-12 x 10^6 cells per a mouse spleen. **Figure A-3** shows C57BL/6 mice adoptively transferred with 5 x 10^5 OT-I/Luc

CD8+ T cells on day -1, and immunized on day 0 with s.c. administration of 10 μg OVA and 0.3 μg MPLA either in soluble or ICMV formulations. Bioluminescence imaging with IVIS performed on day 0 prior to vaccination showed minimal OT-I/Luc signal. However, by day 4, mice immunized with OVA/MPLA-ICMVs had robust bioluminescence signal within inguinal LNs, which are LNs draining the tail base region[28]. In contrast, mice immunized with the soluble form of the vaccine showed much reduced expansion of OT-I/Luc CD8+ T cells within inguinal dLNs.

Using OVA as a model antigen allows monitoring of expansion of endogenous CD8+ T cells specific to immunodominant $OVA_{257-264}$ peptide (SIINFEKL). For an example, C57BL/6 mice were immunized on days 0, 21, and 35 with s.c. administration of 10 μg OVA and 0.3 μg MPLA in either ICMVs or soluble form, and frequencies of SIINFEKL-specific CD8+ T cells among CD8+ T cells in PBMCs were determined by flow cytometric analysis of PBMCs stained with SIINFEKL-H-$2K^b$ tetramer-PE. **Figure A-4A** shows representative flow cytometry scatter plots of SIINFEKL-H-$2K^b$ $tetramer^+$ cells among CD8+ T cells in PBMCs on day 41[6]. Weekly monitoring of PBMCs shown in **Figure A-4B** indicated that soluble OVA vaccine elicited minimal expansion of antigen-specific CD8+ T cell, whereas ICMV vaccination elicited significantly stronger $CD8^+$ T cell responses, achieving a peak 28% SIINFEKL-$tetramer^+$ T cells in the $CD8^+$ T cell population by d 41[6].

A.4 Discussion

The protocol provided in this article describes the synthesis and characterization of a new lipid-based nanoparticle system, termed ICMVs, and provides the process of validating

effectiveness of nanoparticle-based vaccine formulations to induce antigen-specific CD8+ T cell responses. ICMV synthesis is completed in all aqueous condition, which is a major advantage compared with other commonly used polymeric nanoparticle systems (e.g. poly(lactide-co-glycolide) acid particles), which typically require organic solvents for preparation, often resulting in loss of antigenicity in protein antigens[29, 30]. In addition, ICMVs benefit from extensive stability and potential of encapsulating hydrophobic and hydrophilic molecules[6], thus permitting co-delivery of antigens and adjuvants targeted to the same intracellular compartment within APCs[31, 32]. Using ICMVs as a model vaccine nanoparticle, here we have outlined the procedures for (1) nanoparticle synthesis and characterization, (2) validation of nanoparticle drainage to dLNs, and examination of elicitation of antigen-specific CD8+ T cell responses using (3) non-invasive bioluminescence imaging technique and (4) peptide-MHC tetramer staining assay on PBMCs.

It is critical to ensure uniformity in nanoparticle synthesis from batch to batch, especially for particle size and surface charge as they can greatly affect lymphatic draining and uptake by APCs upon *in vivo* administration. DLS and zeta potential analyzer provide quick methods of quality check on particle size and surface charge. For more detailed analyses on morphology of individual particles, these techniques can be complemented with high-resolution electron microscopy, such as scanning electron microscopy (SEM) or transmission electron microscopy (TEM), which are generally compatible with solid core nanostructures that are resistant to dehydration during sample preparation. For hollow core nanomaterials, such as ICMVs based on lipid vesicles, cryo-electron microscopy (cryo-EM) that preserves morphology of "soft" particles in vitrified aqueous layer is more suitable[6, 33, 34].

Particles smaller than 100 nm are generally believed to effectively enter the lymphatic vessels and traffic to dLNs[13], whereas larger microparticles require active transport by tissue-resident DCs[35]. In our hands, ICMVs with the hydrodynamic size ranging from 150-250 nm efficiently localized and persisted in the dLN, resulting in extensive CTL and humoral responses[6, 7]. These studies have utilized fluorophore-tagged nanoparticles and protein antigens to delineate their localization and distribution patterns in dLNs. Confocal microscopy of cryosectioned dLNs allows for additional immunofluorescence histochemistry for identification of LN structures and cells interacting with the formulation components. This technique can be performed in parallel with flow cytometry analyses of cells harvested from dLNs to delineate the subsets of APCs responsible for particle uptake [7, 9] or with whole-animal imaging to quantitate vaccine delivery from injection site to dLNs [36, 37], provided that the fluorescent signals are strong and tissue autofluorescence does not interfere with the signals.

Effective immunization requires robust activation and expansion of antigen-specific cytotoxic T cells, which can be tracked by whole-body bioluminescence imaging after adoptive transfer of bioluminescent, antigen-specific transgenic T cells, followed by vaccination. The added benefit of this method is repeated visualization of CTL trafficking in the same animals for an extended period, potentially reducing the number of animals required for immunological analyses and avoiding the use of laborious cell isolation procedures. Using this imaging technique, we have recently demonstrated that pulmonary administration of ICMVs co-loaded with protein antigen and an immunostimulatory agent led to potent elicitation of antigen-specific CD8+ T cells in the lung and mediastinal LNs and subsequent dissemination of CTLs to distal mucosal tissues, including Peyer's patches, cecum, and vaginal tract[9]. Flow cytometric analyses showed that these newly expanded CD8+ T cells were imprinted with a "mucosal-

homing" phenotype characterized by $\alpha_4\beta_7^+$ integrin expression and mediated protective immune responses against mucosal viral challenge[9]. The whole-animal imaging of bioluminescent CD8+ T cells was also recently utilized by Hailemicheal, *et. al*, who demonstrated that tumor antigen peptide formulated into incomplete Freund's adjuvant (IFA, oil-in-water emulsion) resulted in sequestration of T cells at the site of the injection with vaccine "depot" away from the tumor masses, leading to T cell dysfunction and deletion[38].

Tetramer staining has been used extensively in the past to quantify the level of endogenous CTL responses resulting from various vaccine formulations [21]. This technique is also relevant and commonly utilized in early human cancer immunotherapy clinical trials to confirm CTL responses to specific tumor-associated antigens [39, 40]. Compatibility of this method with flow cytometry allows determination of antigen-specific T cells with memory markers (CD44, CD62L, CD127, Bcl-2, and KLRG-1) to distinguish effector, central memory, and effector memory cells among the tetramer+ T cells[41] or long-lasting tissue resident CTLs [42, 43]. However, tetramer staining assay provides only the initial assessment of CTL responses since highly-expanded antigen-specific T cells may exhibit signs of immune exhaustion [44, 45]. Functional evaluation of CTL responses can be performed by examining cytokine release with enzyme linked immunospot (ELISpot)[46] or intracellular cytokine staining[47] after *ex vivo* stimulation of lymphocytes with minimal epitopes as well as by measuring the intracellular levels of perforin and granzyme B [48] and extracellular expression of CD107a and CD107b upon degranulation [49]. In addition, cytolytic function of CTLs can be directly assessed with CTL cytotoxicity assay performed *in vitro* or *in vivo* [50-52].

A.5 References

1. Irvine, D.J., M.A. Swartz, and G.L. Szeto, *Engineering synthetic vaccines using cues from natural immunity.* Nature materials, 2013. **12**(11): p. 978-90.

2. Moon, J.J., B. Huang, and D.J. Irvine, *Engineering nano- and microparticles to tune immunity.* Advanced materials, 2012. **24**(28): p. 3724-46.

3. Sahdev, P., L.J. Ochyl, and J.J. Moon, *Biomaterials for nanoparticle vaccine delivery systems.* Pharmaceutical Research, 2014.

4. Zhao, L., et al., *Nanoparticle vaccines.* Vaccine, 2014. **32**(3): p. 327-37.

5. van Riet, E., et al., *Combatting infectious diseases; nanotechnology as a platform for rational vaccine design.* Advanced drug delivery reviews, 2014. **74C**: p. 28-34.

6. Moon, J.J., et al., *Interbilayer-crosslinked multilamellar vesicles as synthetic vaccines for potent humoral and cellular immune responses.* Nature Materials, 2011. **10**(3): p. 243-51.

7. Moon, J.J., et al., *Enhancing humoral responses to a malaria antigen with nanoparticle vaccines that expand Tfh cells and promote germinal center induction.* Proceedings of the National Academy of Sciences of the United States of America, 2012. **109**(4): p. 1080-5.

8. DeMuth, P.C., et al., *Releasable layer-by-layer assembly of stabilized lipid nanocapsules on microneedles for enhanced transcutaneous vaccine delivery.* ACS Nano, 2012. **6**(9): p. 8041-51.

9. Li, A.V., et al., *Generation of Effector Memory T Cell-Based Mucosal and Systemic Immunity with Pulmonary Nanoparticle Vaccination.* Science Translational Medicine, 2013. **5**(204): p. 204ra130.

10. Stephan, M.T., et al., *Therapeutic cell engineering with surface-conjugated synthetic nanoparticles.* Nature Medicine, 2010. **16**(9): p. 1035-41.

11. Murdock, R.C., et al., *Characterization of nanomaterial dispersion in solution prior to In vitro exposure using dynamic light scattering technique.* Toxicological Sciences, 2008. **101**(2): p. 239-253.

12. Manolova, V., et al., *Nanoparticles target distinct dendritic cell populations according to their size.* European Journal of Immunology, 2008. **38**(5): p. 1404-1413.

13. Reddy, S.T., et al., *Exploiting lymphatic transport and complement activation in nanoparticle vaccines.* Nature Biotechnology, 2007. **25**(10): p. 1159-1164.

14. Kaur, R., et al., *Manipulation of the surface pegylation in combination with reduced vesicle size of cationic liposomal adjuvants modifies their clearance kinetics from the injection site, and the rate and type of T cell response.* Journal of Controlled Release, 2012. **164**(3): p. 331-7.

15. Zhuang, Y., et al., *PEGylated cationic liposomes robustly augment vaccine-induced immune responses: Role of lymphatic trafficking and biodistribution.* Journal of Controlled Release, 2012. **159**(1): p. 135-42.

16. Hogquist, K.A., et al., *T cell receptor antagonist peptides induce positive selection.* Cell, 1994. **76**(1): p. 17-27.

17. Clarke, S.R.M., et al., *Characterization of the ovalbumin-specific TCR transgenic line OT-I: MHC elements for positive and negative selection.* Immunology and Cell Biology, 2000. **78**(2): p. 110-117.

18. Azadniv, M., et al., *Imaging CD8(+) T cell dynamics in vivo using a transgenic luciferase reporter.* International Immunology, 2007. **19**(10): p. 1165-1173.

19. Kim, D., C.F. Hung, and T.C. Wu, *Monitoring the trafficking of adoptively transferred antigen- specific CD8-positive T cells in vivo, using noninvasive luminescence imaging.* Human gene therapy, 2007. **18**(7): p. 575-88.

20. Rabinovich, B.A., et al., *Visualizing fewer than 10 mouse T cells with an enhanced firefly luciferase in immunocompetent mouse models of cancer.* Proceedings of the National Academy of Sciences of the United States of America, 2008. **105**(38): p. 14342-14346.

21. Altman, J.D., et al., *Phenotypic analysis of antigen-specific T lymphocytes.* Science, 1996. **274**(5284): p. 94-96.

22. Machholz, E., et al., *Manual Restraint and Common Compound Administration Routes in Mice and Rats.* Journal of visualized experiments : JoVE, 2012(67): p. e2771.

23. Bedoya, S.K., et al., *Isolation and Th17 Differentiation of Naive CD4 T Lymphocytes.* Journal of visualized experiments : JoVE, 2013(79): p. e50765.

24. Chen, Y., et al., *Visualization of the interstitial cells of cajal (ICC) network in mice.* J Vis Exp, 2011(53).

25. Scheffold, A., D.H. Busch, and F. Kern, *Detection of Antigen-Specific T-Cells using Major Histocompatibility Complex Multimers or Functional Parameters*, in *Cellular Diagnostics. Basics, Methods and Clinical Applications of Flow Cytometry.*, U. Sack, A. Tárnok, and G. Rothe, Editors. 2009, Karger: Basel. p. 476–502.

26. Wilson, K., et al., *In vitro and in vivo Bioluminescence Reporter Gene Imaging of Human Embryonic Stem Cells.* Journal of visualized experiments : JoVE, 2008(14): p. e740.

27. Golde, W.T., P. Gollobin, and L.L. Rodriguez, *A rapid, simple, and humane method for submandibular bleeding of mice using a lancet.* Lab Animal, 2005. **34**(9): p. 39-43.

28. Tilney, N.L., *Patterns of lymphatic drainage in the adult laboratory rat.* Journal of Anatomy, 1971. **109**(Pt 3): p. 369-83.

29. Stivaktakis, N., et al., *PLA and PLGA microspheres of beta-galactosidase: Effect of formulation factors on protein antigenicity and immunogenicity.* Journal of Biomedical Materials Research Part A, 2004. **70A**(1): p. 139-148.

30. Bilati, U., E. Allemann, and E. Doelker, *Nanoprecipitation versus emulsion-based techniques for the encapsulation of proteins into biodegradable nanoparticles and process-related stability issues.* AAPS PharmSciTech, 2005. **6**(4): p. E594-604.

31. Blander, J.M. and R. Medzhitov, *Toll-dependent selection of microbial antigens for presentation by dendritic cells.* Nature, 2006. **440**(7085): p. 808-12.

32. Iwasaki, A. and R. Medzhitov, *Regulation of Adaptive Immunity by the Innate Immune System.* Science, 2010. **327**(5963): p. 291-295.

33. Dubochet, J., et al., *Cryo-electron microscopy of vitrified specimens.* Quarterly reviews of biophysics, 1988. **21**(2): p. 129-228.

34. Vinson, P.K., Y. Talmon, and A. Walter, *Vesicle-micelle transition of phosphatidylcholine and octyl glucoside elucidated by cryo-transmission electron microscopy.* Biophysical journal, 1989. **56**(4): p. 669-81.

35. Randolph, G.J., V. Angeli, and M.A. Swartz, *Dendritic-cell trafficking to lymph nodes through lymphatic vessels.* Nature Reviews Immunology, 2005. **5**(8): p. 617-628.

36. Liu, H., et al., *Structure-based programming of lymph-node targeting in molecular vaccines.* Nature, 2014. **507**(7493): p. 519-22.

37. Xu, Z., et al., *Multifunctional nanoparticles co-delivering Trp2 peptide and CpG adjuvant induce potent cytotoxic T-lymphocyte response against melanoma and its lung metastasis.* Journal of Controlled Release, 2013. **172**(1): p. 259-65.

38. Hailemichael, Y., et al., *Persistent antigen at vaccination sites induces tumor-specific CD8(+) T cell sequestration, dysfunction and deletion.* Nature Medicine, 2013. **19**(4): p. 465-+.

39. Slingluff, C.L., et al., *Phase I trial of a melanoma vaccine with gp100(280-288) peptide and tetanus helper peptide in adjuvant: Immunologic and clinical outcomes.* Clinical Cancer Research, 2001. **7**(10): p. 3012-3024.

40. Speiser, D.E., et al., *Rapid and strong human CD8(+) T cell responses to vaccination with peptide, IFA, and CpG oligodeoxynucleotide 7909.* Journal of Clinical Investigation, 2005. **115**(3): p. 739-746.

41. Araki, K., et al., *mTOR regulates memory CD8 T-cell differentiation.* Nature, 2009. **460**(7251): p. 108-12.

42. Masopust, D., et al., *Preferential localization of effector memory cells in nonlymphoid tissue.* Science, 2001. **291**(5512): p. 2413-7.

43. Cuburu, N., et al., *Intravaginal immunization with HPV vectors induces tissue-resident CD8+ T cell responses.* Journal of Clinical Investigation, 2012. **122**(12): p. 4606-20.

44. Barber, D.L., et al., *Restoring function in exhausted CD8 T cells during chronic viral infection.* Nature, 2006. **439**(7077): p. 682-7.

45. Wherry, E.J., et al., *Molecular signature of CD8+ T cell exhaustion during chronic viral infection.* Immunity, 2007. **27**(4): p. 670-84.

46. Czerkinsky, C.C., et al., *A solid-phase enzyme-linked immunospot (ELISPOT) assay for enumeration of specific antibody-secreting cells.* Journal of Immunological Methods, 1983. **65**(1-2): p. 109-21.

47. Foster, B., et al., *Detection of intracellular cytokines by flow cytometry.* Current Protocols in Immunology, 2007. **Chapter 6**: p. Unit 6 24.

48. Wonderlich, J., et al., *Induction and measurement of cytotoxic T lymphocyte activity.* Current protocols in immunology 2006. **Chapter 3**: p. Unit 3 11.

49. Betts, M.R., et al., *Sensitive and viable identification of antigen-specific CD8+T cells by a flow cytometric assay for degranulation.* Journal of Immunological Methods, 2003. **281**(1-2): p. 65-78.

50. Brunner, K.T., et al., *Quantitative assay of the lytic action of immune lymphoid cells on 51-Cr-labelled allogeneic target cells in vitro; inhibition by isoantibody and by drugs.* Immunology, 1968. **14**(2): p. 181-96.

51. Noto, A., P. Ngauv, and L. Trautmann, *Cell-based flow cytometry assay to measure cytotoxic activity.* Journal of visualized experiments : JoVE, 2013(82): p. e51105.

52. Quah, B.J., et al., *The use of fluorescent target arrays for assessment of T cell responses in vivo.* Journal of visualized experiments : JoVE, 2014(88): p. e51627.

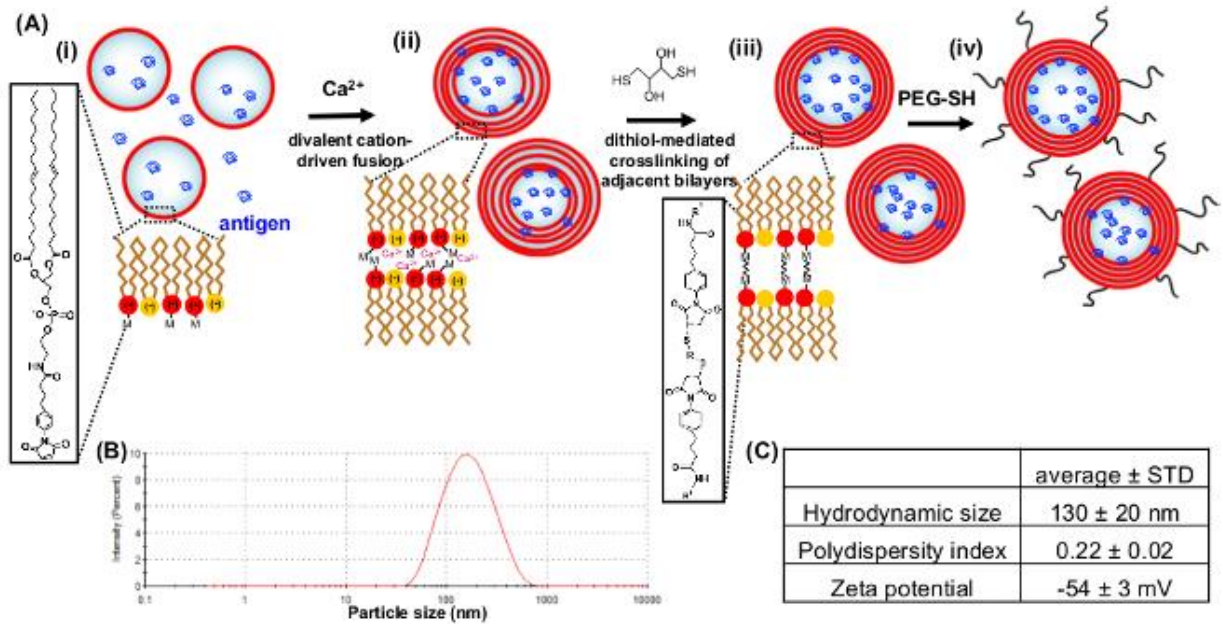

Figure A-1: Synthesis and characterization of interbilayer-crosslinked multilamellar vesicles (ICMVs).

(A) ICMVs are synthesized in the following 4 steps; (i) anionic, maleimide-functionalized liposomes are prepared from dried lipid films; (ii) divalent cations are added to induce fusion of liposomes and the formation of multilamellar vesicles; (iii) membrane-permeable dithiols are added, which crosslink maleimide-lipids on apposed lipid bilayers in the vesicle walls; and (iv) the resulting lipid particles are PEGylated with thiol-terminated PEG. (B) Representative particle distribution as analyzed by DLS is shown. (C) Average hydrodynamic size, polydispersity index, and zeta potential of ICMVs co-loaded with OVA and MPLA are shown. Panel (A) has been modified from Moon et al.[6] with permission.

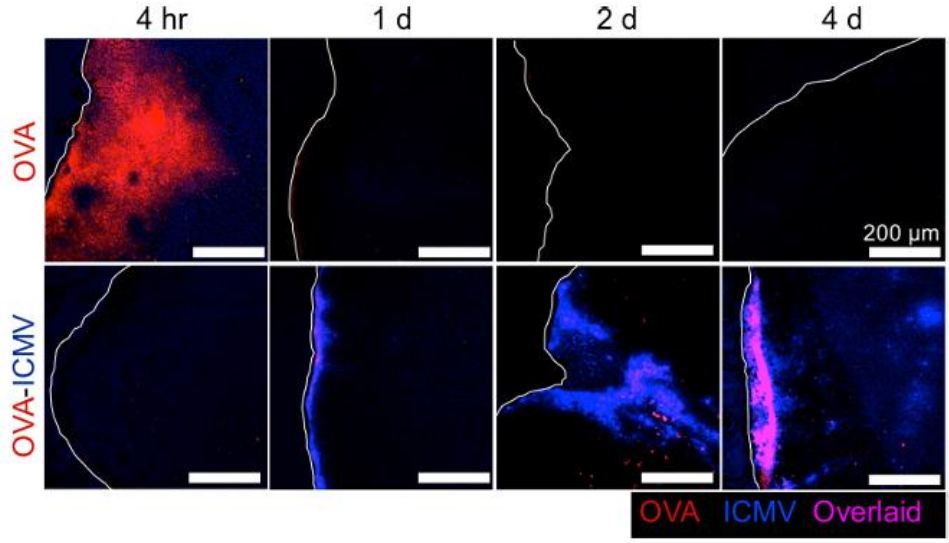

Figure A-2. Analysis of antigen draining to lymph nodes with confocal microscopy.
C57Bl/6 mice were immunized with 100 μg fluorophore-conjugated OVA (shown in red) and 5 μg MPLA either in solution or ICMVs (shown in blue). Draining inguinal lymph nodes were excised at indicated time points, cryosectioned, and imaged with confocal microscopy. Representative confocal micrographs are shown. Pink signals indicate co-localization of OVA and ICMVs. This figure has been modified from Moon et al.[7] with permission.

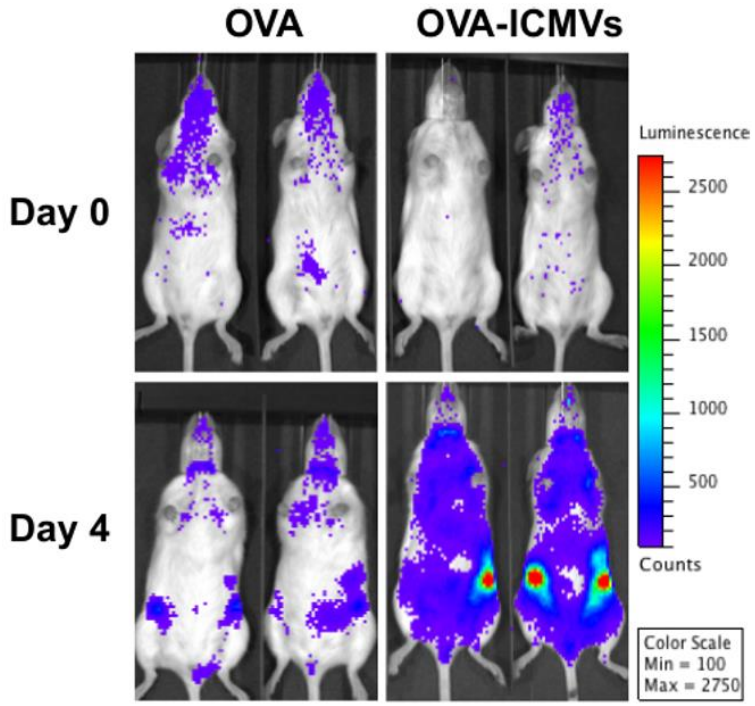

Figure A-3. Monitoring T cell expansion after vaccination.
C57Bl/6 albino mice were adoptively transferred i.v. with 5 x 10^5 Luc^+ OT-I $CD8^+$ T cells on day -1. On day 0, the animals were administered with 10 μg OVA and 0.1 μg MPLA either as soluble or ICMV formulations. The animals were anesthetized with isoflurane and administered with luciferin (150 mg/kg, 300 μl injected i.p.), and bioluminescence signal from Luc^+OT-1 $CD8^+$ T cells was acquired with IVIS.

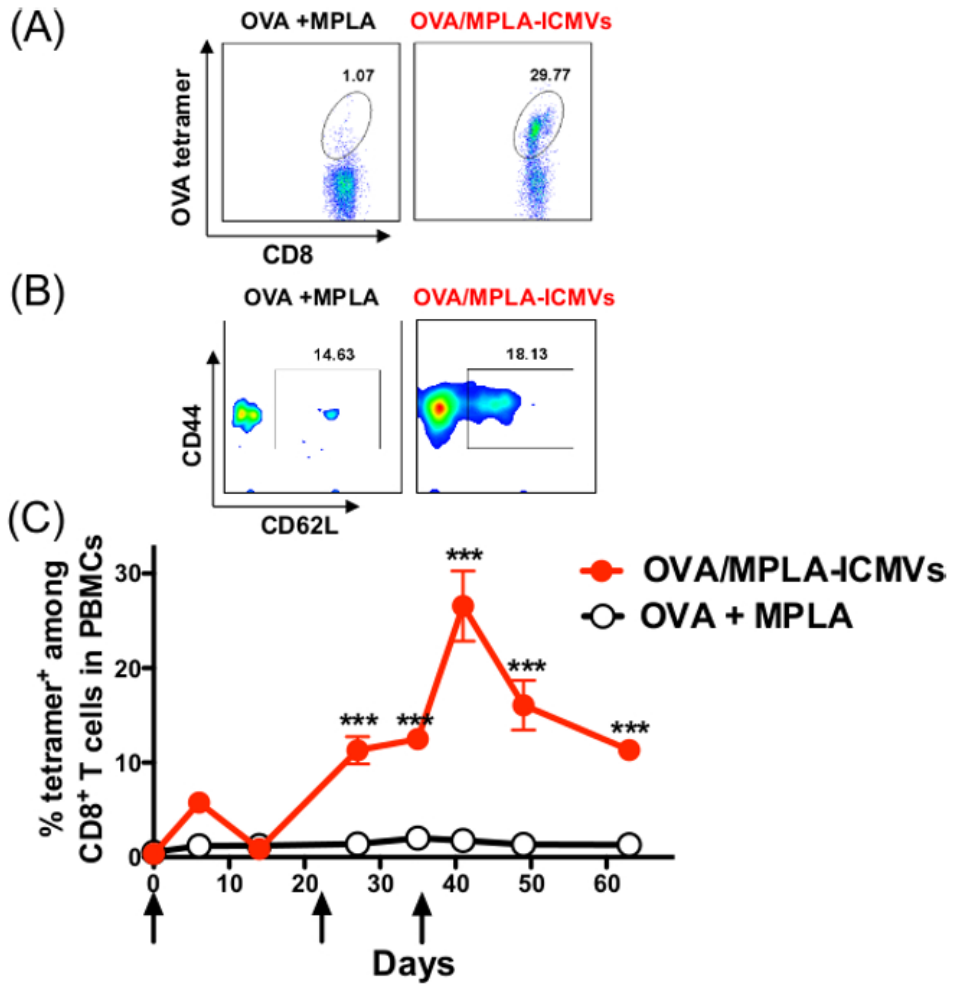

Figure A-4. Expansion of endogenous OVA-specific CD8+ T cells after ICMV vaccination. C57Bl/6 mice were immunized with 10 μg OVA and 0.1 μg MPLA either in solution or ICMVs on days 0, 21, and 35 (arrows). Frequency of OVA-specific T cells among peripheral blood mononuclear cells was assessed over time by flow cytometric analysis of SIINFEKL-MHC-I tetramer^{+} CD8+ T cells. (A) Representative flow cytometry scatter plots from individual mice at day 41 are shown, and (B) overall kinetics of T cell expansion and contraction is shown. This figure has been modified from Moon et al.[6] with permission.